January 2011

Genetic and Chemical Genetic Approaches to Shiga Toxin Inhibition

Jose Saenz
Washington University in St. Louis

Follow this and additional works at: https://openscholarship.wustl.edu/etd

WASHINGTON UNIVERSITY IN ST. LOUIS

Division of Biology and Biomedical Sciences

Molecular Microbiology and Microbial Pathogenesis

Dissertation Examination Committee:
David Haslam, Chair
Michael Caparon
Tom Ellenberger
Daniel Goldberg
Phyllis Hanson
Phil Tarr

GENETIC AND CHEMICAL GENETIC APPROACHES
TO SHIGA TOXIN INHIBITION

by

José Bernardo Sáenz

A dissertation presented to the
Graduate School of Arts and Sciences
of Washington University in St. Louis in
partial fulfillment of the
requirements of the degree
of Doctor of Philosophy

May 2011

Saint Louis, Missouri

ABSTRACT OF THE DISSERTATION

Genetic and Chemical Genetic Approaches to Shiga Toxin Inhibition

by

José Bernardo Sáenz

Doctor of Philosophy in Biology and Biomedical Sciences

Molecular Microbiology and Microbial Pathogenesis

Washington University in St. Louis, 2011

Associate Professor David Haslam, Chairperson

Infection with Shiga toxin-producing bacteria can place patients at risk of developing hemolytic uremic syndrome, a toxemic condition characterized by hemolytic anemia, thrombocytopenia, and acute renal failure. Though hemolytic uremic syndrome remains the leading cause of acute renal failure in children under the age of 5, treatment of this disease remains purely supportive. In order to limit the systemic effects of Shiga toxin, efforts must be undertaken to target intoxicated cells. To this end, we have focused on two aspects of Shiga toxin pathogenesis. One approach relied on a high-throughput screen of a small compound library to identify potential inhibitors of Shiga toxin intracellular transport, as Shiga toxin is known to undergo a stepwise progression through host cells following endocytosis. This screen identified three compounds with distinct effects on Shiga toxin transport. A detailed characterization of one of these inhibitory compounds, golgicide A, shed insight into the role of a guanine nucleotide exchange factor, GBF1, in coordinating bidirectional transport through the Golgi. Golgicide A was found to be a potent and specific inhibitor of GBF1 and represents a novel tool for

probing intra-Golgi transport. Our second approach adapted a siRNA screen of the human kinome to a high-throughput format. In an effort to identify human kinases involved in Shiga toxin pathogenesis, we identified the mitogen-activated protein kinase-activated protein kinase 2 (MK2) as a kinase involved in the host stress response to Shiga toxin. MK2 was activated following ribotoxic stress and contributed to the Shiga toxin-induced acute inflammatory response. Genetic and chemical inhibition of MK2 significantly reduced the expression of the inflammatory cytokines IL-6 and TNFα following Shiga toxin exposure. MK2 thus represents a therapeutic alternative for treating the immunopathological response to Shiga toxin, and future efforts at dissecting its role in an *in vivo* mouse model of hemolytic uremic syndrome will help elucidate the contribution of the inflammatory response to Shiga toxin-mediated disease.

ACKNOWLEDGEMENTS

TABLE OF CONTENTS

CHAPTER I

Introduction

CHAPTER II

**Identification and characterization of small molecules
that inhibit intracellular toxin transport**

CHAPTER III

**Golgicide A reveals essential roles for
GBF1 in Golgi assembly and function**

CHAPTER IV

The MAP kinase-activated protein kinase-activated protein kinase (MK2) contributes to the Shiga toxin-induced inflammatory response

CHAPTER V

Conclusions and Future Directions

LIST OF FIGURES

Chapter IV: The MAP kinase activated protein kinase-activated protein kinase 2 (MK2) contributes to the STx-induced inflammatory response

Chapter V: Conclusions and Future Directions

CHAPTER I

Introduction

Scope of Dissertation

The emergence of Shiga toxin (STx)-producing bacteria, most notably *E. coli* O157:H7, and the relative lack of therapeutic options for the treatment of STx-mediated disease underscore the need to elucidate the mechanisms of STx pathogenesis. While considerable work has enhanced our molecular understanding of intracellular STx transport and the activation of the host stress response to STx, therapeutic alternatives aimed at limiting systemic injury remain limited. The work presented in this thesis focuses on a dual approach to STx inhibition, highlighting the use of high-throughput screens to identify inhibitors of both STx transport and of the STx-induced inflammatory response. The results from these studies have helped to identify three small molecule inhibitors acting at distinct stages in the STx transport pathway. Further characterization of one compound elucidated the function of a host guanine nucleotide exchange factor in mediating anterograde and retrograde transport within the Golgi. In addition, the identification and characterization of a kinase implicated in the inflammatory response to STx offered insight into a potential therapeutic target for mitigating the immunopathology associated with STx-mediated disease. Future endeavors into the role of this kinase in mediating the host response to STx in an *in vivo* model system will be critical to understanding the initiation and regulation of the acute inflammatory response to STx.

"Dans les champs de l'observation, le hasard ne favorise que les esprits préparés."
["In the fields of observation, chance favors only the prepared minds."]
- Louis Pasteur

Shiga Toxin and the Pathophysiology of Hemolytic Uremic Syndrome

Bacterial exotoxins are critical components of bacterial pathogenesis. The contribution of exotoxins to microbial pathogenesis relies on their ability to damage the host through various mechanisms. Apart from the pore-forming toxinss, which bind the plasma membrane where they oligomerize and undergo a conformational change to penetrate and damage the host membrane, most toxins act intracellularly to cause cytotoxicity. Among the intracellular toxins, the AB family of toxins is distinguished by a receptor-binding B moiety that is non-covalently linked to an enzymatic A subunit. Toxin-mediated cytotoxicity depends on the A subunit reaching its cytosolic targets. Several toxins damage host cells by inhibiting protein synthesis: diphtheria toxin (DT) and *Pseudomonas* exotoxin (PE) inhibit protein synthesis through the ADP-ribosylation of elongation factor 2[1,2], whereas Shiga toxin (STx) and the plant toxin ricin inhibit ribosome function by cleaving an adenine residue from the 60S ribosome[3-7]. Still other toxins, such as cholera toxin (CTx) and anthrax edema toxin, induce increases in second messenger levels, resulting in cytotoxicity[8-10].

Despite increasing insight into the mechanisms underlying toxin-mediated disease, bacterial toxins constitute a continuing global health threat. Of particular importance in the U.S. has been the recent emergence of STx-producing bacteria. STx was initially identified in *Shigella dysenteriae* type I, though it is now commonly associated with strains of STx-producing *Escherichia coli* (STEC), among which *E. coli* O157:H7 has become the most clinically relevant. Transmission of STEC is primarily foodborne, with outbreaks emanating from sources ranging from meat products to

vegetables. The incidence of STEC in the U.S. varies by age group, with the highest

incidence occurring in children under 15 years of age[11].

In a subset of patients (3-15%), gastrointestinal infection with STEC may

progress to extraintestinal injury, leading to hemolytic uremic syndrome[12] (HUS; Figure

1). This toxemic syndrome is clinically defined by renal failure, thrombocytopenia, and
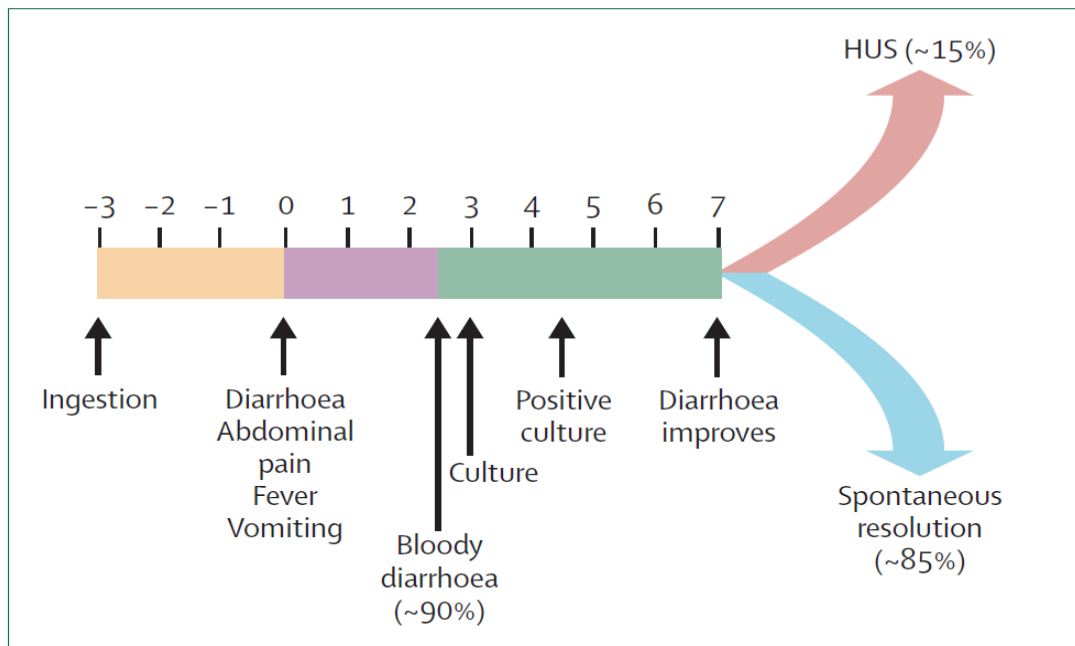
Figure 1. Progression of _E. coli_ 0157:H7 infections in children. Following ingestion of a contaminated vehicle, patients develop bloody diarrhea. In a subset of patients (as high as 15%), intestinal colonization can progress to a toxemic condition known as hemolytic uremic syndrome (HUS). Adapted from Tarr _et al._ [13]

hemolytic anemia, and it remains the leading cause of acute renal failure in children[14,15].

In addition, nearly one third of patients with HUS will experience neurologic

complications, including irritability and altered mental status[12]. While the clinical

characteristics of HUS have become more clearly defined, treatment remains purely

supportive. Indeed, hemodynamic stability through electrolyte and fluid monitoring

represents the most important therapeutic measure in the treatment of HUS and is crucial in preventing progression to renal failure[16].

The pathophysiology of HUS primarily results from STx-mediated effects, and extraintestinal complications of HUS appear to correlate with circulating levels of the toxin. The mechanisms of STx-induced toxicity remain unclear, however. One of the pathologic hallmarks of HUS is the development of thrombotic lesions within the intestinal and renal microvasculature that accounts for the associated hemorrhagic colitis, hemolytic anemia, and renal failure[17]. It has been suggested that STx targeting of endothelial cells that line the microvasculature could account for the characteristic thrombotic microangiopathy associated with HUS[13], and the proposed mechanisms by which STx is believed to induce these changes will be discussed later. While antitoxin therapy through parenteral administration of anti-STx antibodies or STx-binding agents would seem like a logical therapeutic alternative to the more supportive and established measures, clinical trials have consistently showed little therapeutic benefit[18]. By the time of HUS diagnosis, the extraintestinal injury cascade is likely underway, and antitoxin therapy would prove ineffective against cells that have already internalized toxin. It therefore becomes imperative to inhibit STx pathogenesis in intoxicated cells to effectively mitigate HUS pathology and limit systemic injury.

Shiga Toxin Transport

A direct therapeutic approach to inhibiting STx pathogenesis relies on targeting STx transport in intoxicated cells. STx is a member of the AB_5 family of bacterial exotoxins, a group of bacterial toxins with unique trafficking mechanisms. STx, like the

5

bacterial toxin CTx and the plant toxin ricin, is unable to cross host membranes and must progress in a retrograde fashion following endocytosis in order to reach its cytosolic target (Figure 2). Following endocytosis into an early endosome, the toxin bypasses lysosomal degradation and eventually reaches the endoplasmic reticulum (ER) via the
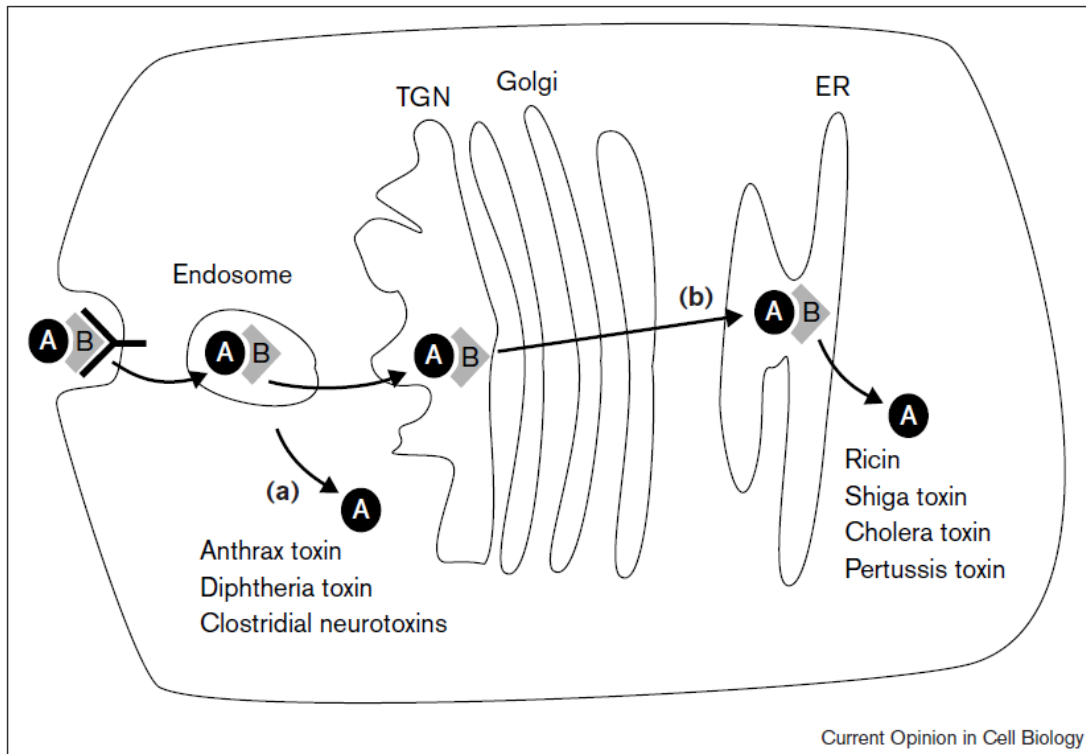
Figure 2. Intracellular transport of protein toxins. Diagram of the stepwise progression of various protein toxins through the host cell. A more detailed description of the retrograde transport of STx is included in the text. Adapted from Falnes, P.O. and Sandvig, K.A.[19]

Golgi. Once in the ER, the catalytic A subunit is retrotranslocated across the ER membrane and accesses the cytosol, where it can target translationally active ribosomes and shut off protein synthesis.

The existence of a retrograde transport pathway was first uncovered by electron microscopic studies tracking the intracellular transport of STx[20], and it has become

increasingly apparent that this retrograde trafficking pathway is not unique to bacterial

toxins. Rather, bacterial toxins are believed to hijack existing host endocytic

mechanisms, and STx has thus emerged as a useful tool for elucidating host mechanisms

underlying its transport. The ability of these toxins to string together existing retrograde

mechanisms translates into a unique system for probing host retrograde transport in its

entirety.

Toxin-receptor interactions

Toxin tropism and the clinical manifestations of toxicity are dictated by toxin-

receptor interactions. Of particular interest is the binding of the STx to its lipid raft-

associated receptor, the neutral glycosphingolipid globotriaosyl ceramide (Gb3). The

association with lipid rafts may serve as a scaffold for the trafficking machinery and

appears to determine the fate of endocytosed toxin. Interestingly, STx is not associated

with lipid microdomains in differentiated monocyte-derived cell lines, which are

relatively resistant to STx's cytotoxic effects[21]. Though the mechanisms underlying lipid

raft internalization remain poorly defined, STx likely subverts endogenous lipid raft

recycling pathways[22] or redirects these pathways at some stage along its transport in

susceptible cells.

Endosome-to-TGN transport

Following the interaction with its receptor, STx internalization consists of uptake

into early endosomes. In contrast to DT and the anthrax toxins, which can enter the

cytosol directly from early endosomes in a pH-dependent manner, STx is unable to cross

host membranes and must rely on a more labored transport to reach its cytosolic targets. This membrane-bound toxin bypasses the late endocytic pathway by retrograde transport from early or sorting endosomes to the *trans*-Golgi network (TGN)[23,24]. Besides cell-type differences in clathrin-dependent endocytosis, increasing evidence suggests that STx is internalized through both clathrin-coated pits and clathrin-independent mechanisms, underscoring the multiple endocytic routes that can be accessed and exploited by the toxin. Despite this complexity, STx converges on early or recycling endosomes while bypassing lysosomal degradation[25]. Studies using STx as an endocytic marker first characterized an alternate pathway that could redirect internalized STxB-containing vesicles away from fusion with late endocytic vesicles en route to the TGN. Several host molecules have been implicated in endosome-to-TGN transport, most notably members of the Rab family of GTP-binding proteins involved in vesicular trafficking[26].

Intra-Golgi transport and retrotranslocation

The molecular components involved in intra-Golgi toxin transport have been less studied than those related to endosome-to-TGN fusion, but retrograde transport within Golgi stacks has proven essential to toxin pathogenesis. As with trafficking through other organelles, the ability of protein toxins to exploit multiple existing trafficking routes within the Golgi has shed insight into the essential components of these pathways. CTx and PE, for example, bear C-terminal KDEL or KDEL-like motifs to make use of the COPI-dependent, KDEL receptor recycling pathway[27,28]. The molecular machinery recruited to COPI-containing vesicles has been extensively studied, and several proteins that constitutively cycle between the ER and Golgi, including ERGIC-53 and the KDEL

receptor, are known to utilize this pathway. STx and ricin, on the other hand, lack KDEL motifs and exhibit COPI-independent transport through the Golgi. These protein toxins exploit a Rab6-dependent pathway, as dominant negative mutants of this small GTP-binding protein blocked STxB delivery to the ER[29]. This COPI-independent pathway is also used for transport to the ER of Golgi-resident glycosyltransferases.

The penultimate destination for STx following retrograde trafficking is the ER. STx has been demonstrated to undergo reverse translocation through the Sec61 translocon in order to reach the cytoplasm. It has been proposed that STxA, like CTx and ricin, is able to mimic the structure of a misfolded protein and thereby exploit the host translocation machinery for transport from the ER to the cytosol[30].

Taken together, the sequential transport of STx occurs through the subversion of preexisting host transport pathways. However, these pathways remain poorly characterized, in part due to inadequate methods to probe individual stages in toxin transport. In the context of STx pathogenesis, enhanced insight into these pathways are significant, as it is believed that this complex retrograde pathway may allow for certain essential steps in toxin activation and transfer; STx has been shown to be cleaved and activated by host proteases[31]. As a result, the necessary stepwise progression of STx through the cell allows for distinct stages in the toxin trafficking pathway to be targeted and enables the characterization of host molecules essential to this process. Moreover, the ability to inhibit toxin trafficking would prove particularly useful in cells that have already internalized toxin, where inhibition of STx transport could potentially inhibit STx-mediated cytotoxicity.

A Small Compound Approach to Shiga Toxin Inhibition

In an effort to dissect and inhibit the stepwise trafficking of STx, our lab developed a quantitative high-throughput luciferase-based assay [32] to screen libraries of small compounds for their ability to block STx-mediated inhibition of protein synthesis. In cells constitutively expressing luciferase mRNA, the level of protein synthesis could be determined by measuring light output from the oxidation of D-luciferin, which is directly proportional to the level of luciferase translation. It was shown that this highly sensitive read-out of protein synthesis could clearly distinguish toxin-susceptible cells exhibiting decreased levels of protein synthesis from untreated cells and cells treated with a combination of toxin plus anti-toxin antibodies [32]. More importantly, this assay could be used to reproducibly screen libraries of small compounds in a high-throughput format.

Previous studies aimed at identifying essential components of the retrograde pathways used by STx, ricin, and CTx have largely focused on standard genetic approaches involving overexpression of dominant negative mutants or siRNA knock-downs of various intracellular targets. While these studies have uncovered novel molecular players at various stages of toxin trafficking, they have equally revealed inconsistencies in their effects on various toxins. For example, disruption of the Golgi apparatus had found that ricin was able to bypass the Golgi apparatus en route to the ER [33]. Whether these alternate routes are physiologically relevant remain to be seen, underscoring a limitation to genetic and irreversible manipulations of trafficking pathways. These approaches have been unable to identify a single trafficking mediator or pathway affecting STx en route to the ER.

The study of microbial pathogenesis through high-throughput screens

Pharmacological compounds have recently gained interest as an alternative to genetic approaches. In particular, small molecules provide an informative chemical genetic method of studying biological activity in live cells in a controlled and reversible manner [34]. The structural diversity of small molecules allows for the screening of large compound libraries for desired phenotypic effects. As these compounds are readily adaptable to high-throughput screens (HTS), numerous commercially available libraries have been used to enhance our understanding of microbial pathogenesis and eukaryotic trafficking. From a library of 12,160 compounds, 24 inhibitors of *Toxoplasma gondii* invasion were identified [35]. These included compounds that inhibited host uptake of the organism as well as inhibitors of *Toxoplasma* gliding motility and microneme-based secretion. Recently, a similar screen identified a small molecule inhibitor of *Vibrio cholera* virulence [36]. 50,000 compounds were screened, from which 109 compounds that inhibited virulence factor expression were identified. Of these, virastatin was characterized and found to inhibit the transcriptional regulator ToxT, thereby suppressing the expression of cholera toxin and the toxin co-regulated pilus.

With respect to toxin trafficking, few studies have used HTS with inhibition of toxin trafficking as the goal. A recent study identified potent antagonists of botulinum neurotoxin A by screening for small molecules that could inhibit the cleavage of vesicle docking proteins by the light chain metalloprotease of the toxin [37]. Though this study did not focus on trafficking of the toxin, another study identified a small molecule, Exo2, that blocked CTx transport by causing disassembly of the Golgi and a redistribution of Golgi proteins to the ER, similar to the effects caused by the well-known fungal metabolite

11

brefeldin A [38] (BFA). While the mechanisms and targets of these small molecules have not been completely solved, these studies highlight the utility of small compounds in our understanding into the biology of retrograde transport and its implications on organelle function and organization.

Identification and characterization of inhibitors of STx transport

A high-throughput screen of over 14,400 small compounds identified several potential inhibitors of Shiga toxicity. Among these, we validated and further characterized two compounds, compounds 75 and 134, that reversibly inhibited Shiga intoxication at distinct steps along its trafficking pathway. Our initial screening results validated the small molecule approach toward our understanding of essential components in toxin transport.

A subsequent screen of a small compound library consisting of biologically active compounds identified golgicide A (GCA), the most potent reported inhibitor of Shiga toxicity. Initial characterization of this compound revealed that it inhibited endosome-to-Golgi transport of STx by reversibly ablating the Golgi and inducing a rapid dissociation of COPI vesicle coats from Golgi membranes. In addition, GCA was found to specifically inhibit GBF1, the guanine nucleotide exchange factor for ARF1, thereby inhibiting bidirectional transport through the Golgi. More importantly, the mechanistic characterization of GCA highlighted the central role of GBF1 in coordinating vesicle transport and maintaining the structural integrity of the Golgi. Our high-throughput screen of small molecule libraries thus yielded three compounds with distinct effects on

12

STx transport. Taken together, small molecules offer a novel approach to studying STx transport and uncovering the host transport mechanisms that underlie it.

From Chemical Genetics Back to Genetics

While small molecule compounds are amenable to high-throughput screening and allow for the reversible manipulation of cellular processes, the rate-limiting step in these studies is the identification of the compound's target. Indeed, the targets of many small compounds pulled out of high-throughput screens have yet to be identified, and the criteria for validating compound specificity are not always met. In addition, "off-target" effects must be considered when using these compounds at relatively high concentrations. As a result, we decided to take an inherently target-based approach to studying STx pathogenesis. By adapting a siRNA screen to a high-throughput format, we screened the human kinome for kinase and kinase-associated genes whose knock-down would protect against Shiga toxicity in HeLa cells.

Kinases and STx transport

As the role of kinases in Shiga toxicity remains largely unexplored, we reasoned that the functional diversity of kinases would enable a multifocal approach to studying STx pathogenesis. On the one hand, the role of kinases in coordinating intracellular transport is not new, and some studies have identified kinases essential to STx internalization and trafficking. Most recently, a study showed that STx binding to the cell surface resulted in the activation of the Src family kinase Syk, leading to the tyrosine phosphorylation of several downstream endocytic components, including the clathrin

heavy chain [39]. Binding of STx to the Gb3 receptor in a renal tubular epithelial

carcinoma cell line also resulted in transient phosphorylation and redistribution of various

proteins involved in cytoskeletal rearrangements [40]. Using ezrin phosphorylation as a

readout for the initiation of downstream signaling events, various kinases were shown to

be involved, including the Src family kinase PTK, PI 3-kinase, and Rho-associated

kinase, but the role of each of these in toxin trafficking beyond internalization into an

endosome was not studied.

The exact mechanism by which the STxB subunit engages its Gb3 receptor

leading to receptor kinase activation and cytoskeletal reorganization remains to be seen.

It is believed that the clustering of bound receptors within lipid rafts provides a scaffold

for toxin internalization and enhances the toxin's interaction with trafficking machinery.

Whether the kinases that function in toxin internalization also contribute to subsequent

steps in toxin trafficking, including endosome fusion with the TGN or intra-Golgi

transport, is not known. As toxins subvert existing host trafficking pathways, a

characterization of kinases at distinct steps in toxin trafficking will likely reveal the role

of kinases in mediating intracellular membrane trafficking.

Kinases and the stress response to STx

Equally important is the critical role of kinases in mediating the stress response to

STx. Perhaps the most studied kinases involved in STx-induced stress pathways are

members of the mitogen-activated protein kinase (MAPK) family. MAPKs are signal-

transducing enzymes involved in a variety of regulatory roles in eukaryotes, including

inflammation, differentiation, and apoptosis [41]. The p38 MAPK (p38) plays a central role

in the response to various insults, including UV radiation, cytokines, and toxic stress [42].

In the context of STx-mediated damage, numerous studies have clearly defined the role

of p38 in inciting inflammatory cytokine release from toxin-treated cells [43,44]. One study,

for example, showed that sequence-specific damage to 28S rRNA by STx stimulated a

ribotoxic stress response that resulted in p38 activation [45].

The contribution of the stress response to HUS pathology remains a debated topic

in the field. Some studies have suggested a direct role for STx in the thrombotic

microangiopathy of HUS. Of note, intravenous injection of STx into the mesenteric

arteries of rats induced hemorrhagic lesions[46]. Another study found that STx treatment of

human glomerular endothelial cells decreased the expression of fibrinolysis factor[47].

Taken together, it has been proposed that STx contributes to HUS by directly injuring

vascular endothelium and inducing a pro-coagulant state through the stimulation of

endothelial thrombotic factors[13]. Moreover, STx-induced cytotoxicity of endothelial cells

may expose a collagen-rich subendothelial matrix conducive to clot formation.

Other lines of evidence support the view that much of the systemic and focal

pathology is immune-mediated. STx has been shown to upregulate endothelial cell

cytokine expression *in vitro*, and pretreatment of endothelial cells with TNFα or IL-1β

enhanced sensitivity to STx by upregulating Gb3 receptor expression[48]. Exposure of

endothelial cells to cytokines *in vitro* also upregulated surface expression of the leukocyte

adhesins ICAM-1 and VCAM-1[49]. Clinically, increased cytokine levels have been

detected in urine samples of HUS patients[50]. It has thus been hypothesized that HUS

could be considered an immunopathologic response to STx, though the immune

mediators of this response remain to be identified.

A synthesis of the two prevailing theories behind HUS pathology would claim that this toxemic syndrome results from a combination of direct toxic effects and toxin-elicited immunopathology. The dual role of kinases in regulating STx transport and STx-mediated cell injury thus makes them an ideal target for studying STx pathogenesis. In particular, the ability to limit the inflammatory response to STx through inhibition of immunomodulatory kinases would prove crucial to reducing Shiga toxicity and provide a therapeutic alternative for the treatment of HUS.

Role of MAP kinase-activated protein kinase 2 (MK2) in the STx-induced inflammatory response

Though the mechanisms behind STx activation of immune signaling cascades remain unclear, a crucial component is the ability of kinases to propagate the stress signal and initiate a cellular response. As a result, kinases are tempting therapeutic targets for limiting STx-mediated cellular injury. For example, inhibition of p38 activation decreased cytokine release following exposure of macrophages to STx [51]. However, p38 inhibition may have limited therapeutic potential, given the ability of p38 to activate various downstream kinases involved in diverse cellular functions. Indeed, mice deficient in p38 are not viable post-natally [52-54], and in human clinical trials p38 inhibition has been met with unanticipated side effects [55]. Moreover, inhibition of p38 kinase activity by overexpression of dominant negative p38 isoforms [56] or by treatment with chemical inhibitors [57] has made probing of specific p38-dependent signaling pathways particularly difficult. Effectors downstream of p38 might therefore be more

specific and functionally relevant to the inflammatory signals induced in response to STx [58].

The mitogen-activated protein kinase-activated protein kinase 2 (MK2) has been recently shown to contribute to the inflammatory response [59]. MK2 is a member of the MK subfamily of calcium/calmodulin-dependent kinases that was originally identified as an *in vivo* substrate of p38 [60]. Activation of MK2 by p38 results primarily in the subsequent phosphorylation of its two main substrates, heat shock protein 27 (Hsp27) and tristetraprolin (TTP). Of note, TTP has been shown to mediate the degradation of cytokine mRNA transcripts bearing AU-rich elements (ARE) in their 3'-UTR. Phosphorylation of TTP by MK2 leads to sequestration of TTP and stabilization of cytokine mRNAs including, but not limited to, IL-6 and TNFα. As a result, MK2 contributes to the inflammatory response through the post-transcriptional stabilization of
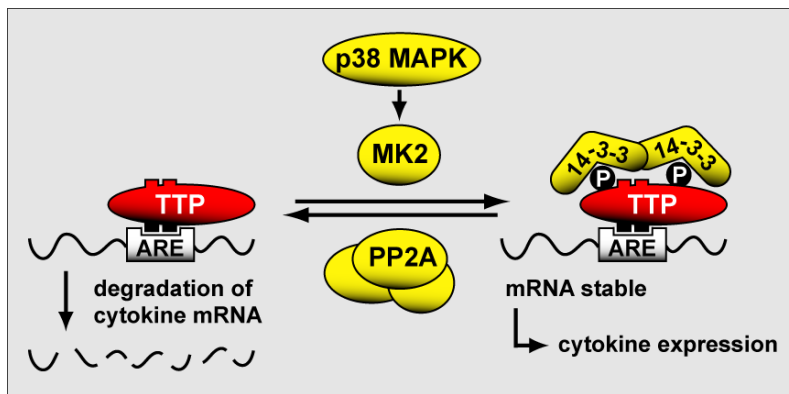
Figure 3. MK2-mediated post-transcriptional stabilization of cytokine mRNAs. Shown is a schematic of the role of MK2 in stabilizing cytokine mRNA transcripts containing AU-rich elements (ARE). Phosphorylation of TTP by MK2 leads to its sequestration by 14-3-3 proteins and subsequent stabilization of cytokine mRNAs. In its unphosphorylated state, TTP binds to the ARE of cytokine mRNAs and directs their degradation. The phosphatase PP2A promotes mRNA degradation by dephosphorylating TTP. TTP, tristretraprolin; MK2, mitogen-activated protein kinase-activated protein kinase 2; PP2A, protein phosphatase 2A. Adapted from http://www.dkfz.de/en/posttrans-genreg/Research.html.

cytokine mRNAs (Figure 3). Although MK2 has been implicated in an *in vivo* inflammatory response to LPS [59], the role of MK2 in STx-mediated toxicity has yet to be explored.

From a high-throughput siRNA screen of the human kinome, knock-down of MK2 was found to protect against Shiga toxicity. Subsequent characterization of MK2 revealed that MK2 activation depends on catalytically active STx following damage to the ribosome. Chemical and genetic inhibition of MK2 significantly reduced the *in vitro* cytokine response to STx, further implicating MK2 as an important modulator of Shiga toxicity.

Mouse model for assessing the In vivo *role of MK2 in Shiga toxicity*

The paucity of adequate animal models that recapitulate the pathological features of HUS has made it particularly difficult to correlate and validate *in vitro* findings in an *in vivo* setting. Though administration of intravenous STx in primates did reproduce elements of HUS pathology[61], the development of small animal models has proven less fruitful. In particular, murine models of HUS, until recently, failed to produce glomerular thrombotic microangiopathy, a clinical hallmark of HUS and a major contributor to acute renal failure. Moreover, some of these studies employed bacterial endotoxin, or lipoplysaccharide (LPS), in combination with STx and obtained varying results that depended on the dose and time of administration[62]. Pretreatment with LPS has been shown to be protective against Shiga toxicity, while later LPS administration enhanced certain elements of STx-induced pathology[63].

18

Recently, a mouse model of HUS using endotoxin-free STx treatment was validated[64]. Mice injected intra-peritoneally with three sublethal STx doses over the course of a week developed anemia, glomerular thrombotic microangiopathy, and acute renal failure (Figure 4).

A)

B)
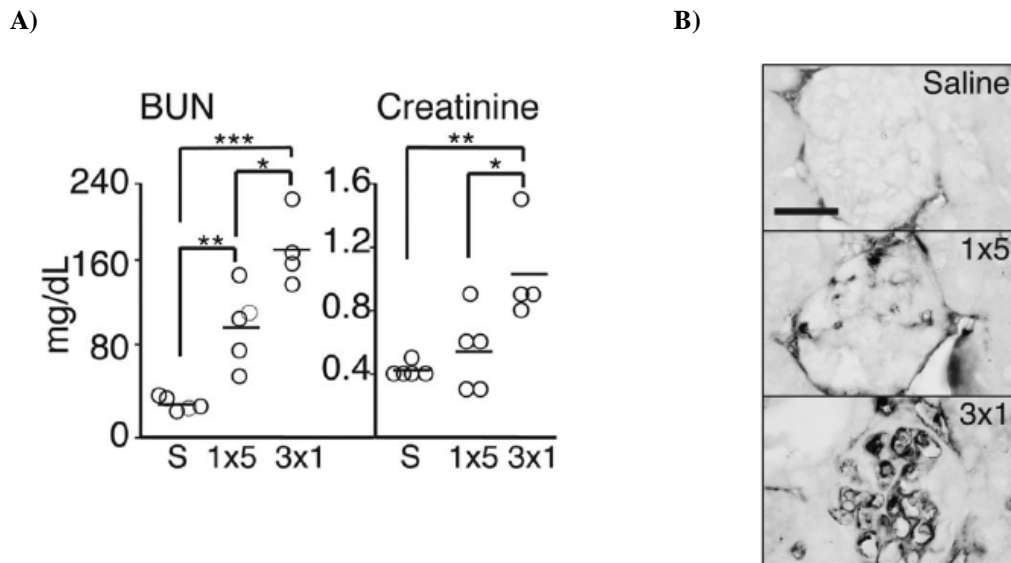
Figure 4. Mouse model of hemolytic uremic syndrome. Shown are two figures taken from Sauter, A.D., et al. (2008). (A) Injection of mice with 3 injections of 1 ng STx2/20 g body weight (3x1) exhibit decreased renal function, as observed by increased serum levels of blood urea nitrogen (BUN) and creatinine compared to saline-treated controls (S). (B) Mice injected with 3 sublethal doses of STx2 (3x1) show increased renal deposition of fibrin/fibrinogen compared to saline-injected mice or mice injected with a single, 5-ng/20g body-weight dose (1x5). Shown are kidney sections stained immunohistochemically for fibrin/fibrinogen. Bar, 20 µm.

We have adopted this model in order to assess the contribution of the inflammatory response to HUS pathology. Given our identification of MK2 as a significant kinase in the immune response to STx, we plan to investigate the contribution of MK2 to Shiga toxicity *in vivo*. More generally, the immunopathological contribution to HUS will be studied through MK2 deletion, as MK2 has been previously shown to modulate the inflammatory response in other pathological states[59]. To that end, we are in the process of adapting the recently validated murine model of HUS to MK2-deficient mice and will compare the development of HUS pathology to wild-type mice. A detailed

assessment of the systemic pathologic features of HUS in wild-type versus MK2-deficent

mice will allow us to more clearly define the contribution of the immune system to the

development of HUS.

REFERENCES

1.   Oh, K.J., Senzel, L., Collier, R.J. & Finkelstein, A. Translocation of the catalytic domain of diphtheria toxin across planar phospholipid bilayers by its own T domain. *Proc Natl Acad Sci U S A* **96**, 8467-70 (1999).

2.   Chaudhary, V.K., Jinno, Y., FitzGerald, D. & Pastan, I. Pseudomonas exotoxin contains a specific sequence at the carboxyl terminus that is required for cytotoxicity. *Proc Natl Acad Sci U S A* **87**, 308-12 (1990).

3.   Endo, Y. & Tsurugi, K. Mechanism of action of ricin and related toxic lectins on eukaryotic ribosomes. *Nucleic Acids Symp Ser*, 187-90 (1986).

4.   Obrig, T.G., Moran, T.P. & Brown, J.E. The mode of action of Shiga toxin on peptide elongation of eukaryotic protein synthesis. *Biochem J* **244**, 287-94 (1987).

5.   Obrig, T.G., Moran, T.P. & Colinas, R.J. Ribonuclease activity associated with the 60S ribosome-inactivating proteins ricin A, phytolaccin and Shiga toxin. *Biochem Biophys Res Commun* **130**, 879-84 (1985).

6.   Reisbig, R., Olsnes, S. & Eiklid, K. The cytotoxic activity of Shigella toxin. Evidence for catalytic inactivation of the 60 S ribosomal subunit. *J Biol Chem* **256**, 8739-44 (1981).

7.   Balint, G.S. [Ricin--2004]. *Orv Hetil* **145**, 2379-81 (2004).

8.   Stryer, L. Transducin and the cyclic GMP phosphodiesterase: amplifier proteins in vision. *Cold Spring Harb Symp Quant Biol* **48 Pt 2**, 841-52 (1983).

9.   Casey, P.J. & Gilman, A.G. G protein involvement in receptor-effector coupling. *J Biol Chem* **263**, 2577-80 (1988).

10. Kumar, P., Ahuja, N. & Bhatnagar, R. Anthrax edema toxin requires influx of calcium for inducing cyclic AMP toxicity in target cells. *Infect Immun* **70**, 4997-5007 (2002).

11. Mead, P.S., Slutsker, L., Griffin, P.M. & Tauxe, R.V. Food-related illness and death in the united states reply to dr. hedberg. *Emerg Infect Dis* **5**, 841-2 (1999).

12. Razzaq, S. Hemolytic uremic syndrome: an emerging health risk. *Am Fam Physician* **74**, 991-6 (2006).

13. Tarr, P.I., Gordon, C.A. & Chandler, W.L. Shiga-toxin-producing Escherichia coli and haemolytic uraemic syndrome. *Lancet* **365**, 1073-86 (2005).

14. Griffin, P.M. & Tauxe, R.V. The epidemiology of infections caused by Escherichia coli O157:H7, other enterohemorrhagic E. coli, and the associated hemolytic uremic syndrome. *Epidemiol Rev* **13**, 60-98 (1991).

15. Karmali, M.A. Infection by verocytotoxin-producing Escherichia coli. *Clinical Microbiology Reviews* **2**, 15-38 (1989).

16. Thorpe, C.M. Shiga toxin-producing Escherichia coli infection. *Clin Infect Dis* **38**, 1298-303 (2004).

17. Proulx, F., Seidman, E.G. & Karpman, D. Pathogenesis of Shiga toxin-associated hemolytic uremic syndrome. *Pediatr Res* **50**, 163-71 (2001).

18. Tzipori, S., Sheoran, A., Akiyoshi, D., Donohue-Rolfe, A. & Trachtman, H. Antibody therapy in the management of shiga toxin-induced hemolytic uremic syndrome. *Clin Microbiol Rev* **17**, 926-41, table of contents (2004).

19. Falnes, P.O. & Sandvig, K. Penetration of protein toxins into cells. *Curr Opin Cell Biol* **12**, 407-13 (2000).

22

20.   Sandvig, K. et al. Retrograde transport of endocytosed Shiga toxin to the endoplasmic reticulum. *Nature* **358**, 510-2 (1992).

21.   Ramegowda, B. & Tesh, V.L. Differentiation-associated toxin receptor modulation, cytokine production, and sensitivity to Shiga-like toxins in human monocytes and monocytic cell lines. *Infect Immun* **64**, 1173-80 (1996).

22.   Nichols, B.J. et al. Rapid cycling of lipid raft markers between the cell surface and Golgi complex. *J Cell Biol* **153**, 529-41 (2001).

23.   Morinaga, N., Kaihou, Y., Vitale, N., Moss, J. & Noda, M. Involvement of ADP-ribosylation factor 1 in cholera toxin-induced morphological changes of Chinese hamster ovary cells. *J Biol Chem* **276**, 22838-43 (2001).

24.   Wilcke, M. et al. Rab11 regulates the compartmentalization of early endosomes required for efficient transport from early endosomes to the trans-golgi network. *J Cell Biol* **151**, 1207-20 (2000).

25.   Mallard, F. & Johannes, L. Shiga toxin B-subunit as a tool to study retrograde transport. *Methods Mol Med* **73**, 209-20 (2003).

26.   Stenmark, H. & Olkkonen, V.M. The Rab GTPase family. *Genome Biol* **2**, REVIEWS3007 (2001).

27.   Jackson, M.E. et al. The KDEL retrieval system is exploited by Pseudomonas exotoxin A, but not by Shiga-like toxin-1, during retrograde transport from the Golgi complex to the endoplasmic reticulum. *J Cell Sci* **112 (Pt 4)**, 467-75 (1999).

28.   Majoul, I. et al. KDEL receptor (Erd2p)-mediated retrograde transport of the cholera toxin A subunit from the Golgi involves COPI, p23, and the COOH terminus of Erd2p. *J Cell Biol* **143**, 601-12 (1998).

29.   White, J. et al. Rab6 coordinates a novel Golgi to ER retrograde transport pathway in live cells. *J Cell Biol* **147**, 743-60 (1999).

30.   Yu, M. & Haslam, D.B. Shiga toxin is transported from the endoplasmic reticulum following interaction with the luminal chaperone HEDJ/ERdj3. *Infect Immun* **73**, 2524-32 (2005).

31.   Garred, O., van Deurs, B. & Sandvig, K. Furin-induced cleavage and activation of Shiga toxin. *J Biol Chem* **270**, 10817-21 (1995).

32.   Zhao, L. & Haslam, D.B. A quantitative and highly sensitive luciferase-based assay for bacterial toxins that inhibit protein synthesis. *Journal of Medical Microbiology* **54**, 1023-30 (2005).

33.   Llorente, A., Lauvrak, S.U., van Deurs, B. & Sandvig, K. Induction of direct endosome to endoplasmic reticulum transport in Chinese hamster ovary (CHO) cells (LdlF) with a temperature-sensitive defect in epsilon-coatomer protein (epsilon-COP). *J Biol Chem* **278**, 35850-5 (2003).

34.   Ward, G.E., Carey, K.L. & Westwood, N.J. Using small molecules to study big questions in cellular microbiology. *Cell. Microbiol.* **4**, 471-482 (2002).

35.   Carey, K.L., Westwood, N.J., Mitchison, T.J. & Ward, G.E. A small-molecule approach to studying invasive mechanisms of Toxoplasma gondii. *Proceedings of the National Academy of Sciences of the United States of America* **101**, 7433-8 (2004).

36. Hung, D.T., Shakhnovich, E.A., Pierson, E. & Mekalanos, J.J. Small-molecule inhibitor of Vibrio cholerae virulence and intestinal colonization. *Science* **310**, 670-4 (2005).

37. Eubanks, L.M. et al. An in vitro and in vivo disconnect uncovered through high-throughput identification of botulinum neurotoxin A antagonists. *Proc Natl Acad Sci U S A* **104**, 2602-7 (2007).

38. Feng, Y. et al. Retrograde transport of cholera toxin from the plasma membrane to the endoplasmic reticulum requires the trans-Golgi network but not the Golgi apparatus in Exo2-treated cells. *EMBO Reports* **5**, 596-601 (2004).

39. Lauvrak, S.U. et al. Shiga toxin regulates its entry in a Syk-dependent manner. *Mol Biol Cell* **17**, 1096-109 (2006).

40. Takenouchi, H. et al. Shiga toxin binding to globotriaosyl ceramide induces intracellular signals that mediate cytoskeleton remodeling in human renal carcinoma-derived cells. *J Cell Sci* **117**, 3911-22 (2004).

41. Ono, K. & Han, J. The p38 signal transduction pathway: activation and function. *Cell Signal* **12**, 1-13 (2000).

42. Zarubin, T. & Han, J. Activation and signaling of the p38 MAP kinase pathway. *Cell Res* **15**, 11-8 (2005).

43. Foster, G.H. & Tesh, V.L. Shiga toxin 1-induced activation of c-Jun NH(2)-terminal kinase and p38 in the human monocytic cell line THP-1: possible involvement in the production of TNF-alpha. *J Leukoc Biol* **71**, 107-14 (2002).

44. Stone, M.K., Kolling, G.L., Lindner, M.H. & Obrig, T.G. p38 mitogen-activated protein kinase mediates lipopolysaccharide and tumor necrosis factor alpha

induction of shiga toxin 2 sensitivity in human umbilical vein endothelial cells. *Infect Immun* **76**, 1115-21 (2008).

45. Smith, W.E. et al. Shiga toxin 1 triggers a ribotoxic stress response leading to p38 and JNK activation and induction of apoptosis in intestinal epithelial cells. *Infect Immun* **71**, 1497-504 (2003).

46. Tashiro, H. et al. Verotoxin induces hemorrhagic lesions in rat small intestine. Temporal alteration of vasoactive substances. *Dig Dis Sci* **39**, 1230-8 (1994).

47. Louise, C.B. & Obrig, T.G. Human renal microvascular endothelial cells as a potential target in the development of the hemolytic uremic syndrome as related to fibrinolysis factor expression, in vitro. *Microvascular Research* **47**, 377-87 (1994).

48. van de Kar, N.C., Monnens, L.A., Karmali, M.A. & van Hinsbergh, V.W. Tumor necrosis factor and interleukin-1 induce expression of the verocytotoxin receptor globotriaosylceramide on human endothelial cells: implications for the pathogenesis of the hemolytic uremic syndrome. *Blood* **80**, 2755-64 (1992).

49. Jacewicz, M.S. et al. Responses of human intestinal microvascular endothelial cells to Shiga toxins 1 and 2 and pathogenesis of hemorrhagic colitis. *Infect Immun* **67**, 1439-44 (1999).

50. Karpman, D., Andreasson, A., Thysell, H., Kaplan, B.S. & Svanborg, C. Cytokines in childhood hemolytic uremic syndrome and thrombotic thrombocytopenic purpura. *Pediatr Nephrol* **9**, 694-9 (1995).

51. Cherla, R.P., Lee, S.Y., Mees, P.L. & Tesh, V.L. Shiga toxin 1-induced cytokine production is mediated by MAP kinase pathways and translation initiation factor eIF4E in the macrophage-like THP-1 cell line. *J Leukoc Biol* **79**, 397-407 (2006).

52. Allen, M. et al. Deficiency of the stress kinase p38alpha results in embryonic lethality: characterization of the kinase dependence of stress responses of enzyme-deficient embryonic stem cells. *J Exp Med* **191**, 859-70 (2000).

53. Mudgett, J.S. et al. Essential role for p38alpha mitogen-activated protein kinase in placental angiogenesis. *Proc Natl Acad Sci U S A* **97**, 10454-9 (2000).

54. Tamura, K. et al. Requirement for p38alpha in erythropoietin expression: a role for stress kinases in erythropoiesis. *Cell* **102**, 221-31 (2000).

55. Dominguez, C., Powers, D.A. & Tamayo, N. p38 MAP kinase inhibitors: many are made, but few are chosen. *Curr Opin Drug Discov Devel* **8**, 421-30 (2005).

56. Somwar, R. et al. A dominant-negative p38 MAPK mutant and novel selective inhibitors of p38 MAPK reduce insulin-stimulated glucose uptake in 3T3-L1 adipocytes without affecting GLUT4 translocation. *J Biol Chem* **277**, 50386-95 (2002).

57. Henry, J.R. et al. Potent inhibitors of the MAP kinase p38. *Bioorg Med Chem Lett* **8**, 3335-40 (1998).

58. Gaestel, M., Kotlyarov, A. & Kracht, M. Targeting innate immunity protein kinase signalling in inflammation. *Nat Rev Drug Discov* **8**, 480-99 (2009).

59. Kotlyarov, A. et al. MAPKAP kinase 2 is essential for LPS-induced TNF-alpha biosynthesis. *Nat Cell Biol* **1**, 94-7 (1999).

60.   Gaestel, M. MAPKAP kinases - MKs - two's company, three's a crowd. *Nat Rev Mol Cell Biol* **7**, 120-30 (2006).

61.   Siegler, R.L., Pysher, T.J., Lou, R., Tesh, V.L. & Taylor, F.B., Jr. Response to Shiga toxin-1, with and without lipopolysaccharide, in a primate model of hemolytic uremic syndrome. *Am J Nephrol* **21**, 420-5 (2001).

62.   Palermo, M. et al. Pretreatment of mice with lipopolysaccharide (LPS) or IL-1beta exerts dose-dependent opposite effects on Shiga toxin-2 lethality. *Clin Exp Immunol* **119**, 77-83 (2000).

63.   Barrett, T.J., Potter, M.E. & Wachsmuth, I.K. Bacterial endotoxin both enhances and inhibits the toxicity of Shiga-like toxin II in rabbits and mice. *Infect Immun* **57**, 3434-7 (1989).

64.   Sauter, K.A. et al. Mouse model of hemolytic-uremic syndrome caused by endotoxin-free Shiga toxin 2 (Stx2) and protection from lethal outcome by anti-Stx2 antibody. *Infect Immun* **76**, 4469-78 (2008).

CHAPTER II

Identification and characterization of small molecules

that inhibit intracellular toxin transport

OVERVIEW

The intracellular transport pathway utilized by Shiga toxin (STx) was first discovered in 1992, and this unique retrograde trafficking mechanism has since been validated in other toxins, including cholera toxin and ricin. The ability of these protein toxins to string together existing host transport mechanisms and direct their transport to intracellular targets makes them ideal probes for studying host retrograde transport in its entirety. Standard genetic approaches, including overexpression of dominant negative mutants or knock-down of candidate genes by siRNA, have been undertaken to identify components essential to these pathways. Most of these studies have produced inconsistent effects on toxin transport, underscoring the complexity of these pathways and the need for novel approaches to systematically investigate dynamic endocytic and trafficking mechanisms. To this end, our lab has turned to small molecules as a means of reversibly manipulating STx trafficking. Using a luciferase-based assay for determining susceptibility to STx, we screened a library of over 14,000 small molecule compounds of unknown function in order to identify inhibitors of Shiga toxicity. Further characterization of inhibitors identified from the screen led to the discovery of two compounds, 75 and 134, that reversibly blocked STx transport at distinct stages in the STx trafficking pathway. Though the targets of these small compounds have yet to be identified, this study validated the small molecule approach to toxin inhibition and provided a preliminary framework for identifying potential therapeutics in the treatment

of toxin-mediated diseases. The work describing these studies is presented in this chapter and published in *Infection and Immunity*[†].

SUMMARY

Shiga toxin (STx), cholera toxin (CTx), and the plant toxin ricin are among several toxins that reach their intracellular destination via a complex route. Following endocytosis, these toxins travel in a retrograde direction through the endosomal system to the trans-Golgi network (TGN), Golgi, and endoplasmic reticulum (ER). There, the toxins are transported across the ER membrane to the cytosol where they carry out their toxic effects. Transport via the ER from the cell surface to the cytosol is apparently unique to pathogenic toxins, raising the possibility that various stages in the transport pathway can be therapeutically targeted. We have applied a luciferase-based high-throughput screen to a chemical library of small molecule compounds in order to identify inhibitors of STx. We report two novel compounds that protect against STx and ricin inhibition of protein synthesis and demonstrate that these compounds reversibly inhibit bacterial transport at various stages in the endocytic pathway. One compound (compound 75) inhibited transport at an early stage of STx and CTx transport and also provided protection against diphtheria toxin, which enters the cytosol from early endosomes. In contrast, compound 134 inhibited transport from recycling endosomes through the Golgi and only protected against toxins that access the ER. Small molecule compounds such as these will provide insight into the mechanism of toxin transport and

---

[†] **Saenz, J.B., Doggett, T.A., and Haslam, D.B.** 2007. Identification and characterization of small molecules that inhibit intracellular toxin transport. *Infect. Immun.* **75**: 4552-4561.

lead to the identification of compounds with therapeutic potential against toxins routed through the ER.

INTRODUCTION

Bacterial and plant toxins are significant agents of human disease and potential vehicles for bioterrorism. Though diverse in their intracellular targets, a common and essential step in their virulence is the ability to reach the cytosol, where most toxins exert their enzymatic effects. The bacterial exotoxins Shiga toxin (STx) and cholera toxin (CTx), as well as the plant toxin ricin, have drawn particular interest for their unique retrograde transport following endocytosis. Members of the AB toxin group, these toxins consist of a receptor-binding B subunit and an enzymatic A subunit. In contrast to anthrax and diphtheria toxins, AB toxins that enter the cytosol directly from early endosomes in a pH-dependent manner[1], these membrane-bound toxins bypass the late endocytic pathway by retrograde transport from early or sorting endosomes to the *trans*-Golgi network (TGN) [2,3]. From the TGN, they traffick through the Golgi to the endoplasmic reticulum (ER), where they are subsequently translocated through the Sec61p channel into the cytosol via ER quality control mechanisms [4-6]. It is believed that this complex retrograde transport may allow for certain essential steps in toxin activation and transfer; STx has been shown to be cleaved and activated by host proteases [7]. Similarly, the ability to reach the ER may enable a chaperone-facilitated transfer to the cytosol, as previously reported for CTx, ricin, and STx [4,6,8,9].

The existence of a retrograde transport pathway was first uncovered by electron microscopic studies tracking the intracellular transport of STx [10]. Since that time, several

toxins, in addition to CTx and ricin, have likewise been found to transit through the ER en route to the cytoplasm. Given the importance of these pathways to intoxication by diverse pathogenic agents, a number of investigations have been directed at identifying host molecules involved in toxin transport. Previous studies aimed at identifying essential components of the retrograde pathways of STx, ricin, and CTx have largely focused on the Rab family of small GTP-binding proteins. Members of the Rab family cycle between their GTP and GDP-bound forms, related to their functions as regulators of vesicular traffic [11]. Standard genetic approaches involving overexpression of dominant negative mutants or siRNA knock-downs of various Rabs have revealed the complexity of toxin trafficking pathways. Inhibition of Rab7 and Rab9, which are involved in lysosome targeting pathways, had no effect on ricin and STx trafficking [12,13]. In contrast, inhibition of Rab6a', involved in endosome-to-TGN transport, inhibited STx transport from endosomes through the Golgi [14-16] but had no effect on ricin transport or intoxication [17]. Similarly, overexpression of a dominant-negative Rab11, implicated in recycling endosome-to-TGN transport, resulted in impaired STx transport but had no effect on ricin [3,12]. Rab22, like Rab6a', has been implicated in endosome-to-TGN transport, though inhibition of Rab22 function has had inconsistent results on retrograde toxin transport [18]. Though these pathways still remain poorly characterized, the sequential retrograde progression utilized by these toxins has translated into a unique system for probing host endocytic mechanisms.

In an effort to dissect and inhibit the stepwise trafficking of STx, we have developed a quantitative and highly sensitive, high-throughput luciferase-based assay to screen a library of small molecule compounds for their ability to block Stx-mediated

inhibition of protein synthesis [19]. Because STx transport involves a multi-step progression through the cell, we predicted that inhibitory compounds could be identified at distinct stages along the retrograde trafficking pathway and could potentially be directed at specific molecular targets. From an initial screen of 14,400 small compounds, we identified several potential inhibitors. Among these, we characterized two compounds (compounds 75 and 134) that reversibly inhibit Shiga intoxication and act at distinct steps along the toxin trafficking pathway. Our results demonstrate the utility of a small molecule approach to elucidating toxin transport pathways and will lead to the identification of novel therapeutic approaches targeting diseases caused by ER-routed toxins.

RESULTS

High-throughput screen for compounds that inhibit STx activity in host cells.

Several toxins damage host cells by inhibiting protein synthesis. Diphtheria toxin (DT) and *Pseudomonas* exotoxin (PE) inhibit protein synthesis through the ADP-ribosylation of elongation factor 2 [20,21], whereas STx and the plant toxin ricin inhibit ribosome function by cleaving an adenine residue from the 60S ribosome [22-26]. Still other toxins, such as CTx and anthrax edema toxin, induce increases in second messenger levels, resulting in cytotoxicity [27-29]. In order to quantify the effects of various protein synthesis-inhibiting toxins on host cells, we had previously established a luciferase-based assay that could readily determine the susceptibility of various cell lines to Stx, ricin, DT, and PE[30]. In cells constitutively expressing an mRNA encoding destabilized

firefly luciferase, luciferase enzyme activity served as a surrogate measure of protein synthesis.

This assay was adapted to a high-throughout screen (HTS) and applied to a screen of small molecule compounds that inhibit toxin susceptibility. The ICCB facility at Harvard University contains a number of commercial libraries consisting of synthetic and natural products. An initial screen of biological compounds with known effects yielded positive hits such as brefeldin A (BFA) and D,L-*threo*-1-phenyl-2- decanoylamino-3-morpholino-1-propanol (PDMP; data not shown), two compounds previously shown to inhibit STx susceptibility through distinct mechanisms [31,32] and serving as positive controls for the detection of STx-inhibitory compounds. In addition, the assay detected known inhibitors of the proteasome, such as MG-132. This was an expected result, as the discriminatory power of the assay is dependent on rapid degradation of luciferase following translation[30].

We next screened the ChemDiv 3 library at the ICCB facility, consisting of 14,400 compounds of unknown function. The compounds included in this library were selected for their structural diversity, chemical stability, and "drug-like properties." As these compounds were commercially available and their functions currently undefined, we reasoned that novel inhibitors could be identified. Among these were selected the top 1% of compounds yielding the highest luciferase signal in the presence of toxin, all of which resulted in a signal at least twice baseline. As the initial screen lacked a counterscreen to exclude compounds affecting luciferase turnover, each compound was subsequently tested for its effect on luciferase signal following cycloheximide treatment. Cycloheximide-mediated inhibition of protein synthesis is independent of intracellular

transport, and its mechanism of ribosomal inactivation is distinct from that of STx [33].

Therefore, compounds that provided protection against cycloheximide-mediated

inhibition of luciferase signal must be acting in a toxin-independent manner (e.g., by

inhibiting luciferase degradation), and these were excluded from further analysis. After

excluding compounds that affected cycloheximide-induced suppression of luciferase

signal, eight compounds with toxin-specific effects were selected for further analysis.

Notably, subsequent screens have incorporated a cycloheximide counterscreen in order to

exclude compounds with toxin-independent effects prior to secondary analysis (Figure 1).

Figure 1. A sample plate from the high-throughput screen. Vero cells were transduced with pAD-Luc, seeded in 384-well plates, and incubated for 1 h with various known biological compounds, followed by treatment with Shiga toxin (STx; 1 ng/ml) or cycloheximide (CHX; 2 mg/ml) for 5 h. SuperLight Reagent was added, and relative light output (RLU) was determined. Replicates (up/down arrowheads) of STx- or CHX-treated samples are presented by sample number, and the insets demonstrate Z' and Z factors calculated for each replicate plate. Since each plate contains 16 negative controls (wells treated with STx or CHX but lacking compound) and 16 positive controls (wells treated with neither toxin, CHX, nor compound), the Z'- and Z-factors can be calculated for each plate. The Z'-factor (a measure of the ability of an assay to distinguish positive controls from negative controls) ranged from 0.61 to 0.74. The Z-scores (the ability of an assay to distinguish true hits from negative controls) ranged from 0.46 to 0.62 for the known biologicals, and, as expected, varied depending on the composition of the library. An assay having Z'- and Z-scores greater than 0.5 is considered excellent for HTS purposes [34]. In contrast to proteasomal inhibitors MG-132 and 3,4-dichloroisocoumarin, which were positive on STx- and CHX-treated replicates, some compounds scored as positives on the STx-treated plates and were negative on the CHX-treated plates (circles), including brefeldin A (BFA), a known inhibitor of STx intracellular transport.
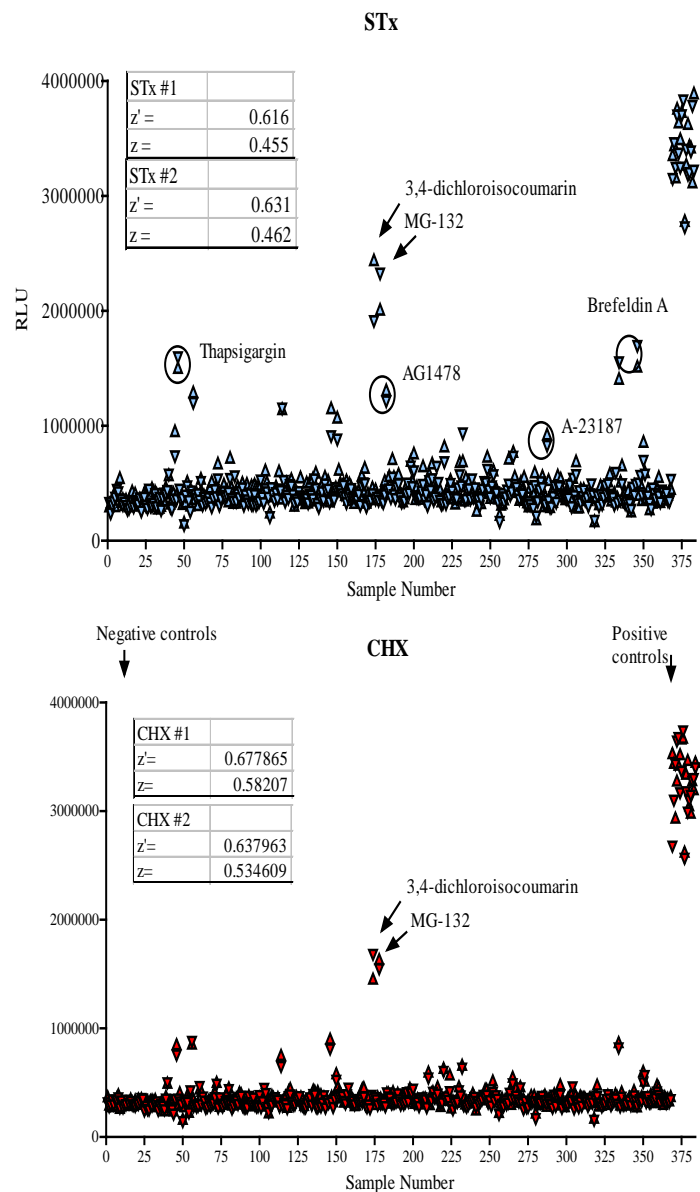
Secondary analysis to determine potency and efficacy of inhibitory compounds

The optimal protective concentration for each identified hit was determined using a radioactive assay for protein synthesis [35] that was modified for medium-throughput analysis in a multi-well format (see Methods). As some of these compounds could exhibit non-specific effects at increased concentrations, the lowest concentration providing significant protection against STx compared to untreated Vero cells was considered to be optimal. Compounds classified as inhibitors showed half-maximal

activity between 10 to 50 µM (data not shown). Compounds were used above their half-maximal concentrations but below their maximal concentrations for all subsequent assays (25 µM for compound 75 and 50 µM for compound 134).
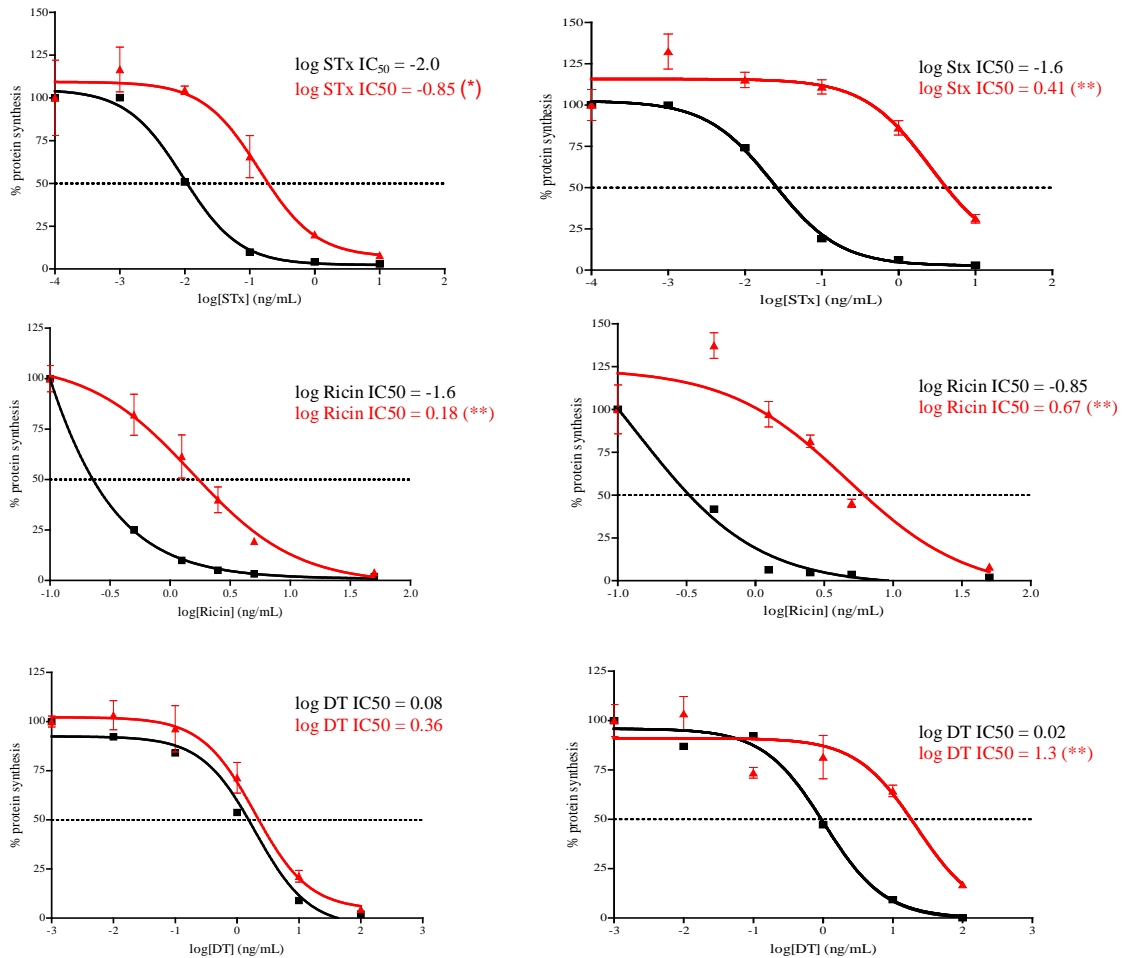
Figure 2. Protective effects of inhibitory compounds against STx, ricin, and DT. (A, B) Protein synthesis levels for control (black line, no compound) and compound-treated (red line) Vero cells were determined using the radioactive amino acid incorporation assay (see Methods). Percent protein synthesis is expressed as the amount of radioactive amino acid incorporation in control or compound-treated cells at a given toxin concentration as a percentage of radioactive amino acid incorporation in cells lacking toxin treatment. Toxin-response curves, toxin IC_{50} values, and statistical comparisons between control and compound-treated cells were calculated (see Methods). Data points (mean ±SD) represent triplicate data at the indicated toxin concentration from one representative experiment. **(A)** Compound 134 (50 µM; left panels) protects against STx- and ricin-mediated decreases in protein synthesis. Toxin IC_{50} values for STx and ricin in compound-treated cells were found to be statistically different (*, $p<0.05$) from control cells. **(B)** Compound 75 (25 µM; right panels) protects against STx-, ricin-, and DT-mediated decreases in protein synthesis. Toxin IC_{50} values for all three toxins in compound-treated cells were found to be highly statistically different (**, $p<0.01$) from those in control cells.

The ability of these compounds to protect against increasing STx concentrations was expressed as toxin IC_{50}, the concentration of toxin needed to reduce protein synthesis by 50% (see Methods). Using these criteria, compounds 75 and 134, at their respective optimal concentrations, exhibited the greatest protective effects among the hits identified from the initial screen. Both compounds showed statistically significant increases in STx IC_{50} compared to cells containing no compound (Figure 2).

At higher concentrations, these compounds exhibited up to 1,000-fold increases in Stx IC_{50} (not shown). Neither of these compounds affected luciferase degradation in the presence of cycloheximide (not shown). An initial characterization of compounds showing highly protective effects against STx led us to consider whether these compounds could protect against other toxins that inhibit protein synthesis. Both compounds 75 and 134 similarly showed statistically significant increases in ricin IC_{50} (Figure 2; $p<0.01$). Protection against both STx and ricin was also greater than previously observed protective effects using an overexpressed dominant negative mutant of Rab6, a small GTP-binding protein found to be essential to STx transport through the Golgi [17].

Interestingly, compound 134 failed to show a statistically significant effect against DT-mediated protein synthesis inhibition (Figure 2A), while compound 75 demonstrated greater protection (Figure 2B). Vero cells lacking compound treatment demonstrated a similar susceptibility profile to DT as to STx and ricin. STx and ricin, following endocytosis, are known to traffick from an endosomal compartment to the ER via the Golgi [36]. DT, however, directly accesses the cytosol from early endosomes, as the low endosomal pH is believed to allow for a conformational change in the holotoxin and

promote shuttling of the A moiety across the endosomal membrane [20]. The lack of

protection against DT suggests that compound 134 affects toxin transport at a post early-

endosome stage but has no effect on trafficking from plasma membrane to the early

endosomal compartment. In contrast, the protective effect of compound 75 against all

three toxins suggests that this compound affects transport mechanisms common to all

three pathways, presumably at an earlier stage in endocytosis than the site of action of

compound 134.

Effects of compounds 75 and 134 on toxin transport

In order to determine the site at which inhibitory compounds were affecting toxin activity, the endocytosis and transport of fluorescent STx and CTx B-subunits (STxB and CTxB, respectively) were examined. The retrograde transport of protein toxins is believed to occur exclusively from early and/or recycling endosomes [37]. In order to determine whether endocytosis and trafficking of STxB to early and recycling endosomes were affected by compound 134, STxB transport was compared to fluorescently-labeled transferrin (Tf), which is known to accumulate in recycling endosomes at 22°C due to a block in recycling endosome-to-TGN transport at this temperature [15].
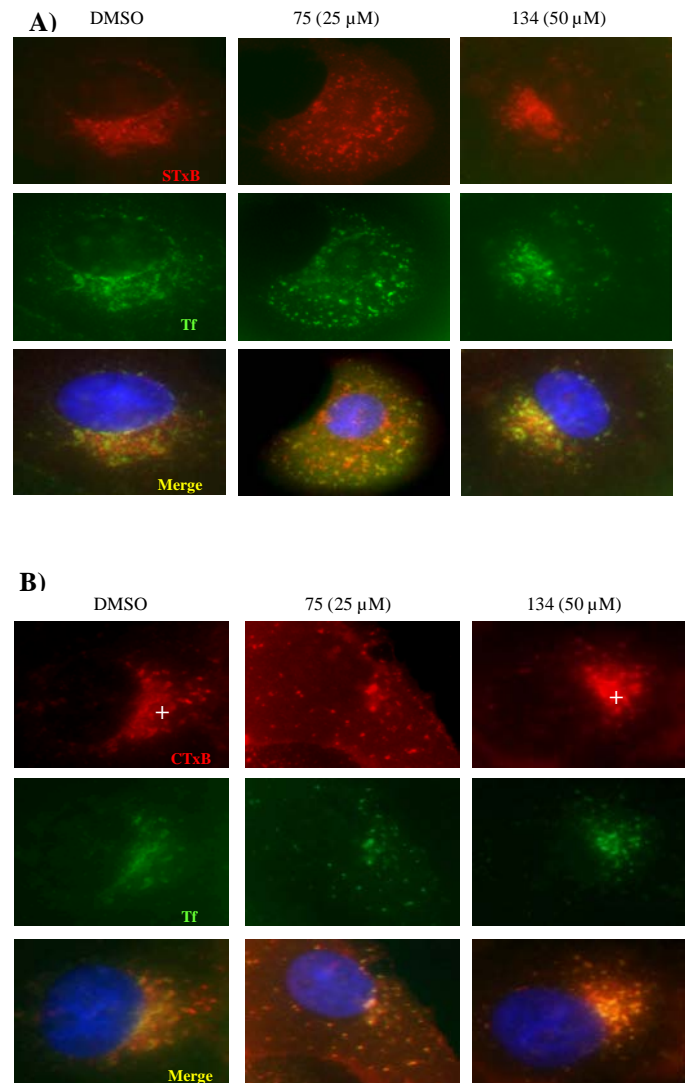
Figure 3. Compound 75 impedes STxB/CTxB and transferrin ligand trafficking to recycling endosomes. **(A)** Vero cells were incubated with AlexaFluor 594-labeled STxB (1 µg/ml) and 488-labeled Tf (1 µg/ml) for 1 h at 4°C in serum-free medium, then shifted to 22°C for an additional hour and developed for immunofluorescence, as described in Methods. In control (0.5% v/v DMSO) and compound 134-treated cells, STxB reaches a perinuclear, Tf-positive compartment previously described as recycling endosomes (cross). In compound 75-treated cells, however, no perinuclear staining was observed, and Tf and STxB were confined to early endosomes (punctate staining). **(B)** Neither CTxB nor Tf reaches the perinuclear Tf-positive recycling endosome compartment in 75-treated Vero cells compared to control and 134-treated cells. Results are representative of two similar experiments. Images were obtained at 1000X magnification. Tf, transferrin; blue, nuclei.

Consistent with previous reports, STxB colocalized with Tf-positive compartments in control cells at 22°C (Figure 3A). STxB trafficking to Tf-positive compartments in 134-treated cells was not significantly different than in control cells, showing a similar level of colocalization with the perinuclear recycling endosome compartment (Figure 3A, cross). Similar results were seen with CTxB, which also accumulated in a Tf-positive perinuclear compartment.

(Figure 3B, cross). In addition, compound 134 did not affect binding of CtxB or STxB to the cell surface (Figure 4), suggesting that this compound was not occupying toxin receptor binding sites or significantly decreasing receptor expression. Taken together with the relative lack of protection of compound 134 against DT-mediated protein synthesis inhibition (Figure 2A), these results collectively suggest that
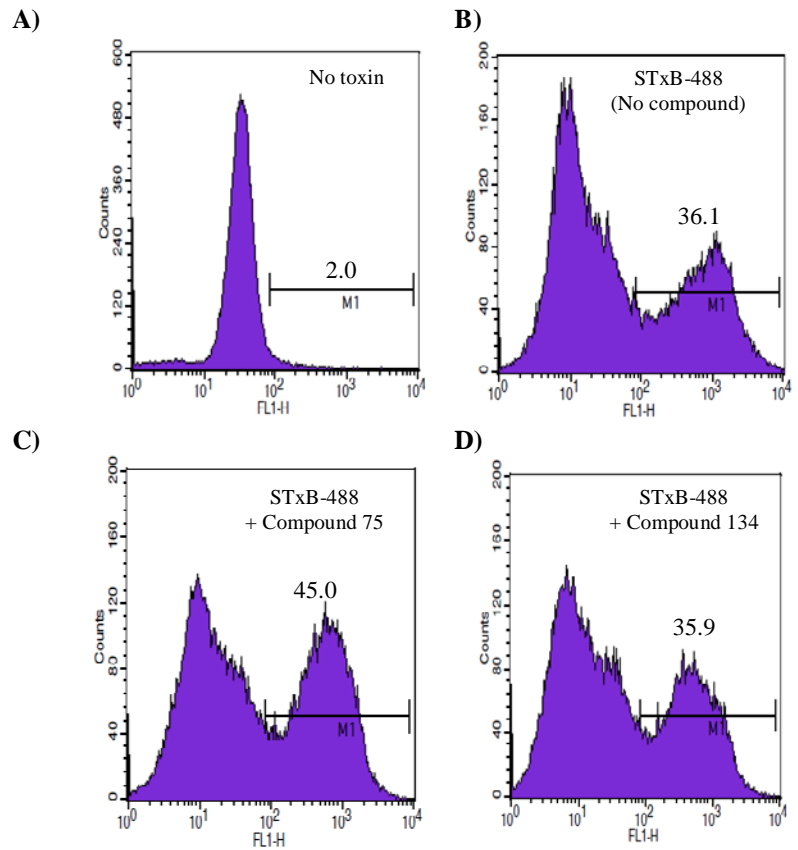
Figure 4. Compound treatment does not downregulate Gb3 receptor expression. **(A-D)** Vero cells were grown to confluency and shifted to 4°C for 15 min. STxB-488 was added at 1µg/mL, and cells were kept at 4°C for an additional 45 min to allow for STxB binding to Gb3 receptors. Cells were washed 5 times with cold PBS prior to scraping the cells into 750 µL of cold PBS. STxB-positive cells were sorted by FACS (M1 gate), and the proportion of STxB-positive cells relative to the total number of cells (% total) was determined by CellQuest 9 (Becton-Dickinson). For compound-treated cells, compound was added at the indicated concentrations at 37°C for 30 min prior to the binding of STxB at 4°C. Neither compound 75 **(C)** nor 134 **(D)** decreased the proportion of STxB-positive cells compared to DMSO-treated cells **(B)** at the indicated concentrations. **(A)** represents untreated Vero cells lacking STxB.

compound 134 maintains STx and CTx transport to recycling endosomes.

Compound 75, like compound 134, did not inhibit STxB binding to its receptor or decrease receptor expression (Figure 4). However, treatment with compound 75 appeared to inhibit transport of both STxB/CTxB and Tf to perinuclear recycling endosomes. Most of the toxin and Tf were located in peripheral vesicular structures (Figure 3), likely early endosomes. These results, in addition to those demonstrating effects of compound 75 on DT susceptibility, collectively suggest that this compound inhibits STx and CTx transport to recycling endosomes.

Immunohistochemical analysis of compound-treated cells revealed morphological changes to the Golgi (not shown). The dispersal of the Golgi apparatus is a morphological effect that has been observed under several conditions that impair retrograde and intra-Golgi transport [38]. To exclude the possibility that the effects of these compounds were non-specific to intracellular toxin transport, we sought to rule out processes that are known to have effects on Golgi morphology. In particular, during the process of apoptosis, the Golgi becomes fragmented [39]. In order to rule out that compounds 75 and 134 were inducing Golgi fragmentation through apoptosis, ATP levels in compound-treated cells were compared to those in untreated cells or cells treated with staurosporine, a known apoptosis-inducing agent[40]. Treatment with compounds 75 and 134 failed to deplete ATP levels over 24 hours as was observed following staurosporine

A)

B)

| 134 (50 µM) | Staurosporine (20 µM) | Anisomycin (5 µg/mL) | BFA (25 µg/mL) | Nocodazole (10 µg/mL) |
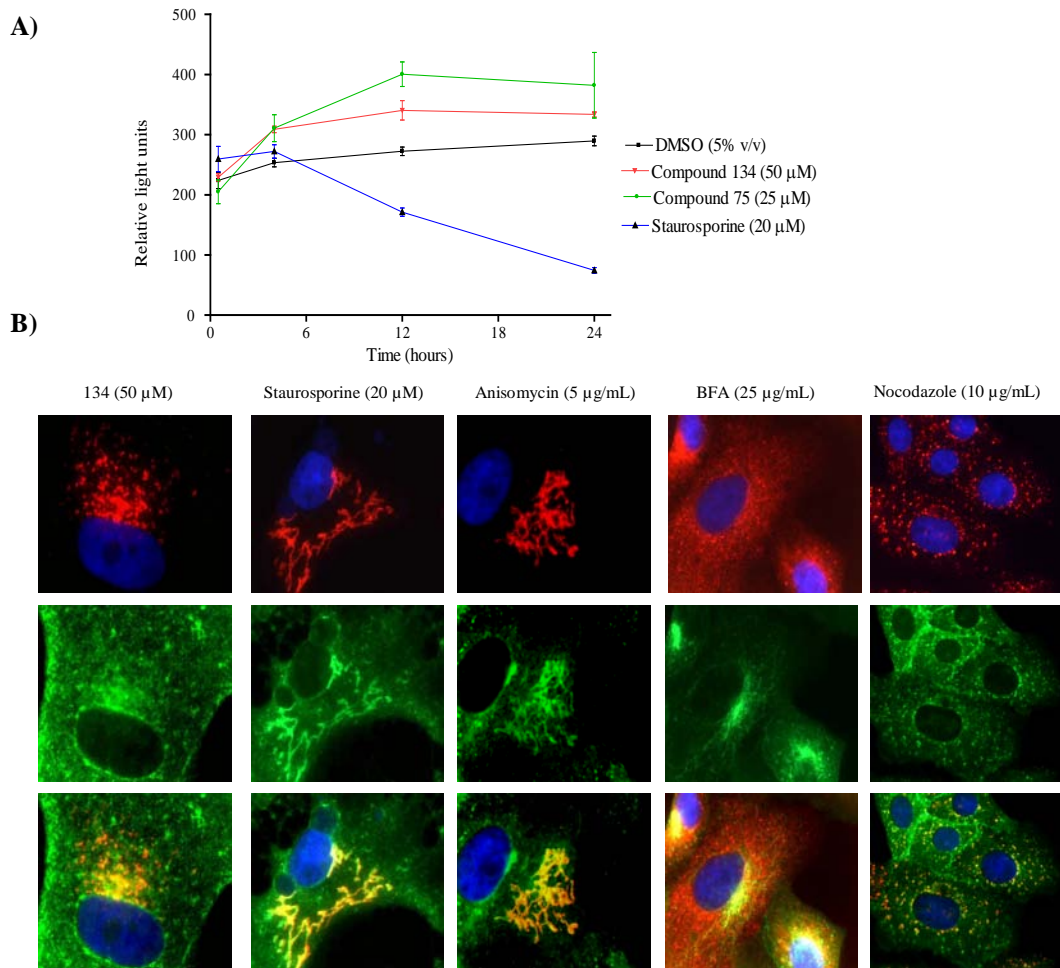
Figure 5. Biochemical and morphologic effects of compound treatment are distinct from those produced by apoptosis-inducing or Golgi-disturbing agents. **(A)** Compound treatment does not deplete ATP levels. Vero cells were incubated with compounds 75, 134, staurosporine, or DMSO for up to 24 h at 37°C at the indicated concentrations. ATP levels were determined by the CellTiter-Glo Luminescent Cell Viability Assay (see Methods). Luminescence (relative light units) is linearly related to ATP levels in viable cells. Results (mean ±SD) are triplicate data for each time point from one representative experiment. **(B)** Compound 134 produces changes in Golgi morphology distinct from those generated by known apoptosis-inducing (staurosporine, anisomycin) or Golgi-disturbing agents (nocodazole, brefeldin A). Vero cells were treated for 1 h with the specified compounds at the indicated concentrations prior to incubation with 1 µg/mL Alexa Fluor 488-labelled CTxB at 4°C for 1 h. Toxin was internalized for 1 h at 37°C. Cells were fixed, permeabilized, and stained with an antibody against the Golgi marker giantin. Compound 75 produced a similar dispersal of the Golgi as seen with compound 134 (not shown). BFA, brefeldin A; blue, nuclei. Images were obtained at 1000X magnification.

treatment, suggesting that the compounds were not cytotoxic or apoptosis-inducing at the

specified concentrations over the time course studied (Figure 5A). In addition,

compound-treated cells consistently showed a more punctate and swollen Golgi

compared to the more tubulated Golgi in staurosporine-treated cells (Figure 5B). The

Golgi morphology of compound-treated cells also differed from the characteristic Golgi

architecture of cells treated with anisomycin, a peptidyl transferase inhibitor shown to

induce apoptosis in HeLa cells [41]. Other small molecule compounds known to affect

Golgi morphology include nocodazole [38], a microtubule-disrupting agent, and brefeldin

A, a known trafficking inhibitor that causes complete dispersal of the Golgi [42]. The

morphological effects on the Golgi for compounds 75 and 134 were distinct from each of

these (Figure 5B). As a result, effects on the Golgi, induced by these compounds as early

as 30 minutes following compound treatment (not shown), were consistently distinct

from the characteristic morphological and biochemical changes observed with known

apoptosis-inducing and Golgi-disturbing agents.

As another means of determining and quantifying the effect of compounds 75 and

134 on toxin transport from early endosomes to the TGN, sulfation of a STxB construct

bearing a tandem of C-terminal sulfation sites (STxB-Sulf$_2$) was evaluated. Sulfation of

endogenous proteins occurs in the TGN, and sulfation of internalized STxB-Sulf$_2$ has

shown that it trafficks through this compartment [43]. Trafficking of fluorescently-labeled

STxB-Sulf$_2$ (Figure 6A, green) showed similar Golgi localization as native STxB-594 in

untreated cells (Figure 6A, red) and thus could serve as a suitable assay for toxin

trafficking through the TGN. Consistent with its effect at an early stage in toxin

trafficking, compound 75 inhibited STxB sulfation to 47 % of compound-negative

samples (Figure 6B). By contrast, compound 134 modestly reduced sulfation (72% of

control) over the 3-hour incubation. Sulfation of endogenous proteins, as assessed by

total [^{35}S] incorporation, was unaffected by compound treatment, implying that the

compounds were not inhibiting sulfotransferase enzymatic activity (not shown).

Together with previous results, these results are consistent with compound 75 inhibiting transport at an early stage in endocytosis and compound 134 blocking transport at a post-recycling endosome stage (including recycling endosome-to-TGN transport).

Figure 6. Compounds 75 and 134 affect trafficking of STxB through the *trans*-Golgi network (TGN). (A) A STxB construct containing a tandem of sulfation sites and a histidine tag for purification (see Methods) was used to track STxB transport through the TGN in Vero cells. (B) The degree of sulfation of the STxB-Sulf2 construct was determined as described in Methods. % signal indicates the band density relative to the band signal in DMSO-treated cells from one representative experiment. Results are representative of two similar experiments. Compound 75 was used at 25 μM and 134 at 50 μM.

Compounds 75 and 134 reversibly target toxin retrograde transport.

Small molecule compounds may act by reversible or irreversible mechanisms. In general, irreversible inhibitors act by covalent interaction with or modification of target molecules, such as through oxidation or acylation. Reversible compounds often act as competitive inhibitors of enzymatic activity or of protein-target interactions. Morphological effects on the Golgi produced by compound 75 and 134 treatment were found to be reversible. Following washout of the compounds, the Golgi reassembled in compound-treated cells at a time point at which BFA-treated cells

maintained an altered Golgi morphology (Figure 7A). More importantly, Vero cells lost

protection against STx following washout of either compound (Figure 7B).
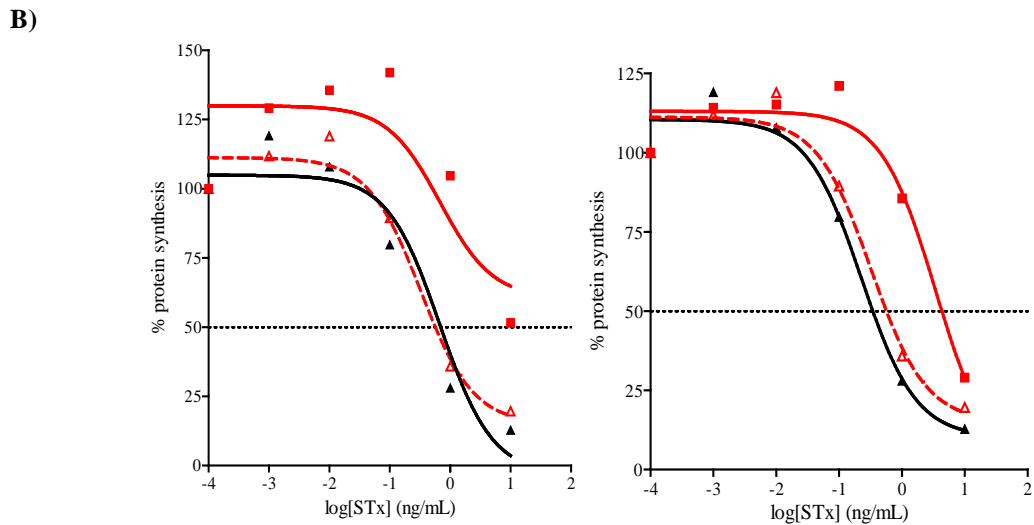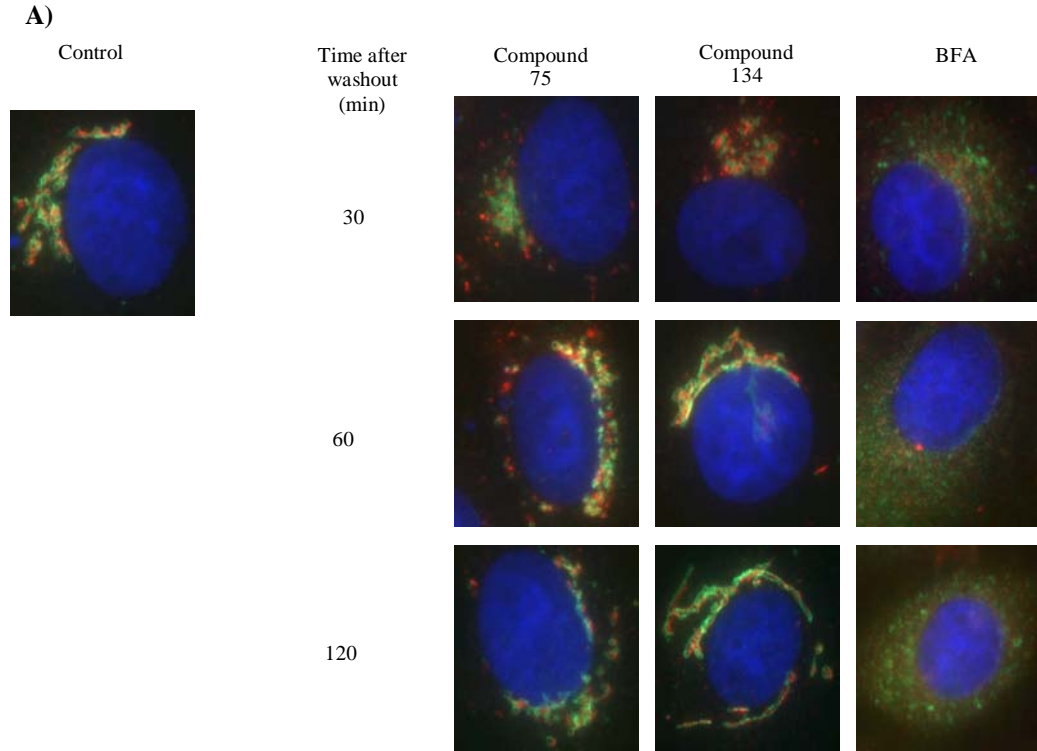
Figure 7. Effects of compounds on Golgi structure are reversible. (A) Vero cells were treated with compounds 75 (25 µM), 134 (50 µM), or BFA (25 µg/mL) for 1 h at 37ºC, followed by washing with prewarmed media and an additional incubation at 37ºC in media alone for the indicated times. Cells were fixed, permeabilized, and stained with anti-giantin (green) and anti-TGN46 (red) antibodies. Control indicates cells treated with DMSO (0.5% v/v) and fixed 2 h after washing as with compound-treated cells. **(B)** Vero cells were pretreated with compounds 75 (left) and 134 (right) for 1 h at 37ºC at the concentrations used in (A), followed by washing with prewarmed media and an additional incubation at 37ºC in media alone for 2 h. Cells were then treated with STx for 4 h and assessed for levels of protein synthesis using the radioactive amino acid incorporation assay, as described in Methods. Black line, untreated; red line, compound treatment with no washout; red dotted line, compound treatment with washout. BFA, brefeldin A.

Effects of compounds on anterograde transport

The toxin trafficking pathway, from early endosomes to the ER via the Golgi, is almost the mirror inverse of the biosynthetic and secretory pathways. The degree of overlap between the retrograde and anterograde pathways, however, remains largely unresolved. Since no host molecules have been shown to traffic from endosomes all the way to the ER, the ability to track bacterial toxins and identify compounds that potentially block their transport allows us to specifically probe the retrograde pathway in its entirety.

To study the effects of these compounds on general anterograde transport, the sequential trafficking of a temperature-sensitive VSVG-GFP (*ts*O45) fusion protein [44] in transiently transfected Vero cells was examined. In cells incubated at 42°C, the VSVG-GFP protein was seen to be retained within the ER. An hour following a shift to 32°C, the VSVG-GFP protein had made an anterograde progression to the Golgi (Figure 8A). Compounds 75 and 134 also maintained VSVG-GFP transport from the ER to the Golgi, as evidenced by colocalization of VSVG-GFP with TGN46 as early as 1 h following the shift to 32°C (Figure 8A, yellow). BFA has been shown to impede ER to Golgi transport [42], and cells treated with BFA showed a dispersed Golgi with VSVG-GFP restricted to the ER over the time course studied. We conclude that both compounds 75 and 134 preserve ER-to-Golgi transport of VSVG-GFP, suggesting that generalized anterograde transport mechanisms from the ER to the Golgi remain unaffected.

49

To examine the effects of compounds 75 and 134 on the secretory pathway beyond the Golgi, the secretion of a GFP construct bearing an amino-terminal neuropeptide Y secretion signal (NPY-GFP) was assessed by ELISA. In contrast to BFA and compound 75, compound 134 had a minimal effect on NPY-GFP secretion (Figure 8B, 86% and 89% GFP secretion compared to untreated cells at 1 and 2h, respectively). Compound 75 decreased GFP secretion to a similar extent as BFA, a known inhibitor of anterograde transport. It

Figure 8. Effects of compound treatment on anterograde transport. (A) Both compounds 75 and 134 maintain ER-to-Golgi transport. Anterograde transport of VSVG-GFP (green) was assessed by immunofluorescence in Vero cells transiently transfected with pCDM8.1 expressing VSVG-GFP *ts*045, as described in Methods. Following fixation at indicated times, cells were permeabilized and labeled with anti-TGN46 (red). **(B)** Compound 75 and BFA decrease post-Golgi secretion of NPY-GFP. NPY-GFP secretion at 1 and 2 h following CHX treatment was assessed by ELISA of cell supernatants. Mean absorbance values for control wells containing DMEM alone were subtracted from sample wells. Results (mean ±SD) are pooled data from one representative experiment. BFA, brefeldin A; OD, optical density.

should be noted that NPY-GFP secretion was only reduced by approximately 50% after 1

50

h of BFA. This likely represents the pool of protein that had already reached the Golgi prior to BFA or compound 75 treatment. We conclude that, when compared to its effects on retrograde transport of toxin, compound 134 exhibits a less pronounced and less significant effect on the anterograde secretory pathway.

DISCUSSION

A luciferase-based assay for determining cell susceptibility to STx-mediated inhibition of protein synthesis was adapted to HTS and used to screen a chemical library of small compounds. Compounds 75 and 134 showed marked potency and selectivity against intracellular toxin transport. Both compounds demonstrated strong protective effects against STx and ricin, and compound 75 was shown to equally protect against DT. We thus report two novel compounds demonstrating efficacy against multiple bacterial toxins, with toxin IC_{50} values nearly an order of magnitude greater than previously reported values using knock-down approaches for toxin inhibition [17,45].

Screens at the ICCB have recently identified small molecule inhibitors of *Toxoplasma* invasion and *Vibrio cholera* virulence. From a library of 12,160 compounds, 24 inhibitors of *Toxoplasma gondii* invasion were identified [46]. These included compounds that inhibited host uptake of the organism as well as inhibitors of *Toxoplasma* gliding motility and microneme-based secretion. Effective doses of these compounds ranged from 3 to 100 µM. Recently, a similar screen identified a small molecule inhibitor of *Vibrio cholera* virulence [47]. 50,000 compounds were screened, from which 109 compounds that inhibited virulence factor expression were identified. Of these, a compound named virastatin inhibited the transcriptional regulator ToxT, thereby

suppressing the expression of cholera toxin and the toxin co-regulated pilus. The minimal inhibitory concentration of virastatin against CTx expression ranged from 3 to 40 µM, depending on the bacterial strain. As a result, recent screens underscore the utility of small molecule assays in the identification of compounds that inhibit microbial virulence or block intracellular trafficking pathways.

The ability of compound 134 to specifically protect against STx and ricin but not DT suggested that it targeted a step common to the transport of STx and ricin but distinct from the DT transport pathway. Since DT is known to access the cytosol directly from an endosomal compartment [20], compound 134 was presumed to act on a site downstream of the early endosome. However, compound 134 had little to no effect on toxin colocalization with a perinuclear, Tf-positive compartment previously reported as recycling endosomes [48], implying that toxin transport to early/ recycling endosomes was unaffected. If we consider that toxin transport to the Golgi was delayed compared to control cells and that the sulfation of STxB-Sulf$_2$ was modestly reduced, it seems likely that compound 134 inhibits toxin transport at a post-recycling endosome stage (including recycling endosome-to-TGN transport). Compound 75, on the other hand, consistently impeded toxin localization to the recycling endosome and exhibited a more pronounced effect on transport through the TGN, as evidenced by the decreased sulfation of STxB-Sulf$_2$. We thus conclude that compounds 75 and 134 are conferring toxin-protective effects by disrupting transport at distinct steps along the toxin trafficking pathway.

Both compounds produced a fragmented Golgi phenotype and delayed, but did not inhibit, toxin transport to this disrupted compartment. Toxin transport to the ER, though significantly reduced compared to control cells, was apparent by

immunofluorescence (not shown), suggesting that toxin transport through the Golgi was not completely blocked. Consistent with these findings, these compounds, at the inhibitory concentrations used, did not completely protect susceptible cells against toxin-mediated decreases in protein synthesis, as has been observed following BFA treatment [49]. The strong protective effect of BFA, however, comes at the expense of a collapsed Golgi structure and disrupted anterograde transport [38]. Morphological analysis of compound-treated cells revealed dispersed Golgi-derived vesicles, but their pronounced toxin-protective effects were distinct from apoptosis-inducing or cytotoxic agents.

More importantly, the disrupted Golgi membranes showed competent anterograde trafficking in compound 134-treated cells, implying that this compound was preferentially targeting components of the retrograde pathway. A similar Golgi fragmentation has been observed in HeLa cells depleted of Cog3p, and the disrupted Golgi membranes were equally capable of anterograde trafficking of VSVG protein [50]. Though it also exhibited a strong protective effect against toxin-mediated protein synthesis inhibition, compound 75 appeared to have a more pronounced effect on the post-Golgi trafficking of NPY-GFP. Nonetheless, the identification of two compounds preferentially targeting the retrograde pathway could represent a useful tool in elucidating similarities and differences between anterograde and retrograde trafficking.

A previous study examining toxin transport found that disruption of the Golgi apparatus by the expression of a temperature-sensitive mutant of ε-COP did not inhibit ricin transport in Chinese hamster ovary cells, and it was concluded that ricin was capable of bypassing the Golgi apparatus altogether through a normally inaccessible

route [51]. Though we cannot rule out the possibility that compound treatment is inducing

an alternate toxin trafficking pathway, it seems unlikely that toxin is bypassing the Golgi

to any appreciable extent in compound-treated cells, given that STxB and CTxB still

traffic to the disrupted Golgi apparatus. Rather, our results indicate that an intact Golgi is

required for efficient STx trafficking and toxicity. The reversibility of compound effects

on Golgi structure concomitant with the loss of protection against STx following Golgi

reassembly suggest that STx transits retrogradely through the Golgi using a pathway that

is equally responsible for maintaining Golgi structure.

In contrast to standard genetic approaches that have been extensively employed to

understand the retrograde pathways used by bacterial and plant toxins, small compounds

provide an informative chemical genetic method for studying intracellular toxin transport

in a controlled and reversible manner [52]. Pharmacological agents derived from small

compounds have enhanced our understanding into the biology of retrograde transport and

its implications on Golgi organization [38]. Retrograde flow through the Golgi is believed

to balance anterograde flow in order to establish a membrane equilibrium while

maintaining Golgi polarity [53]. It has been suggested that components regulating

retrograde trafficking of glycolipid toxin receptors could also serve a role in the

retrograde recycling of Golgi membranes [54]. Indeed, it remains to be seen if the recycling

of different resident Golgi proteins is being directly or indirectly targeted by protein

toxins and, more importantly, whether the inhibitory effects of either or both of these

compounds is targeting this host membrane recycling machinery. Future studies with

fluorescently modified or biotinylated compounds that can be efficiently tracked and used

to identify molecular targets will elucidate our understanding of toxin subversion of retrograde, membrane recycling pathways.

Our study identifies two small compounds that protect against toxin-mediated inhibition of protein synthesis by selectively and reversibly disrupting toxin trafficking. As the mechanisms underlying endocytic transport become clearer, the ability to manipulate and alter these pathways through small molecules will serve as an invaluable tool in probing both the retrograde and anterograde trafficking mechanisms.

ACKNOWLEDGEMENTS

MATERIALS AND METHODS

Reagents and antibodies

Small chemical compounds were purchased from ChemDiv and reconstituted to 5 mg/mL stocks in DMSO. All compounds were checked for purity by mass spectroscopy. Shiga-like toxin 1 (referred to as STx1 in the text) and diphtheria toxin were from List Biological Laboratories, and ricin was from Sigma. Recombinant Alexa Fluor 488-labeled CTxB, Alexa Fluor 594-labeled human transferrin, SlowFade Gold mounting reagent with or without DAPI, and Alexa Fluor-labeled goat or donkey anti-IgG secondary antibodies were obtained from Molecular Probes. Rabbit anti-p115 and mouse anti-GM130 were purchased from BD Transduction Laboratories. Rabbit anti-giantin was from Covance, sheep anti-human TGN46 from Serotec. Dulbecco's Modified Eagle's Medium (DMEM), Eagle's Minimum Essential Medium (EMEM), streptomycin, and penicillin were from BioWhittaker. Non-essential amino acids (NEAA) were purchased from Mediatech. Cycloheximide, DMSO, brefeldin A, nocodazole, anisomycin, and staurosporine were from Sigma. Trans [^{35}S] was purchased from MP Biomedicals, and [^{35}S]O$_4$ was obtained from American Radiolabeled Chemicals.

Cell culture

Vero and HeLa cells were grown and maintained at 37ºC and 5% CO$_2$. Vero cells were maintained in DMEM supplemented with 10% fetal calf serum (FCS, Sigma), 100 µg/mL streptomycin, 100 U/mL penicillin, and 1% NEAA. HeLa cells were maintained in EMEM supplemented with 5% FCS, 100 µg/mL streptomycin, 100 U/mL penicillin, and 1% NEAA.

Purification of Shiga toxin B subunit (STxB)

Recombinant STx-B was isolated from periplasmic extracts of *E. coli* BL21(DE3) cells (Invitrogen) containing the expression vector pT7B5-1, as previously described [35]. Briefly, periplasmic extracts were subjected to anion-exchange chromatography on a Q-sepharose column (Pharmacia), and pentameric STxB was isolated following further purification of the Q-sepharose peak on a Superdex 75R 10/30 gel filtration column (Pharmacia). Fractions containing STxB were identified by SlotBlot (Hoefer) using a polyclonal rabbit anti-STxB antibody [35], and positive fractions were combined and concentrated to 1 mg/ml using Ventricon Plus-20 filters (Millipore). STxB purity was verified by SDS-PAGE on a 4-20% Tris-HCl gel stained with Coomassie Blue. AlexaFluor-488 and -594 conjugation was performed following the manufacturer's recommendations (Molecular Probes).

Luciferase-based assay for measuring protein synthesis

The luciferase-based assay has been described [19] and was applied to a high-throughput screen of small molecules consisting of known biological as well as unknown compounds at the ICCB facility at Harvard University. The luciferase protein has been modified by Promega by the addition of a PEST sequence, resulting in its short intracellular half-life [55]. The luciferase-PEST cDNA was cloned into an adenoviral expression plasmid [19], and high titer viral stocks were generated (pAD-Luc). Vero or HeLa cell monolayers were transduced with pAD-Luc (MOI of 200) and incubated for 24 h at 37^oC in 5% CO_2, then seeded into 384-well black polystyrene plates (Corning) at 1×10^4 cells/well for an additional 24 h. Cells were then treated for 30 min at 37ºC with

known biological and unknown compounds at 5 mg/mL. STx was added at 1 ng/mL, and cells were incubated for an additional 4 h at 37ºC. To determine luciferase expression, the SuperLight Luciferase Reporter Gene Assay was used according to the manufacturer's instructions (BioAssay Systems), and light output was detected using an LMax 1.1L luminometer (Molecular Devices). To be considered protective, the compound must increase the luciferase signal at least 2-fold above the mean observed from cells treated with toxin alone. Compounds maintaining luciferase expression levels in the presence of cycloheximide alone (100 µM) were excluded from further analysis.

Radioactive amino acid incorporation assay

Experiments measuring radioactive [^{35}S] incorporation were used to confirm positive hits from the luciferase-based high-throughput screen. This assay was adapted to a multi-well format to enable testing on a large number of samples. Vero cells were cultured overnight at 37°C in 5% CO_2 in 96-well plates at 2.5×10^4 cells/well, whereupon media was removed and replaced with either prewarmed media (plus 0.5% DMSO v/v) or media containing compound. Following a 1 h incubation at 37°C, toxin was added to wells in triplicate, and cells were shifted to 37°C for an additional 4 h. The media was then removed from all wells and replaced with media containing Trans [^{35}S] label at 10 µCi/mL. Cells were incubated at 37°C for 45 min, then washed with PBS (pH 7.4) and lysed (1 mg/mL BSA, 0.2% deoxycholic acid, 0.1% SDS, 20mM Tris pH 7.4) at 4°C for 12 h. Proteins from the lysed cells were TCA-precipitated (final concentration 15%), transferred to multi-screen HA plates (Millipore), and the filters were washed with ice-cold 20% TCA. Filters were then removed from the plate, placed in 2 mL Bio-Safe II

scintillation fluid (RPI), and [^{35}S] incorporation quantitated using a beta counter (Beckman). Independent experiments were performed at least three times for potent compounds, and data were analyzed using Prism v4.0 software (2003).

Toxin and transferrin internalization

For toxin trafficking experiments, Vero cells were grown in chamber slides (2.5 x 10^4 cells/chamber) and treated with medium containing DMSO, compound, or known agents at indicated concentrations for 1 h at 37°C, then placed on ice for 15 min prior to the addition of toxin. Toxin was bound for 45 min at 4°C, followed by washing of unbound toxin with ice-cold PBS (pH 7.4). Fresh, prewarmed media was added, and cells were shifted to 37°C for the indicated times to allow for toxin internalization. In transferrin trafficking experiments, cells were pretreated with compounds in serum-free culture medium, and transferrin and toxin were bound to cells at 4°C for 1 h, followed by a shift to 22°C for 1 h. For all immunofluorescence experiments, cells were fixed in 4% paraformaldehyde in cold PBS, permeabilized in culture medium containing 0.1% Triton-X100, and blocked with culture medium containing 0.1% BSA (w/v), all at room temperature. All primary and secondary (Alexa Fluor 488, 594, or 555-labeled donkey anti-IgG) antibodies were diluted in blocking buffer. Cells were rinsed thoroughly in PBS prior to mounting in SlowFade Gold reagent with or without DAPI. Fluorescence imaging used EpiFluorescence (Zeiss) microscopy.

Expression and trafficking of VSVG-GFP

Vero cells were transiently transfected with VSVG-GFP *ts*045, as previously described for other cell lines [44]. Briefly, 10^6 Vero cells were transfected with 20 µg of pCDM8.1 expressing VSVG-GFP *ts*045 and a Lipofectamine2000 (Invitrogen) mixture in antibiotic-free medium (DMEM with 10% FCS), followed by overnight incubation at 37^oC in 5% CO_2. Cells were collected and placed into chamber slides (Lab-Tek) for an additional 8-10 h at 37^oC before their transfer to 42^oC for 12-16 h. Cells were then treated with compounds or brefeldin A (25 µg/mL) in prewarmed, antibiotic-free medium for 1 h at 42^oC before their transfer to 32^oC. Thirty minutes prior to the shift to 32^oC, all chambers were treated with cycloheximide (100 µM) to prevent *de novo* protein synthesis. Cells were fixed following various incubation times at $32°C$. Fixation, permeabilization, staining, and imaging were performed as described for toxin and transferrin internalization experiments.

Cell viability assay

The viability of cells treated with compound was evaluated using the CellTiterGlo Lumninescent Cell Viability Assay (Promega), a luciferase-based assay. Vero cells (5 x 10^4 cells/well) were added to 96-well plates and grown at 37^oC in 5% CO_2 overnight. Media was then removed and replaced with either prewarmed media with DMSO or compound in triplicate. Following incubation at $37°C$ for various times, an equal volume of CellTiter Reagent (50 µL) was added according to the manufacturer's instructions, and light output was measured using the Lmax 1.1L luminometer. Independent experiments were performed three times.

Assessment of NPY-GFP secretion

Approximately 5×10^6 Vero cells were infected overnight at 37ºC in 5% CO_2 with pAD-NPY-GFP. Cells were then washed, trypsinized, and seeded into each well of a 6-well plate (~1 x 10^6 cells/well). The next day, media was removed, and cells were washed twice with serum-free media. Media was subsequently replaced with serum-free DMEM containing DMSO or compounds for 30 min at 37ºC. Cells were all treated with cycloheximide (100 µM) to inhibit *de novo* protein synthesis and to synchronize NPY-GFP trafficking. At various time points following cycloheximide treatment, supernatants were collected, and GFP secretion was assessed by ELISA as described in the manufacturer's instructions (Pierce). ELISA plates were analyzed by the Gen5 software program (BioTek) using the Synergy 2 spectrophotometer (BioTek). Mean absorbance for control wells containing DMEM alone were subtracted from sample wells before analysis.

Cloning and expression of StxB-Sulf₂-His6

In order to add overlapping sulfation sites to the carboxyl terminus of Stx B-subunit, the STxB gene from pNAS-13 [35] was amplified with primers Sulf1, 5'-GGTGCTCAAGGAGTATTGTGTAATATGAAAAAAACATTATTAATA-GC-3' and Sulf-2, 5'GGATTCAGCGAAGTTATTTTTCGTGGAGAGGAACCTGAG-TATGGAGAAGAGGAACCTGAGTATGGAGAAAGCGGCCGAAAAAAGTAGGC-G-3', which encodes the two overlapping sulfation sites added to STxB by Johannes *et al.*[56]. The amplified product was ligated into expression plasmid pCRT7-TOPO (Invitrogen). Sequencing of one such product revealed a nucleotide deletion at base 312

61

of the STxB coding region, such that the sulfation sites were intact and the frame-shift resulted in read-through in frame into the pCRT7 flanking sequence encoding a V5 epitope, a histidine tag, and a stop codon. This protein was found to be expressed at a high level from BL21 (DE3) cells and was used in future studies. The protein was expressed from BL21 (DE3) cells by the addition of 0.1 M IPTG (Fischer) to cultures growing at late log phase. After 2 h incubation at 30°C, the bacteria were harvested by centrifugation, and periplasmic extract was prepared by osmotic lysis. The material was mixed with 2 mL Ni-NTA resin (Qiagen) and incubated overnight at 4°C with rocking. The resin and periplasmic extract were then applied to an empty column, the beads were washed with several column volumes of PBS, followed by PBS containing imidazole at 25, 50, 250 and 500 mM. The STxB-Sulf$_2$-His protein, which remained associated with the column at 500 mM imidazole, was released by the addition of 5 ml 2M imidazole in PBS. The eluted protein was dialyzed twice against PBS (pH 7.4), aliquoted, and stored at 4ºC. In order to demonstrate that addition of the sulfation, V5, and histidine tags did not affect binding and transport of the toxin, STxB-Sulf$_2$-His was labeled with AlexaFluor-488 following the manufacturer's instructions (Molecular Probes). Vero cells were incubated with 1 µg/mL each of STxB-Sulf$_2$-His-488 and wild-type STxB labeled with AlexaFluor-594. After binding at 4ºC for 1 h, the cells were washed and warmed to 37ºC for 1 h, fixed with 4% paraformaldehyde, and visualized by epifluoresence microscopy.

Sulfation of STxB-Sulf$_2$-His

Vero cells were seeded overnight at 37ºC in 5% CO_2 (1 x 10^6 cells/well). The next day, media was replaced with serum-free DMEM lacking sulfate (Washington University Tissue Culture Support Center), and cells were incubated for an additional 3.5 h at 37ºC. Media was replaced with sulfate-free DMEM containing DMSO or compound for 30 min at 37ºC, then replaced with prewarmed sulfate-free media containing 1 mCi/mL [^{35}S]O$_4$ for 3 h at 37ºC. Wells were washed with cold PBS (pH 7.4) and lysed with PBS containing 1% Triton X-100. The protein concentration of post-nuclear supernatants were determined by the BCA Protein Assay Kit (Pierce), and 250 µg lysates were added to 40 µL Ni-NTA Superflow beads and rotated at 4ºC overnight. The next day, beads were spun down at 5,000 rpm for 5 min, and the unbound fraction was collected. Total [^{35}S]-incorporated counts were determined by measuring radioactive counts from TCA-precipitated proteins of unbound lysates. Beads were washed once with PBS containing 1% Triton X-100 and twice with PBS. Beads were resuspended in imidazole (1.5 M in PBS), and eluates were denatured with 1X SDS gel-loading buffer (50 mM Tris HCl, 100 mM β-mercaptoethanol, 2% SDS, 0.1% bromophenol blue, 10% v/v glycerol) and boiling. Eluates were resolved on a 10-20% Tris-HCl denaturing gel, fixed, and developed overnight in a Phosphorimager cassette.

Statistics

Data are expressed as mean ± SD. Toxin IC$_{50}$ values were determined by a nonlinear regression curve fit to the observed data as determined by Prism v4.0 (2003), and statistical differences between toxin IC$_{50}$ values were calculated by the F test.

Differences were considered statistically significant for $p \leq 0.05$ (*) or highly statistically significant for $p \leq 0.01$ (**).

REFERENCES

1.   Guidi-Rontani, C., Weber-Levy, M., Mock, M. & Cabiaux, V. Translocation of Bacillus anthracis lethal and oedema factors across endosome membranes. *Cell Microbiol* **2**, 259-64 (2000).

2.   Morinaga, N., Kaihou, Y., Vitale, N., Moss, J. & Noda, M. Involvement of ADP-ribosylation factor 1 in cholera toxin-induced morphological changes of Chinese hamster ovary cells. *Journal of Biological Chemistry* **276**, 22838-43 (2001).

3.   Wilcke, M. et al. Rab11 regulates the compartmentalization of early endosomes required for efficient transport from early endosomes to the trans-golgi network. *Journal of Cell Biology* **151**, 1207-20 (2000).

4.   Schmitz, A., Herrgen, H., Winkeler, A. & Herzog, V. Cholera toxin is exported from microsomes by the Sec61p complex. *Journal of Cell Biology* **148**, 1203-1212 (2000).

5.   Tsai, B., Rodighiero, C., Lencer, W.I. & Rapoport, T.A. Protein disulfide isomerase acts as a redox-dependent chaperone to unfold cholera toxin. *Cell* **104**, 937-948 (2001).

6.   Yu, M. & Haslam, D.B. Shiga toxin is transported from the endoplasmic reticulum following interaction with the luminal chaperone HEDJ/ERdj3. *Infection & Immunity* **73**, 2524-32 (2005).

7.   Garred, O., van Deurs, B. & Sandvig, K. Furin-induced cleavage and activation of Shiga toxin. *Journal of Biological Chemistry* **270**, 10817-21 (1995).

8.   Simpson, J.C. et al. Ricin A chain utilises the endoplasmic reticulum-associated protein degradation pathway to enter the cytosol of yeast. *FEBS Letters* **459**, 80-4 (1999).

9.   Yu, M., Haslam, R.H. & Haslam, D.B. HEDJ, an Hsp40 co-chaperone localized to the endoplasmic reticulum of human cells. *Journal of Biological Chemistry* **275**, 24984-92 (2000).

10.   Sandvig, K. et al. Retrograde transport of endocytosed Shiga toxin to the endoplasmic reticulum. *Nature* **358**, 510-2 (1992).

11.   Stenmark, H. & Olkkonen, V.M. The Rab GTPase family. *Genome Biol* **2**, REVIEWS3007 (2001).

12.   Iversen, T.G. et al. Endosome to Golgi transport of ricin is independent of clathrin and of the Rab9- and Rab11-GTPases. *Molecular Biology of the Cell* **12**, 2099-107 (2001).

13.   Sandvig, K. et al. Ricin transport into cells: studies of endocytosis and intracellular transport. *International Journal of Medical Microbiology* **290**, 415-420 (2000).

14.   Girod, A. et al. Evidence for a COP-I-independent transport route from the Golgi complex to the endoplasmic reticulum. *Nature Cell Biology* **1**, 423-30 (1999).

15.   Mallard, F. et al. Early/recycling endosomes-to-TGN transport involves two SNARE complexes and a Rab6 isoform. *Journal of Cell Biology* **156**, 653-64 (2002).

16. White, J. et al. Rab6 coordinates a novel Golgi to ER retrograde transport pathway in live cells.[erratum appears in J Cell Biol 2000 Jan 10;148(1):followi]. *Journal of Cell Biology* **147**, 743-60 (1999).

17. Chen, A., AbuJarour, R.J. & Draper, R.K. Evidence that the transport of ricin to the cytoplasm is independent of both Rab6A and COPI. *Journal of Cell Science* **116**, 3503-10 (2003).

18. Mesa, R. et al. Overexpression of Rab22a hampers the transport between endosomes and the Golgi apparatus. *Experimental Cell Research* **304**, 339-53 (2005).

19. Zhao, L. & Haslam, D.B. A quantitative and highly sensitive luciferase-based assay for bacterial toxins that inhibit protein synthesis. *Journal of Medical Microbiology* **54**, 1023-30 (2005).

20. Oh, K.J., Senzel, L., Collier, R.J. & Finkelstein, A. Translocation of the catalytic domain of diphtheria toxin across planar phospholipid bilayers by its own T domain. *Proc Natl Acad Sci U S A* **96**, 8467-70 (1999).

21. Chaudhary, V.K., Jinno, Y., FitzGerald, D. & Pastan, I. Pseudomonas exotoxin contains a specific sequence at the carboxyl terminus that is required for cytotoxicity. *Proc Natl Acad Sci U S A* **87**, 308-12 (1990).

22. Endo, Y. & Tsurugi, K. Mechanism of action of ricin and related toxic lectins on eukaryotic ribosomes. *Nucleic Acids Symposium Series*, 187-90 (1986).

23. Obrig, T.G., Moran, T.P. & Brown, J.E. The mode of action of Shiga toxin on peptide elongation of eukaryotic protein synthesis. *Biochemical Journal* **244**, 287-94 (1987).

24. Obrig, T.G., Moran, T.P. & Colinas, R.J. Ribonuclease activity associated with the 60S ribosome-inactivating proteins ricin A, phytolaccin and Shiga toxin. *Biochemical & Biophysical Research Communications* **130**, 879-84 (1985).

25. Reisbig, R., Olsnes, S. & Eiklid, K. The cytotoxic activity of Shigella toxin. Evidence for catalytic inactivation of the 60 S ribosomal subunit. *Journal of Biological Chemistry* **256**, 8739-44 (1981).

26. Balint, G.S. Ricin--2004. *Orvosi Hetilap* **145**, 2379-81 (2004).

27. Stryer, L. Transducin and the cyclic GMP phosphodiesterase: amplifier proteins in vision. *Cold Spring Harb Symp Quant Biol* **48 Pt 2**, 841-52 (1983).

28. Casey, P.J. & Gilman, A.G. G protein involvement in receptor-effector coupling. *J Biol Chem* **263**, 2577-80 (1988).

29. Kumar, P., Ahuja, N. & Bhatnagar, R. Anthrax edema toxin requires influx of calcium for inducing cyclic AMP toxicity in target cells. *Infect Immun* **70**, 4997-5007 (2002).

30. Zhao, L. & Haslam, D.B. A quantitative and highly sensitive luciferase-based assay for bacterial toxins that inhibit protein synthesis. *J Med Microbiol* **54**, 1023-30 (2005).

31. Sherwood, A.L. & Holmes, E.H. Brefeldin A induced inhibition of de novo globo- and neolacto-series glycolipid core chain biosynthesis in human cells. Evidence for an effect on beta 1-->4galactosyltransferase activity. *Journal of Biological Chemistry* **267**, 25328-36 (1992).

32. Kok, J.W. et al. PDMP blocks brefeldin A-induced retrograde membrane transport from golgi to ER: evidence for involvement of calcium homeostasis and

dissociation from sphingolipid metabolism. *Journal of Cell Biology* **142**, 25-38 (1998).

33.   Sutton, C.A., Ares, M.J. & Hallberg, R.L. Cycloheximide restance can be mediated through either ribosomal subunit. *Proc. Natl. Acad. Sci. USA* **75**, 3158-3162 (1978).

34.   Zhang, J., Chung, D.Y. & Oldenburg, K.R. A simple statistical paramater for use in evaluation and validation of high throughput screening assays. *J. Biomol. Screen.* **4**, 67-73 (1999).

35.   Elliott, S.P., Yu, M., Xu, H. & Haslam, D.B. Forssman synthetase expression results in diminished shiga toxin susceptibility: a role for glycolipids in determining host-microbe interactions. *Infection & Immunity* **71**, 6543-52 (2003).

36.   Lord, J.M., Smith, D.C. & Roberts, L.M. Toxin entry: how bacterial proteins get into mammalian cells. *Cellular Microbiology* **1**, 85-91 (1999).

37.   Mallard, F. & Johannes, L. Shiga toxin B-subunit as a tool to study retrograde transport. *Methods in Molecular Medicine* **73**, 209-20 (2003).

38.   Dinter, A. & Berger, E.G. Golgi-disturbing agents. *Histochemistry & Cell Biology* **109**, 571-90 (1998).

39.   Machamer, C.E. Golgi disassembly in apoptosis: cause or effect? *Trends Cell Biol* **13**, 279-81 (2003).

40.   Kabir, J., Lobo, M. & Zachary, I. Staurosporine induces endothelial cell apoptosis via focal adhesion kinase dephosphorylation and focal adhesion disassembly independent of focal adhesion kinase proteolysis. *Biochem J* **367**, 145-55 (2002).

41. Tscherne, J.S. & Pestka, S. Inhibition of protein synthesis in intact HeLa cells. *Antimicrob Agents Chemother* **8**, 479-87 (1975).

42. Orlandi, P.A., Curran, P.K. & Fishman, P.H. Brefeldin A blocks the response of cultured cells to cholera toxin. Implications for intracellular trafficking in toxin action. *Journal of Biological Chemistry* **268**, 12010-6 (1993).

43. Lauvrak, S.U., Torgersen, M.L. & Sandvig, K. Efficient endosome-to-Golgi transport of Shiga toxin is dependent on dynamin and clathrin. *Journal of Cell Science* **117**, 2321-31 (2004).

44. Hirschberg, K. & Lippincott-Schwartz, J. Secretory pathway kinetics and in vivo analysis of protein traffic from the Golgi complex to the cell surface. *Faseb J* **13 Suppl 2**, S251-6 (1999).

45. Abujarour, R.J., Dalal, S., Hanson, P.I. & Draper, R.K. p97 Is in a complex with cholera toxin and influences the transport of cholera toxin and related toxins to the cytoplasm. *Journal of Biological Chemistry* **280**, 15865-71 (2005).

46. Carey, K.L., Westwood, N.J., Mitchison, T.J. & Ward, G.E. A small-molecule approach to studying invasive mechanisms of Toxoplasma gondii. *Proceedings of the National Academy of Sciences of the United States of America* **101**, 7433-8 (2004).

47. Hung, D.T., Shakhnovich, E.A., Pierson, E. & Mekalanos, J.J. Small-molecule inhibitor of Vibrio cholerae virulence and intestinal colonization. *Science* **310**, 670-4 (2005).

48. Falguieres, T. et al. Targeting of Shiga toxin B-subunit to retrograde transport route in association with detergent-resistant membranes. *Molecular Biology of the Cell* **12**, 2453-68 (2001).

49. Kojio, S. et al. Caspase-3 activation and apoptosis induction coupled with the retrograde transport of shiga toxin: inhibition by brefeldin A. *FEMS Immunol Med Microbiol* **29**, 275-81 (2000).

50. Zolov, S.N. & Lupashin, V.V. Cog3p depletion blocks vesicle-mediated Golgi retrograde trafficking in HeLa cells. *J Cell Biol* **168**, 747-59 (2005).

51. Llorente, A., Lauvrak, S.U., van Deurs, B. & Sandvig, K. Induction of direct endosome to endoplasmic reticulum transport in Chinese hamster ovary (CHO) cells (LdlF) with a temperature-sensitive defect in epsilon-coatomer protein (epsilon-COP). *J Biol Chem* **278**, 35850-5 (2003).

52. Ward, G.E., Carey, K.L. & Westwood, N.J. Using small molecules to study big questions in cellular microbiology. *Cell. Microbiol.* **4**, 471-482 (2002).

53. Shorter, J. & Warren, G. Golgi architecture and inheritance. *Annu Rev Cell Dev Biol* **18**, 379-420 (2002).

54. Yoshino, A. et al. tGolgin-1 (p230, golgin-245) modulates Shiga-toxin transport to the Golgi and Golgi motility towards the microtubule-organizing centre. *Journal of Cell Science* **118**, 2279-93 (2005).

55. Rechsteiner, M. PEST sequences are signals for rapid intracellular proteolysis. *Seminars in Cell Biology* **1**, 433-40 (1990).

56.   Johannes, L., Tenza, D., Antony, C. & Goud, B. Retrograde transport of KDEL-

bearing B-fragment of Shiga toxin. *Journal of Biological Chemistry* **272**, 19554-

61 (1997).

CHAPTER III

Golgicide A reveals essential roles for

GBF1 in Golgi assembly and function

OVERVIEW

In contrast to some members of the AB toxin family, the bacterial exotoxin Shiga toxin (STx) undertakes a more labored route to reach its intracellular target in host cells. Following endocytosis into an early endosome, the membrane-bound STx is transported in a retrograde manner to the endoplasmic reticulum (ER) via the Golgi. It has been proposed that STx exploits underlying host mechanisms to gain access to the cytosol, where it can exert its enzymatic effects. Though the stepwise progression of STx through the cell has become more clearly defined, the host molecules essential to distinct steps in STx transport remain largely unidentified. In addition, no host molecules have been shown to be transported from endosomes all the way back to the ER. As a result, STx has become a useful probe for studying the retrograde pathway in its entirety. Using a recently developed high-throughput assay for screening compound libraries for potential inhibitors of STx transport, we identified Golgicide A (GCA), a potent and highly specific inhibitor of Shiga toxicity. Further characterization of GCA found that it strongly protects against Shiga toxicity by inhibiting GBF1, a *cis*-Golgi-localized guanine nucleotide exchange factor for ADP-ribosylation factor 1 (ARF1). A more detailed structural analysis suggested a putative binding site of GCA on GBF1 that could be critical for GDP/GTP exchange on ARF1. More importantly, GCA represents a novel tool for preferentially targeting ARF1 at the *cis*-Golgi and for studying the role of GBF1 in mediating host trafficking within the Golgi. The work describing these studies is

74

presented in this chapter and published in Nature Chemical Biology[†]. The contributions of the authors to different sections of the project are indicated.

SUMMARY

The small GTPase ADP-ribosylation factor 1 (ARF1) plays a critical role in regulating secretory traffic and membrane transport within the Golgi of eukaryotic cells. ARF1 is activated by Golgi-localized guanine nucleotide exchange factors (ARFGEFs), which confer spatiotemporal specificity to vesicular transport. From a phenotypic screen aimed at identifying small molecule inhibitors of Shiga toxin (STx) trafficking, we identified a novel compound, golgicide A (GCA), that reversibly caused Golgi disassembly while maintaining endocytic transport to recycling endosomes. The morphological effects on the Golgi resemble those caused by the fungal metabolite brefeldin A (BFA), but further characterization reveals that GCA specifically targets coatomer protein I (COPI)-dependent transport within the Golgi while maintaining adaptor protein 1 (AP-1)-mediated trafficking. More specifically, the phenotypic effects of GCA mimicked overexpression of the dominant-negative GBF1-E794K mutant. However, overexpression of a GBF1 point mutant (GBF1-M830L) conferred resistance to GCA and reversed the effects of GCA on the Golgi, indicating that GCA specifically disrupts COPI-dependent trafficking by targeting the *cis*-Golgi-localized ARFGEF, GBF1. As a specific and reversible inhibitor of GBF1, GCA will serve as a useful alternative to BFA for examining the role of GBF1 in maintaining Golgi structure and function.

[†] **Saenz, J.B., Sun, W.J.,** *et al.* 2009. Golgicide A reveals essential roles for GBF1 in Golgi assembly and function. *Nat. Chem. Biol.* **5**: 157-165.

INTRODUCTION

The family of small GTP-binding proteins known as ADP-ribosylation factors (ARFs) mediate eukaryotic vesicular transport and membrane trafficking [1]. Mammalian ARFs fall into three categories based on sequence similarity: class I (ARF1-3), class II (ARF4 and ARF5), and class III (ARF6) [2]. The most extensively characterized of the ARFs, ARF1 is a major regulator of vesicular transport within the *cis/medial*-Golgi as well as between the *trans*-Golgi network (TGN) and endosomes. A member of the Ras superfamily of small GTPases, ARF1 cycles between its inactive, GDP-bound form, and an active, GTP-bound state. Inactive ARF1-GDP is primarily cytosolic and can associate weakly with Golgi membranes, whereas active ARF1-GTP coordinates coated vesicle assembly following its tight interaction with membranes [3].

Activation of ARF1 at the Golgi is catalyzed by ARF1-specific guanine nucleotide exchange factors (ARFGEFs) that confer spatiotemporal specificity to vesicular transport. The ARFGEFS are further divided into two families consisting of the large brefeldin A (BFA)-susceptible molecules, which localize to the Golgi and TGN, and the smaller BFA-resistant ARNO-family GEFs, which predominantly localize to endosomes [4,5]. Crucial to their guanine nucleotide exchange activity is a highly conserved region of roughly 200 amino acids known as the Sec7 domain, whose central hydrophobic groove binds to nucleotide-free ARF1[6,7]. Activation of ARF1 at the *cis*-Golgi is catalyzed by the mammalian ARFGEF Golgi BFA resistance factor 1 (GBF1), while ARF1 is activated at the TGN by the ARFGEFs BIG1 and BIG2 (Figure 1)[8-12]. Following activation by GBF1, ARF1-mediated COPI coat recruitment enables vesicle transport between the Golgi and endoplasmic reticulum (ER) [13]. Activation by BIG1 and

BIG2 results in ARF1 recruitment of adaptor protein 1 (AP-1), a protein implicated in

clathrin vesicular transport from the Golgi to endosomes, AP-3, involved in clathrin

vesicular transport from the Golgi to lysosomes and vacuoles, AP-4, an adaptor protein

functioning at the TGN, and Golgi-associated, gamma adaptin ear containing, ARF-

binding proteins (GGA 1-3), monomeric proteins involved in trafficking from the TGN

and within the endosomal compartment [14-19]. ARF1 has also been demonstrated to

modulate phospholipase D activity, thus affecting membrane compositional integrity and

continuous remodeling of the Golgi [20].

The crucial role of ARFGEFs in vesicular transport has been highlighted by the effects of BFA, a heterocylic lactone that inhibits ARF1 activation at the *cis*- and *trans*-Golgi (TGN) by stabilizing an abortive complex between ARF1-GDP and its cognate ARFGEF [21]. At the *cis*-Golgi, BFA inhibits ARF1 activation by GBF1 and

Figure 1. Schematic diagram of Golgi-localized ARFGEFs. ARF1 exists in the cytoplasm in its inactive, GDP-bound form. At the cis-Golgi, the ARFGEF GBF1 catalyzes GDP/GTP exchange on ARF1, thereby activating it. Activated ARF1 (ARF1-GTP) recruits COPI coat protein, which mediates ER-to-Golgi and intra-Golgi transport. At the *trans*-Golgi (TGN), GTP exchange on ARF1 is catalyzed by the TGN-localized ARFGEFs BIG1/BIG2. Activated ARF1 recruits AP-1 coat protein, which mediates bidirectional transport between endosomes and the TGN. ARF1, ADP-ribosylation factor 1; GBF1, Golgi BFA-resistance factor 1; BIG1/2, BFA-inhibited guanine nucleotide exchange factors 1/2; AP-1, adaptor protein 1; COPI, coat protein I; ER, endoplasmic reticulum; ERGIC, ER-Golgi intermediate compartment.
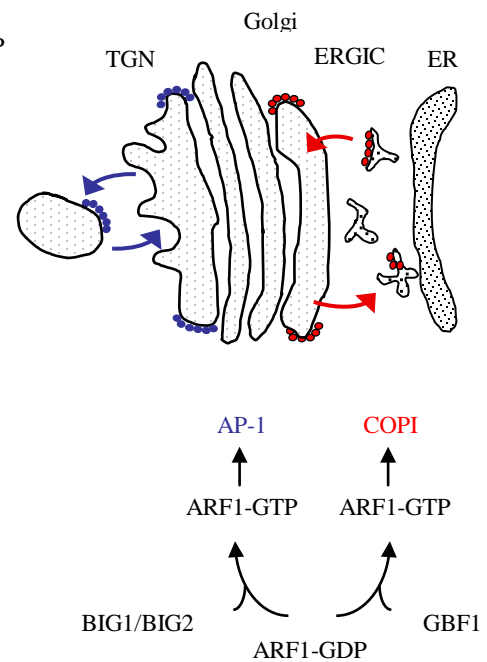
blocks COPI-dependent trafficking that is essential to maintaining Golgi integrity. This results in a redistribution of Golgi membranes and proteins to the ER. Similarly, inhibition of BIG1/BIG2 at the TGN halts AP-1-dependent TGN-endosome trafficking and leads to a fusion of both compartments. In addition to its effects on ARFGEF activity, BFA has other less-characterized effects on intracellular transport molecules, including inhibition of BARS and Golgi-associated phospholipase D activities [22-24].

Recently, the function of individual ArfGEFs has been explored. Among the ARFGEFs, GBF1 has been studied most intensively, either by siRNA-mediated silencing [10,25-27] or by the expression of dominant-negative forms [9,11,28,29]. The phenotypic and functional effects of these perturbations have not been in complete agreement but nevertheless demonstrate crucial roles for GBF1 in intra-Golgi transport. We describe here the discovery and characterization of a potent, highly specific, and rapidly reversible small molecule inhibitor of GBF1 function. This compound, which we called Golgicide A (GCA), reveals diverse roles for GBF1 in maintaining structure and function of the Golgi and *trans*-Golgi network.

RESULTS

Golgicide A (GCA) is a potent and highly effective inhibitor of Shiga toxin activity.

From a high-throughput screen for small molecules that inhibit the effect of bacterial toxins on host cells [30,31], we identified a compound that potently and effectively protected Vero cells from Shiga toxin (STx). STx inhibits protein synthesis by inactivating an adenine residue on the 28S ribosome. To quantify the effects of STx on protein synthesis, a luciferase-based assay was used to screen the Harvard ICCB facility's ChemDiv4 library, composed of approximately 14,000 commercially available small molecule compounds selected for their structural diversity, chemical stability, and "drug-like" properties. GCA (Figure 1A) was identified as protective by the initial high-throughput screen, maintaining light output at least 3 standard deviations above STx-treated Vero cells lacking compound (not shown). The potency of GCA, determined from the compound IC_{50} (the compound concentration resulting in 50% inhibition of STx activity in STx-treated Vero cells; see Methods) was found to be 3.3 µM (Figure 1B). At a GCA concentration of 10 µM, the STx IC_{50}, or the STx concentration required to reduce protein synthesis by 50%, was significantly increased over untreated cells (Figure 1C). This protection was similar to that observed with BFA, which has been considered the most efficacious STx-protective agent.
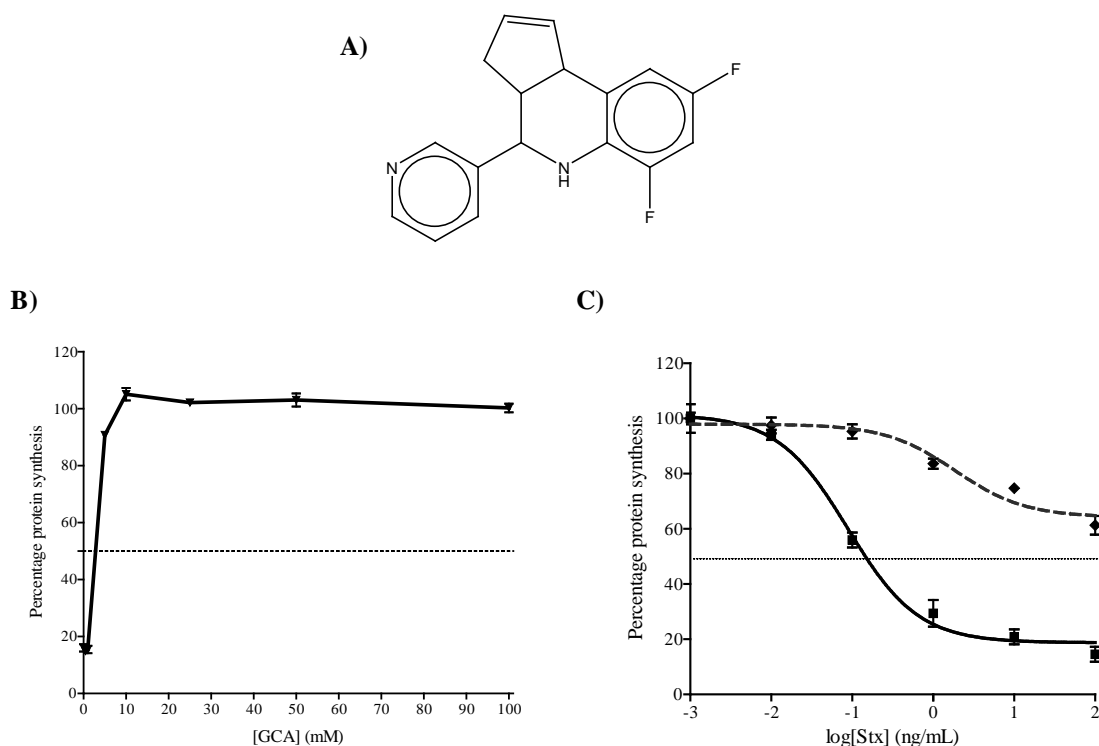
Figure 2. GCA is a potent and effective inhibitor of STx susceptibility. **(A)** Structure of GCA. **(B)** Vero cells were pretreated for 30 min at 37ºC with varying concentrations of GCA, followed by incubation with STx (1 ng/mL) for 4 h at 37ºC. Percentage protein synthesis indicates the amount of radioactive amino acid incorporation in GCA-treated cells as a percentage of radioactive amino acid incorporation in cells lacking STx treatment. Protein synthesis levels and compound-response curves were determined as described in Methods. **(C)** Protein synthesis levels for control (solid line; no compound) or GCA-treated (dotted line; 10 μM) Vero cells were determined using the radioactive amino acid incorporation assay as described in (B). Percentage protein synthesis is expressed as the amount of radioactive amino acid incorporation in untreated or GCA-treated cells at a given toxin concentration as a percentage of radioactive amino acid incorporation in cells lacking STx treatment. Toxin IC_{50} values for GCA-treated cells were significantly increased over control cells ($p<0.01$; see Methods). For (A) and (B), data points (mean ±SD) represent triplicate data at the indicated compound or toxin concentrations, respectively, from one representative experiment. STx, Shiga toxin; GCA, Golgicide A.

Other compounds identified in this screen acted through the inhibition of intracellular toxin transport [32], leading us to examine the effect of GCA on toxin trafficking and on intracellular organelle morphology.

Immunofluorescence experiments demonstrated dramatic effects of GCA on the Golgi and TGN. Whereas the Golgi remains as a tightly organized perinuclear ribbon in untreated cells, GCA caused complete dispersal of the Golgi marker giantin. This effect was seen at concentrations as low as 5 μM (not shown). Within two minutes of GCA

80
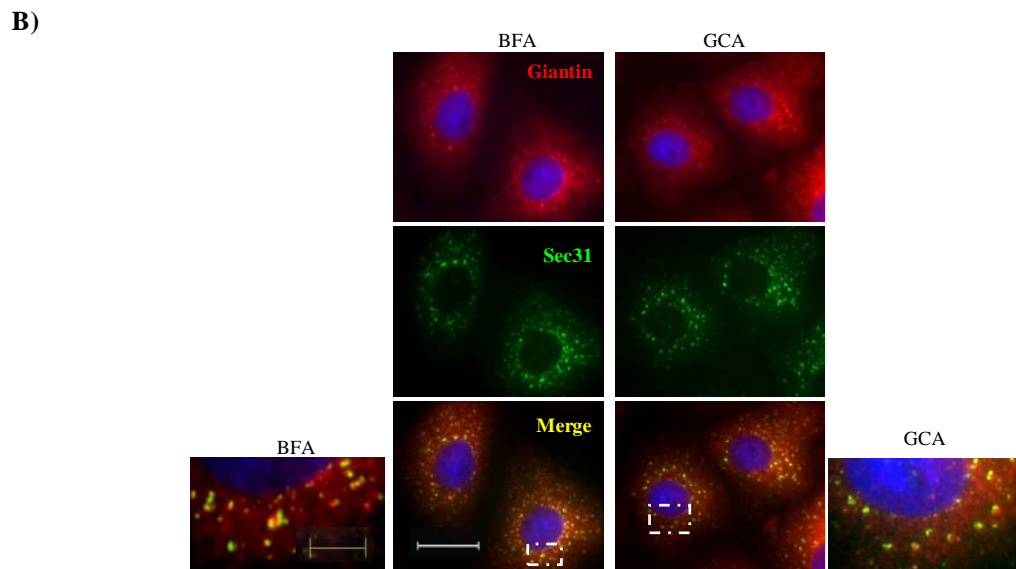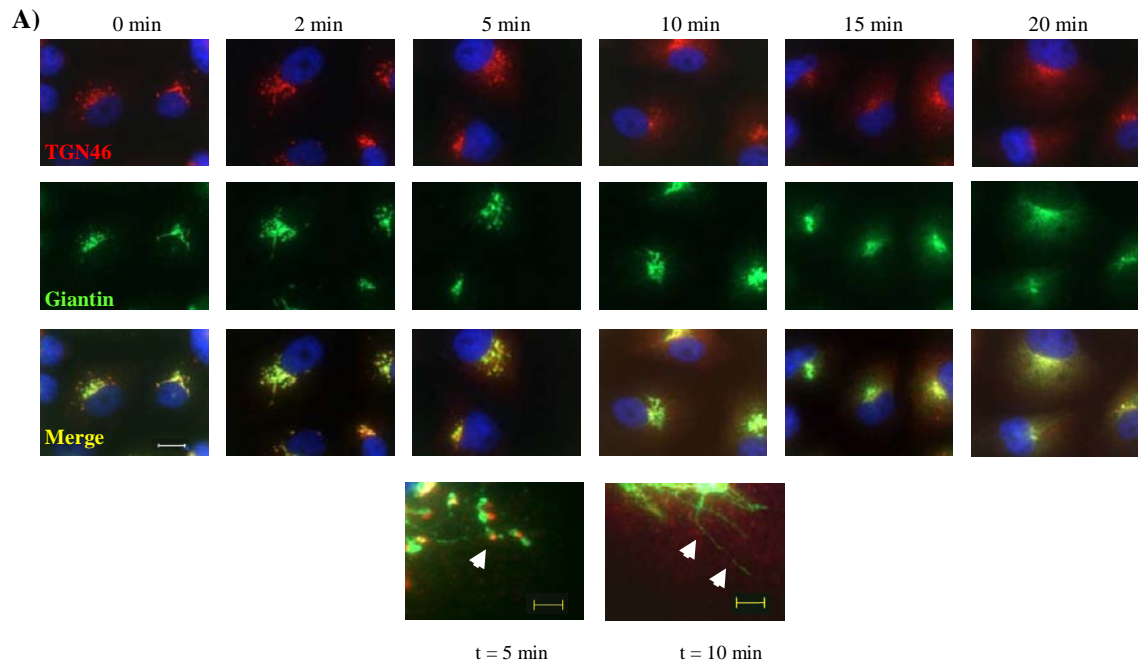
Figure 3. GCA causes tubulation and dispersal of the Golgi and TGN. (A) Vero cells were treated with GCA (10 μM) for the indicated times prior to fixation and labeling with anti-TGN46 (red) and anti-giantin (green) antibodies. Both the TGN and *medial*-Golgi begin to disassemble within 5 min of treatment. Insets demonstrate giantin-positive tubules (arrowheads) at the indicated times. White scale bars, 20 μm. Yellow scale bars, 5 μm. **(B)** BFA and GCA disperse the *medial*-Golgi marker giantin to a partially punctate pattern adjacent to ERES. Vero cells were treated with BFA (10 μg/ml) or GCA (10 μM) for 60 min, then fixed and labeled with antibodies against giantin (red) or Sec31 (green). Both compounds cause giantin redistribution into a hazy and punctate pattern. Giantin-positive punctate structures are closely approximated to Sec31-labeled ERES. White scale bars, 10 μm. Yellow scale bars, 5 μm. BFA, brefeldin A; TGN, *trans*-Golgi network; ERES, endoplasmic reticulum exit sites.

addition, giantin labeling became extensively tubulated and had completely dispersed by

15 min (Figure 3A). These morphological effects were highly reminiscent of those

caused by BFA [33,34]. The distribution of *cis*-Golgi *(*GM130 and p115; not shown) and *medial*-Golgi (giantin; Figure 3B) markers were essentially identical following either GCA or BFA treatment.

Treatment with GCA resulted in a diffuse and punctate distribution of the *medial*-Golgi marker giantin. The punctate structures were in contact with Sec31-positive foci, indicative of their association with ER exit sites (ERES; Figure 3B). These findings were also similar to BFA treatment, which causes Golgi matrix proteins to concentrate at ERES[35]. Effects of these compounds on the TGN, however, were subtly different. Whereas BFA induced the formation of tubules derived from TGN and endosomes, GCA caused the TGN to disperse into small vesicles that subsequently disseminated throughout the cell (Figure 3A).

A)

| DMSO (0.5% v/v) | GCA (10 μM) | Nocodazole (5 μg/mL) |

B)

| DMSO (0.5% v/v) | GCA (10 μM) | Cytochalasin B (25 μM) |
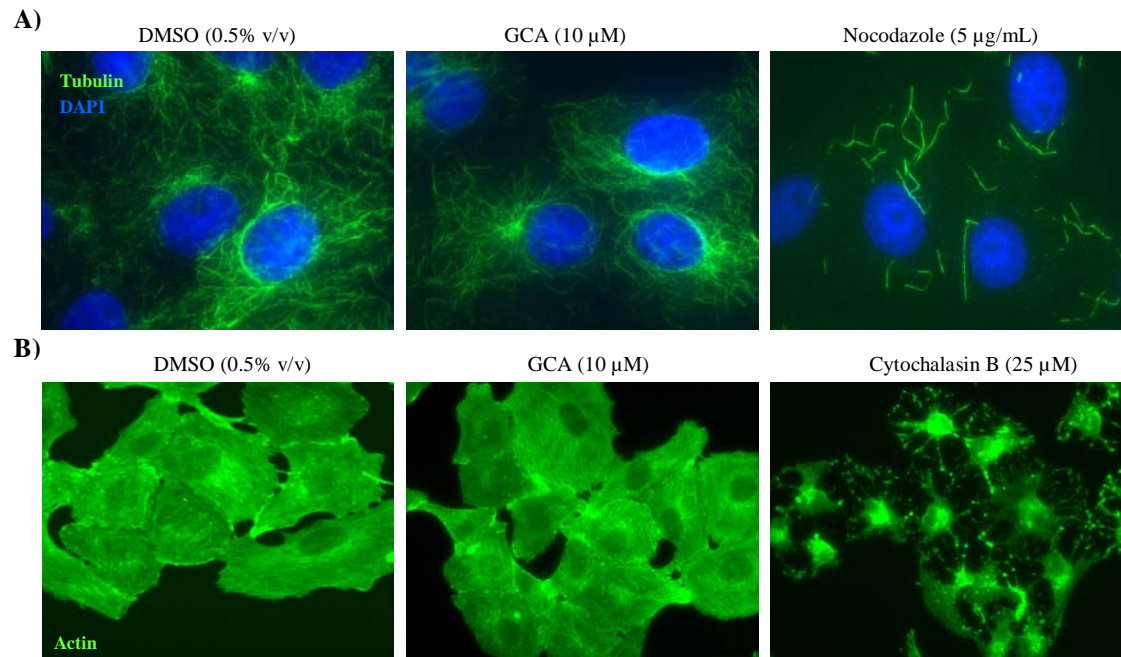
Figure 4. GCA does not affect microtubular or actin cytoskeletons. **(A)** Vero cells were treated for 30 min at 37°C with DMSO, GCA, or nocodazole at the indicated concentrations prior to fixation and immunostaining, as described in Methods. At 10 μM, GCA had no observable effects on microtubules, while nocodazole, an inhibitor of microtubule polymerization, produced drastic morphological effects. **(B)** Vero cells were treated with DMSO, GCA, or cytochalasin B at the indicated concentrations and developed for immunofluorescence, as in (A). GCA showed no effects on actin microfilaments compared to DMSO-treated cells, while the actin-depolymerizing agent cytochalasin B induced significant changes to actin morphology.

The morphologic effects of GCA did not result from disruption of microtubules or actin cytoskeleton (Figure 4). Finally, the effects of GCA were found to be rapidly reversible. Within 15 minutes of removing the compound, the Golgi and TGN began to reassemble (Figure 5A). The effects of GCA on protein secretion (Figure 5B) were likewise found to be completely reversible within 1 h of compound removal.

A)

Giantin

B)
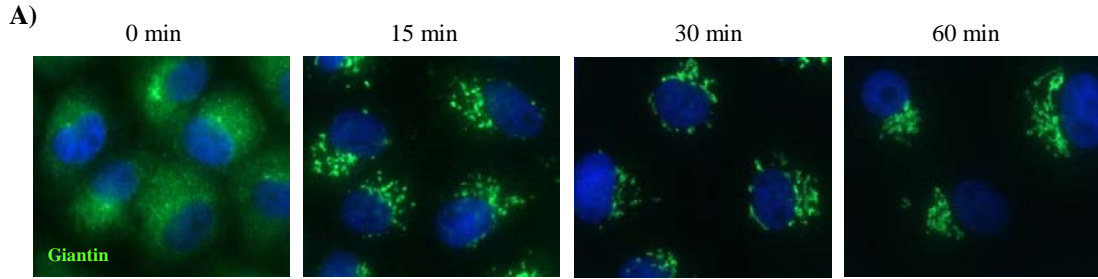
Figure 5. The effects of GCA are rapidly reversible. (A) Vero cells were treated with GCA (10 µM) for 1 h. To remove GCA, cells were washed three times with PBS and incubated at 37ºC in media alone for various times (t = 0, 15, 30, and 60 min) prior to fixation and labeling with an anti-giantin antibody. The *medial*-Golgi (green) reassembles by 60 min following GCA removal. **(B)** The effects of GCA on protein secretion are reversible. Vero cells were transduced with adenovirus expressing NPY-GFP and were treated with DMSO or GCA for 1 h at the indicated concentrations. In cells with compound washout, DMSO or GCA was removed as described in (A), and cells were incubated in media alone for 1 h. The amount of secreted GFP was assessed 2 h later by ELISA (see Methods). GCA treatment alone inhibits NPY-GFP secretion, while NPY-GFP secretion was restored to control levels following GCA removal. NPY-GFP, GFP construct bearing a neuropeptide Y secretion signal; O.D., optical density.
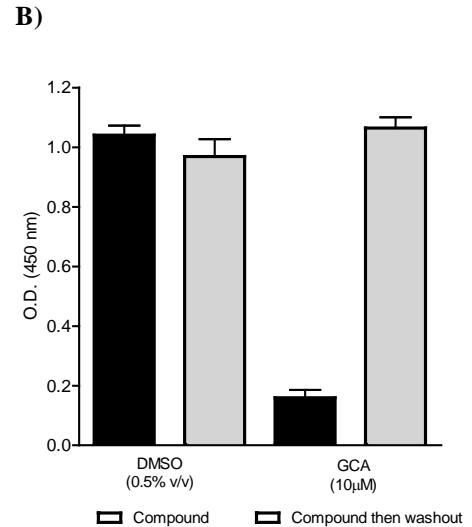
GCA depletes COPI at the *cis*-Golgi with no effect on AP-1 or GGA3 at TGN.

While the mechanisms behind the dramatic morphological changes induced by BFA have not been completely elucidated, the effects of BFA on both the *cis/medial*-Golgi and the TGN are in part due to the specific inhibition of ARFGEFs acting at both of these compartments [1,36]. BFA inhibits GBF1 activity within the Golgi by stabilizing an abortive complex between ARF1-GDP and the catalytic Sec7 domain of GBF1 [37], thereby disrupting COPI-mediated retrograde transport and resulting in a redistribution of Golgi contents into the ER. At the TGN, BFA forms a similar complex between ARF1-GDP and the TGN-localized BIG1/2, inhibiting anterograde transport beyond the TGN [38,39]. As a result of the delocalization of various vesicular transport mediators at the TGN, including clathrin coat and the adaptor proteins AP-1, AP-3, and GGA3 [22], the

TGN tubulates and subsequently fuses with a proportion of endosomes. The dual targeting by BFA of both Golgi- and TGN-localized ARFGEF activity thus appears to underlie many of its morphological effects.

Consistent with previous reports [40-42], COPI delocalization preceded Golgi collapse in BFA-treated cells: within 5 min following BFA treatment, β-COP staining was diffuse (Figure 6D), and this dispersal preceded morphologic changes to Golgi structure, as evidenced by juxtanuclear staining with the Golgi structural marker GM130 (Figure 6B). In addition, BFA almost immediately induced AP-1 (Figure 6E) and GGA3 (Figure 6F) dispersal from TGN membranes. Since compound GCA had similar effects on the *cis*/*medial*-Golgi to BFA (Figures 6A-B), we compared the effects of these compounds on COPI, AP-1 and GGA3 localization. GCA treatment equally resulted in a rapid loss of COPI from the Golgi complex prior to its collapse. However, AP-1 (Figure 6E) and GGA3 (Figure 6F) remained associated with the TGN until the Golgi and TGN began to disperse. Taken together, GCA and BFA have similar phenotypic effects on *medial*- and *cis*-Golgi which correlate with rapid dispersal of COPI from Golgi membranes. In contrast, these two compounds have differing morphologic effects on the TGN and distinct effects on AP-1 and GGA3 localization. This led us to investigate whether GCA specifically targeted a *cis*/*medial*-Golgi-localized molecule that could explain the compartment-specific effects.
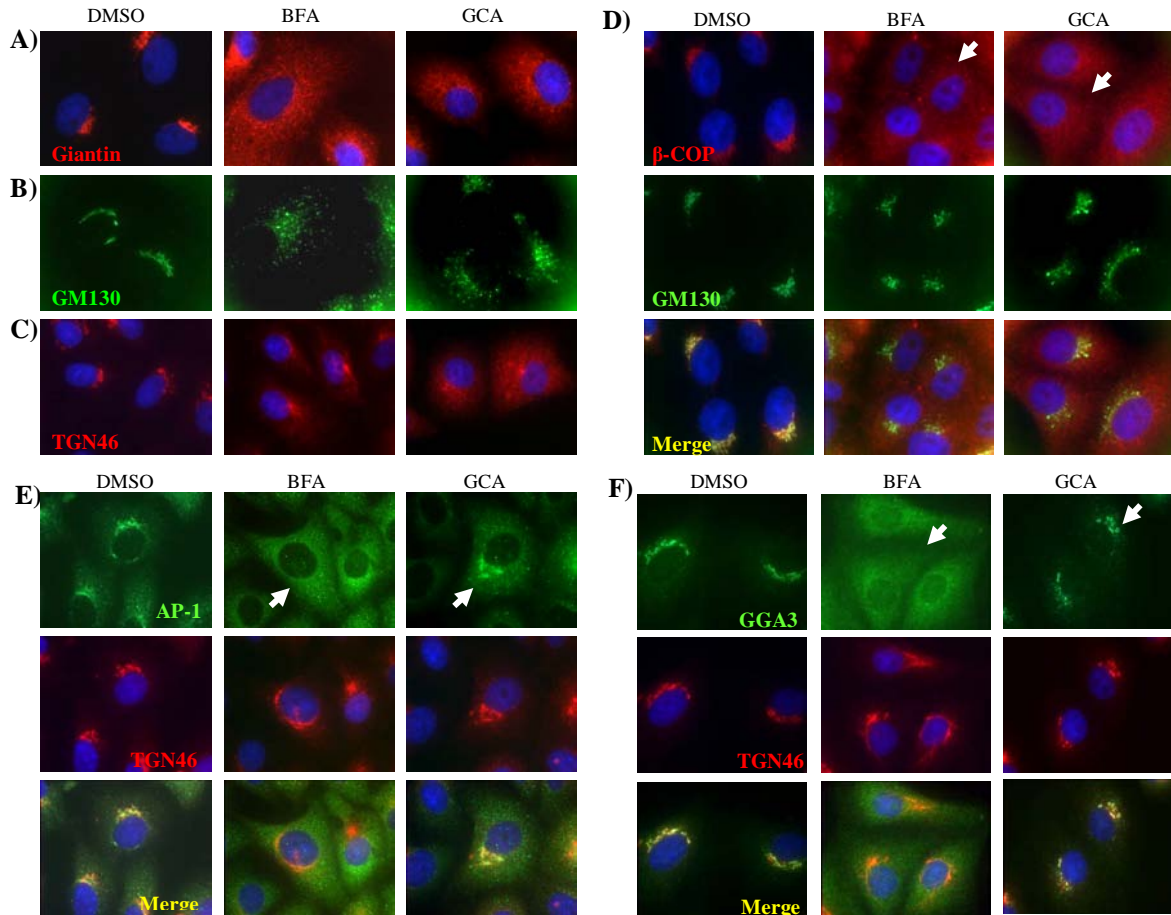
Figure 6. GCA disperses Golgi structure and inhibits recruitment of COPI coat while maintaining AP-1 and GGA3 coat recruitment to the TGN. (A-C) Vero cells were treated with DMSO (0.5% v/v), GCA (10 µM), or BFA (10 µg/mL) for 1 h prior to fixation and staining with the indicates antibodies (see Methods). GCA and BFA treatment resulted in the dispersal of giantin (*medial*-Golgi) and GM130 (*cis*-Golgi). **(D-F)** Vero cells were treated for 5 min with the indicated compounds (at concentrations used in A-C) and stained with the indicated antibodies. Both GCA and BFA cause rapid dispersal of COPI **(D)**, but, unlike BFA, GCA maintains AP-1 **(E)** and GGA3 **(F)** localization. Blue, nuclei.

GCA treatment phenotypically mimics overexpression of dominant negative GBF1.

Given GCA's distinct effects on *cis*/*medial*-Golgi, we hypothesized that GCA could be specifically targeting GBF1, the ARFGEF responsible for ARF1 activation and COPI recruitment to *cis*-Golgi membranes, while maintaining BIG1/BIG2-mediated activation and AP-1/GGA3 vesicle coat recrtuitment at the *trans*-Golgi (Figure 1). Consistent with this possibility, we found that expression of GBF1-E794K, a catalytically

inactive, dominant-negative GBF1 [9], resulted in dispersal of β-COP from Golgi

membranes and disruption of TGN and *medial*-Golgi structure (Figure 7A),

phenotypically similar to the effects of GCA. This GBF1 mutant was previously shown

to localize to the ER-Golgi intermediate compartment (ERGIC) [9]: indeed, wild-type

GBF1 colocalized with ERGIC-53, a marker for this compartment, following GCA

treatment (Figure 7B). Moreover, overexpression of the TGN-localized ARFGEF, BIG1,

partially reversed BFA's morphologic effects on the TGN (Figure 7C), consistent with

previous studies highlighting BFA's dual inhibition of ARFGEFs at the *cis*/*medial*- and
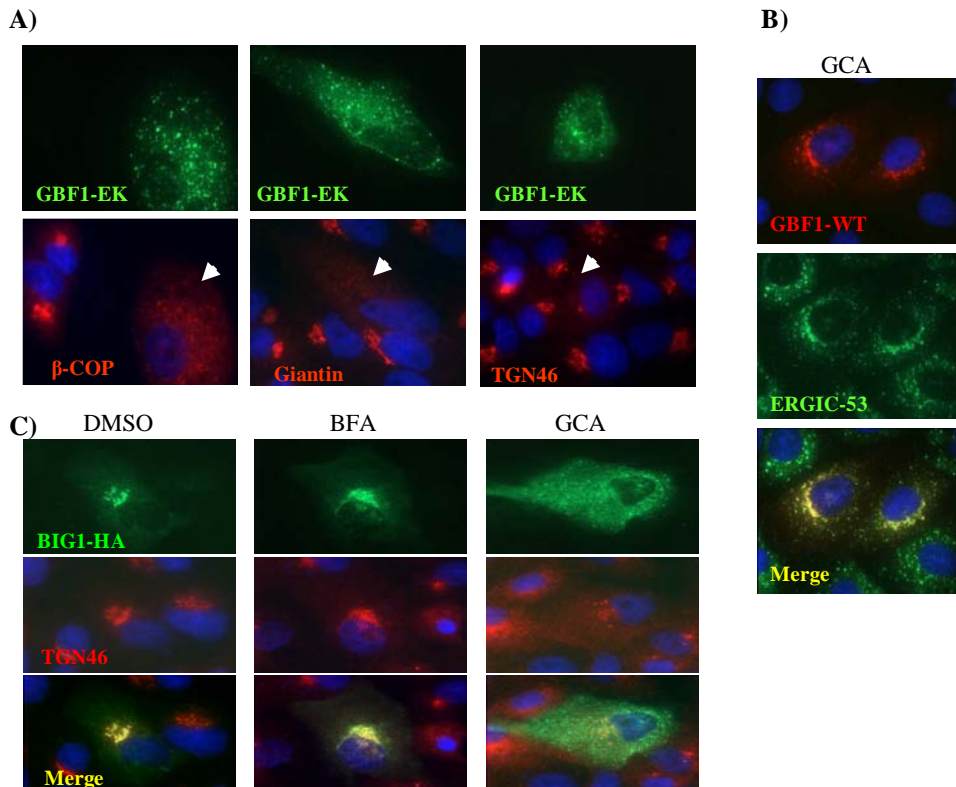
Figure 7. Treatment with GCA phenotypically resembles overexpression of inactive GBF1. (A) Vero cells overexpressing the GBF1-E794K (GBF1-EK) mutant show dispersed COPI, giantin, and TGN staining. Arrowheads indicate GBF1-EK-overexpressing cells. **(B)** GCA treatment (10 µM) of cells overexpressing wild-type GBF1 (GBF1-WT) causes trapping of GBF1 in the ERGIC, as shown by colocalization with the ERGIC marker, ERGIC-53. **(C)** BIG1 overexpression partially rescues the effects of BFA (10 µg/mL) on the TGN but fails to reconstitute TGN morphology in GCA (10 µM)-treated cells. ERGIC, ER-Golgi intermdiate compartment; Blue, nuclei.

trans-Golgi [25]. However, BIG1 overexpression did not rescue the morphological effects

on the Golgi in GCA-treated cells. These results point to a phenotypic similarity between

GCA treatment and overexpression of catalytically inactive GBF1 and support the

possibility that GBF1 is the target of GCA.

A single nucleotide substitution in canine GBF1 results in resistance to GCA[†].

In the course of examining the effect of GCA on several cell types, we found that

Madin-Darby canine kidney (MDCK) cells were resistant to GCA, as evidenced by a lack

of effect of this compound on Golgi morphology and β-COP localization (Figure 8A),

viability (not shown), and protein secretion (not shown). The Golgi apparatus of MDCK
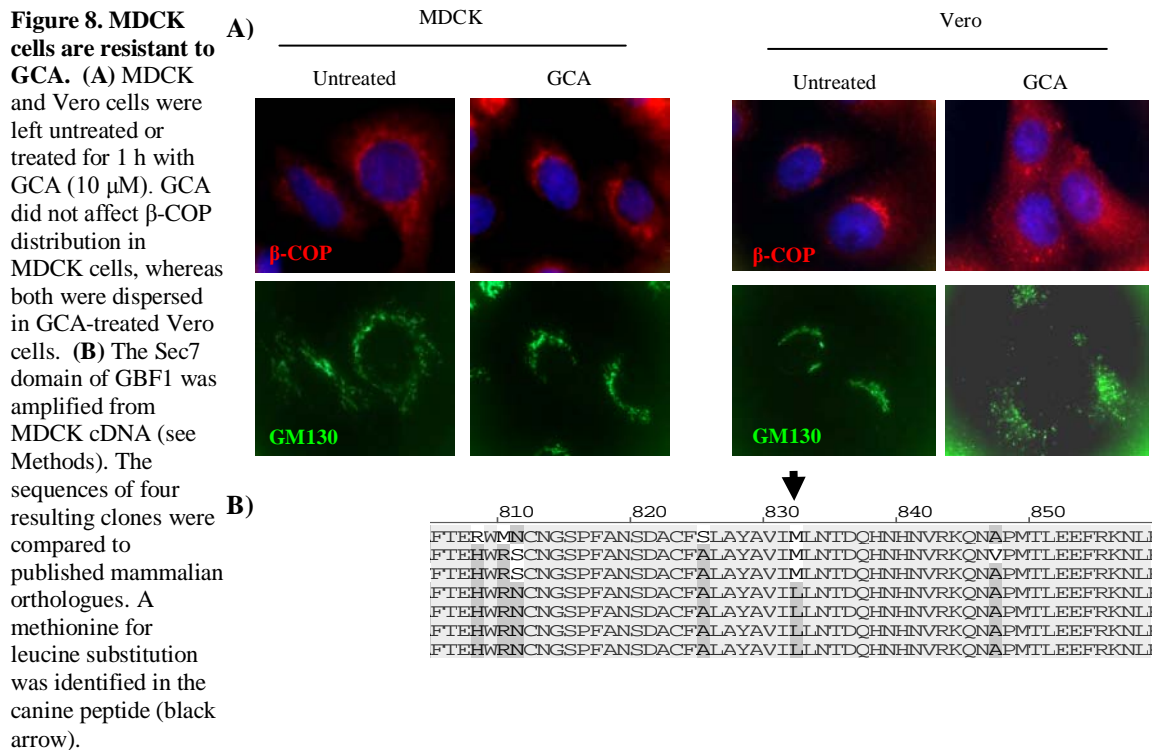
Figure 8. MDCK cells are resistant to GCA. (A) MDCK and Vero cells were left untreated or treated for 1 h with GCA (10 μM). GCA did not affect β-COP distribution in MDCK cells, whereas both were dispersed in GCA-treated Vero cells. **(B)** The Sec7 domain of GBF1 was amplified from MDCK cDNA (see Methods). The sequences of four resulting clones were compared to published mammalian orthologues. A methionine for leucine substitution was identified in the canine peptide (black arrow).

cells has also been reported to be resistant to the effects of BFA[43-45]. Given that BFA is known to bind within the highly-conserved Sec7 domain of Golgi-associated ARFGEFs and that we suspected GBF1 to be the target of GCA, we examined the possibility that differences in the canine GBF1 Sec7 domain accounted for MDCK cell resistance to both compounds. We amplified, cloned, and sequenced the canine GBF1 Sec7 domain. Analysis of several independent clones revealed a leucine substitution for methionine at residue 832 of the full-length protein (numbering corresponds to the human GBF1 sequence). Comparison with all other mammalian GBF1 homologues revealed this substitution to be unique to the canine gene (Figure 8B). Interestingly, mutagenesis of the corresponding methionine to leucine in the yeast ARFGEF homologue Gea1 and the human GBF1 resulted in resistance to BFA[32, 37,46].

The M832L substitution was introduced into the hamster GBF1, and the effect of its expression on GCA susceptibility was examined in transfected cells. Vero cells expressing this mutant were highly resistant to GCA, as evidenced by maintenance of COP localization, TGN morphology, and *cis*-Golgi structure, even at compound concentrations as high as 100 μM (Figure 9). As described later,
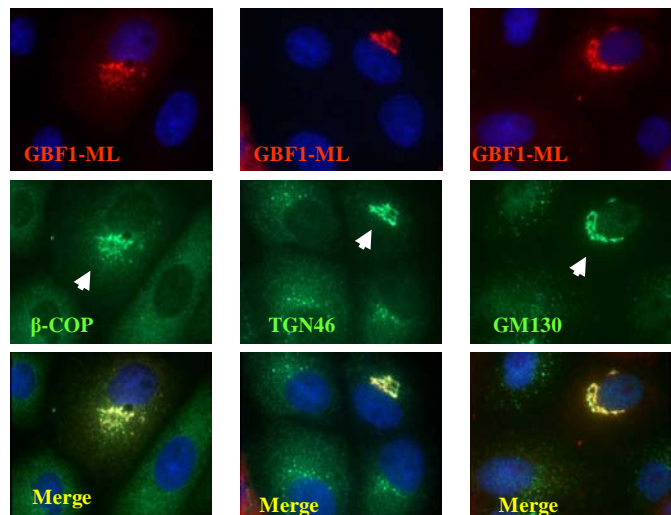
Figure 9. Overexpression of the GBF1-ML mutant protects against GCA's effects on Golgi morphology. Vero cells were transiently transfected with GBF1-M832L (GBF1-ML) and treated for 1 h with GCA (100 μM) prior to staining with the indicated antibodies. GCA has little to no effect on Golgi morphology in cells overexpressing GBF1-ML (arrowheads).

expression of GBF1-M832L rescued the functional effects of GCA on secretion and on

retrograde toxin transport. The ability of this mutant to fully protect Vero cells against

the phenotypic and functional effects of this compound indicate that GCA specifically

targets GBF1 and does not have evident "off-target" effects.

Molecular modeling of GCA selectivity for GBF1[†]

The results presented thus far suggest that GCA has high selectivity for GBF1 and

does not affect BIG1. The mechanism of GCA specificity for GBF1 was investigated by
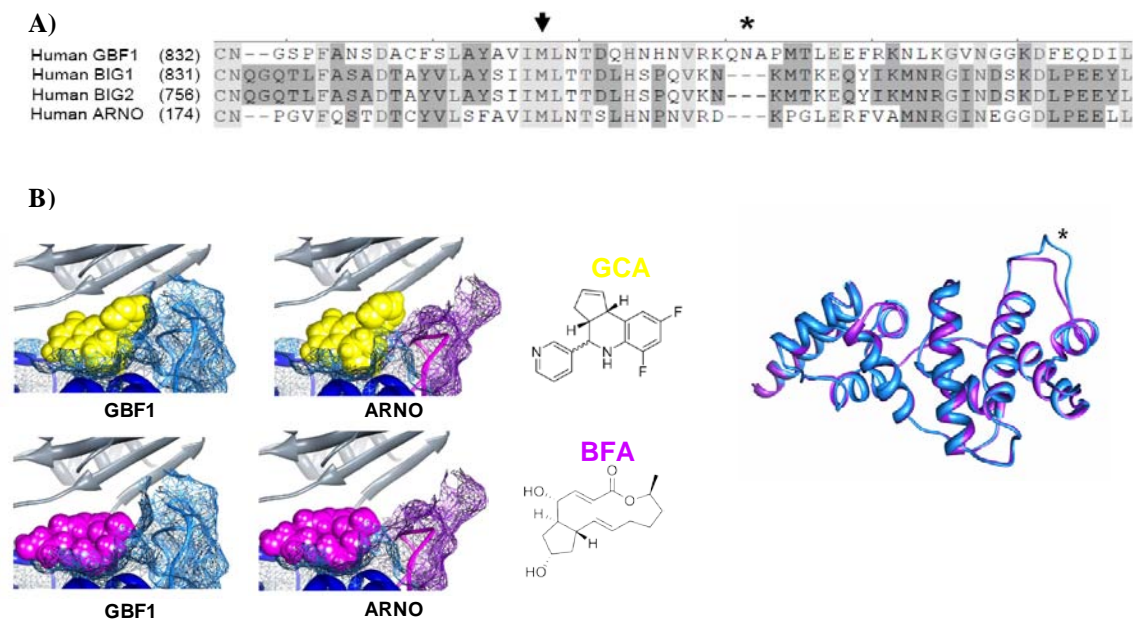
Figure 10. Molecular modeling of the potential GCA-GBF1 interaction identifies a tripeptide loop that could account for GCA's selectivity for GBF1. **(A)** Sequence alignment of the Sec7 domains of various human ARFGEFs identifies the M832 residue (arrowhead) and a tripetide loop (asterisk) present in GBF1 but absent from the other human ARFGEFs. **(B)** (left) GCA (yellow) and BFA (magenta) were docked onto the BFA binding pocket on GBF1 (blue) and ARNO (magenta). GCA, but not BFA, contacts a tripeptide loop on GBF1 that is absent in ARNO. The structures of GCA and BFA are also provided (middle panel). (right) The GBF1 Sec7 domain (residues 693 to 887) was threaded onto the previously reported ARNO-ARF1-BFA complex. Only the Sec7 domains of GBF1 (blue) and ARNO (purple) are shown. The asterisk highlights the tripeptide loop on GBF1 that is lacking in ARNO.

[†] Molecular modeling of the GCA-GBF1 interaction was carried out by Badry Bursulaya and Nathanael Gray. Functional characterization of the GBF1 loop mutants was carried out by David Haslam, and the following section highlights those findings.

molecular modeling and site-directed mutagenesis. The GBF1 Sec7 domain was

modeled in complex with ARF1 using the published structure of the ARF1-ARNO-BFA

complex[47]. Although there is considerable sequence divergence between GBF1 and

BIG1/BIG2 (Figure 10A), the predicted tertiary structure of the GBF1 Sec7 domain is

very similar to that of ARNO (Figure 10B). When the ARNO-ARF1 and predicted

GBF1-ARF1 complexes were compared, the BFA-interacting regions of the interfacial

cleft were virtually identical. Nevertheless, the observation that the GBF1-M832L

mutant was resistant to both BFA and GCA suggested that these compounds may bind

within the same GBF1-ARF1 interfacial region. When GCA was docked into this

pocket, it was found to extend past the BFA-binding region to contact a tripeptide loop

that exists in GBF1 and is lacking in other ARFGEFS, including ARNO, BIG1 and BIG2

(Figure 10B, asterisk).

The contribution of the GBF1 tripeptide extension to GCA susceptibility was

investigated by mutagenesis. Deletion of residues 845 to 848 or substitution of alanines

for all three residues resulted in resistance to GCA, as indicated by the ability of these

mutants to maintain Golgi morphology in the presence of the compound (Figure 11A).

However, as expected, these mutants remained susceptible to BFA, as this loop lies

outside the BFA-binding pocket and would not be expected to contribute to BFA

susceptibility (Figures 10B and 11A). Further mutagenesis of individual residues

revealed that substitution of alanine for arginine 843, glutamine 845 or asparagine 846

resulted in loss of susceptibility to GCA (Figure 11B) while none of these residues were

required for BFA susceptibility (not shown). Lysine 844, which protrudes from the

opposite side of the GBF1 loop, did not affect GCA susceptibility. In summary, these

results reveal that GCA susceptibility is dependent upon residues within a tripeptide found within the GBF1 Sec7 domain.

A)

B)
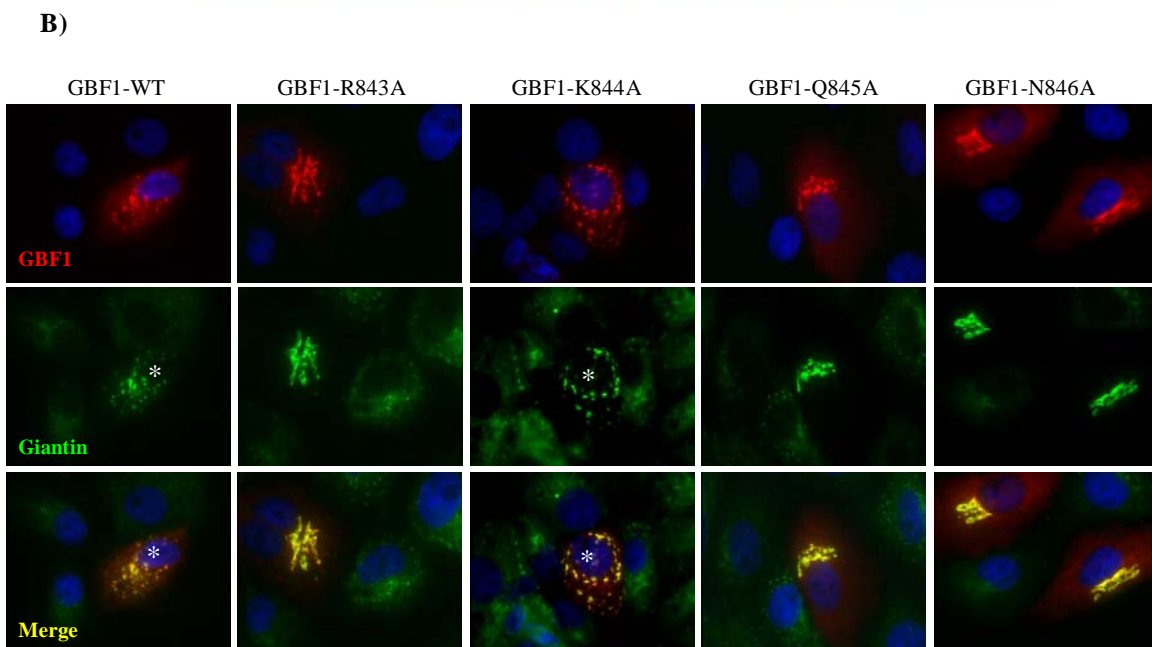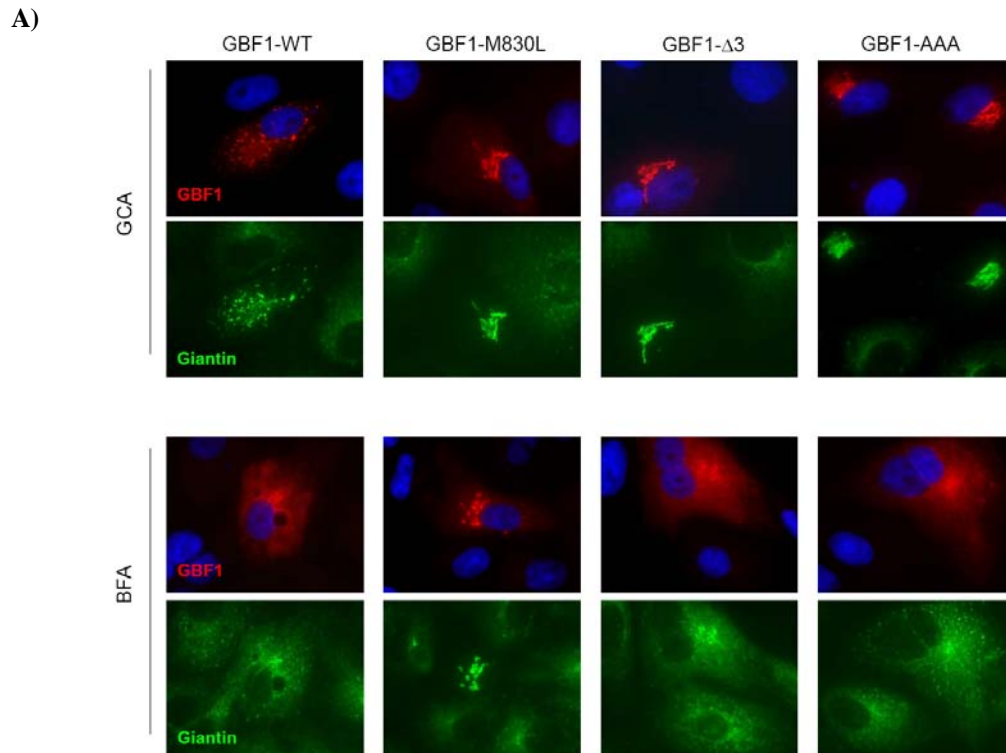
Figure 11. A distinct tripeptide loop in GBF1 accounts for GCA's selecticvity for GBF1. **(A)** Vero cells were transfected with wild-type GBF1 (GBF1-WT) or GBF1 mutants prior to a 1-h treatment with GCA (10 µM) or BFA (10 µg/mL). Cells overexpressing the GBF1-M830L mutant (Figure 9) or the loop mutants (GBF1-Δ3 and GBF1-AAA) are protected against the effects of GCA on the Golgi. Overexpression of the loop mutants shows no protection against the effects of BFA. **(B)** Site-directed mutagenesis of specific residues within the GBF1 tripeptide loop shows that R843, Q845, and N846 are critical to GCA susceptibility, while K844 appears to not be involved in binding to GCA. GBF1-Δ3, GBF1 mutant lacking the tripeptide loop; GBF1-AAA, GBF1 mutant with tripeptide replaced with three consecutive alanine residues (see Methods). Blue, nuclei.

GCA prevents GBF1-mediated GTP exchange on ARF1.

GBF1 activates ARF1 by catalyzing GDP/GTP exchange on Golgi membranes[8,11]. In order to assess the effect of GCA on GBF1 activity, *in vivo* ARF1-GTP levels were quantified in cells treated with either BFA or GCA. This assay took advantage of the ability of immobilized GGA3 to specifically pull down ARF1-GTP from cellular extracts[48]. GCA treatment significantly reduced levels of ARF1-GTP, with an approximate 33% decrease compared to DMSO-treated controls (Figure 12A). BFA, on the other hand, reduced ARF1-GTP levels to nearly 25% of control levels. This is consistent with BFA's more promiscuous effects on ARFGEFs at the *cis/medial*-Golgi and TGN compared to GCA's more specific targeting of GBF1.

To confirm that the observed decrease in ARF1-GTP levels were specific to GCA inhibition of GBF1, cells were transduced with an adenoviral construct expressing the previously identified GBF1-ML mutant (Figure 9; see Methods). Overexpression of the GCA-resistant GBF1-ML mutant restored ARF1-GTP levels in GCA-treated cells to control levels (86%) but had a marginal effect on restoring ARF1-GTP levels in BFA-treated cells (45%). Because adenoviral transduction did not result in overexpression in 100% of the cells (Figure 12B), overexpression of the GBF1-ML mutant was likely unable to completely restore ARF1-GTP to control levels. Nonetheless, overexpression of a GCA-resistant GBF1 mutant attenuated GCA's inhibitory effect on GBF1-mediated GTP exchange on ARF1. Moreover, the ability to rescue ARF1-GTP levels was

93

dampened in BFA-treated cells, presumably because BFA targets ARFGEFs besides

GBF1. Together, these results further confirm that GCA specifically targets GBF1 and

inhibits this ARFGEF's GDP/GTP exchange function. More importantly, these results

provide an estimate of the relative contribution of GBF1 and other ARFGEFs on ARF1

activation. These data would suggest that, in Vero cells growing under tissue culture

conditions, GBF1 accounts for approximately 30% of activated ARF1 and BIG1/BIG2

for 45%, with the remainder attributed to BFA-resistant ARFGEFs.

A)

Figure 12. GCA specifically inhibits GBF1-mediated activation of ARF1. **(A)** Vero cells left untransduced (No transduction) or transduced with an adenoviral construct overexpressing the GBF1-ML mutant were treated with DMSO (0.5% v/v; None), BFA (10 µg/mL), or GCA (10 µM) for 1 h. Intracellular ARF1-GTP levels were assessed (see Methods). Percentages indicate band intensity as a percentage of DMSO-treated controls. Graphs indicate mean (±S.D.) from three independent experiments, and statistical analyses are provided in Methods. **(B)** Vero cells were transduced with an adenoviral construct overexpressing GBF1-ML (GBF-1) prior to a 1-h treatment with GCA (10 µM). Cells were subsequently stained with antibodies against the HA epitope (red) and giantin (green). Approximately 85% of transduced cells express detectable GBF1-ML. Blue, nuclei.

B)

94
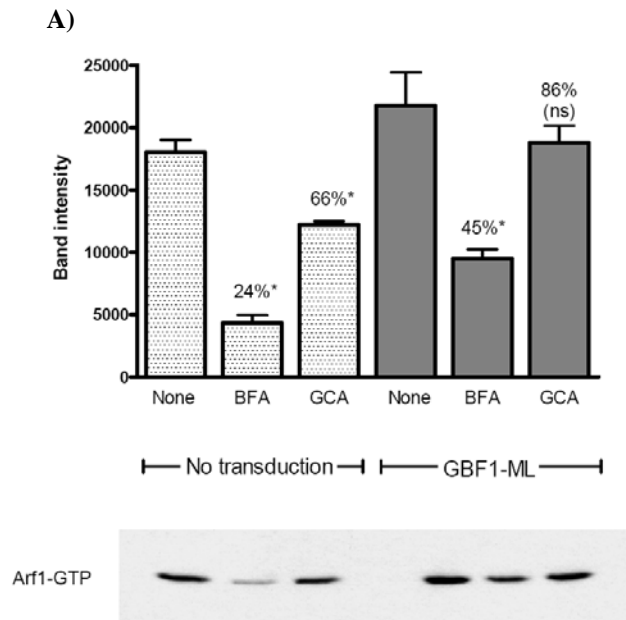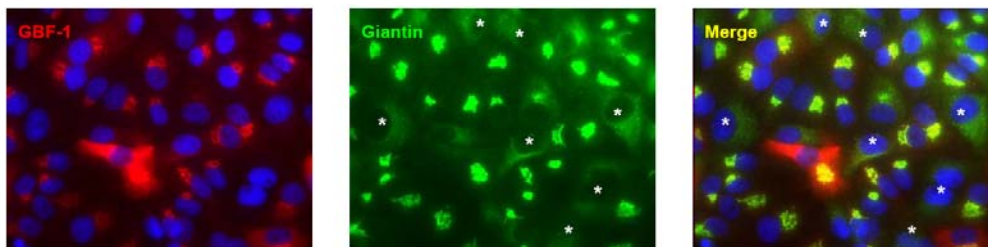
GBF1 inhibition arrests protein secretion[†]

Having demonstrated that GCA was a specific inhibitor of GBF1 function, we used this compound to examine the role of GBF1 in secretory transport. Previous studies with a dominant negative mutant indicated that GBF1 function was required for maturation of ER-Golgi intermediate vesicles to a transport-competent state[10,11]. Recent studies with siRNA-mediated inhibition suggested that GBF1 was required for anterograde transport of membrane-anchored cargo but was not required for secretion of soluble molecules[10].

To assess the role of GBF1 in secretion of membrane-anchored proteins, we examined the effect of GCA on transport of a GFP-tagged, temperature sensitive VSV-G mutant, *ts*VSVG-GFP[49]. At the non-permissive temperature of 40^oC, this protein is retained and accumulates in the ER. Following a shift to the permissive temperature (32^oC), *ts*VSVG-GFP transits through the ERGIC to the Golgi and ultimately to the plasma membrane. Cells were transfected either with *ts*VSVG-GFP alone or co-transfected with plasmid encoding GBF1-WT or GBF1-M832L, and the fate of *ts*VSV-G was followed in GCA-treated cells. In untreated cells, *ts*VSVG-GFP was transported from the ER to Golgi within 60 min and was located predominantly at the plasma membrane by 4 h (Figure 13A). GCA treatment, however, caused *ts*VSVG-GFP to be partially retained in a reticular, ER-like distribution as well as in diffuse punctate structures. GBF1-WT overexpression did not overcome the block in *ts*VSVG-GFP secretion in GCA-treated cells, whereas co-transfection with GBF1-M832L restored *ts*VSVG-GFP transport to the plasma membrane.

[†] Experiments involving the effects of overexpression of a GCA-resistant mutant on protein secretion were carried out by David Haslam, and this section highlights those findings.

Expression of the GCA-resistant GBF1 loop mutants also restored transport of

(*ts*VSVG-GFP) to the plasma membrane in the presence of GCA (not shown). GCA

treatment did not completely block *ts*VSVG-GFP transport from the ER, as this protein

was also found in peripheral punctate structures after a 60-min incubation. These
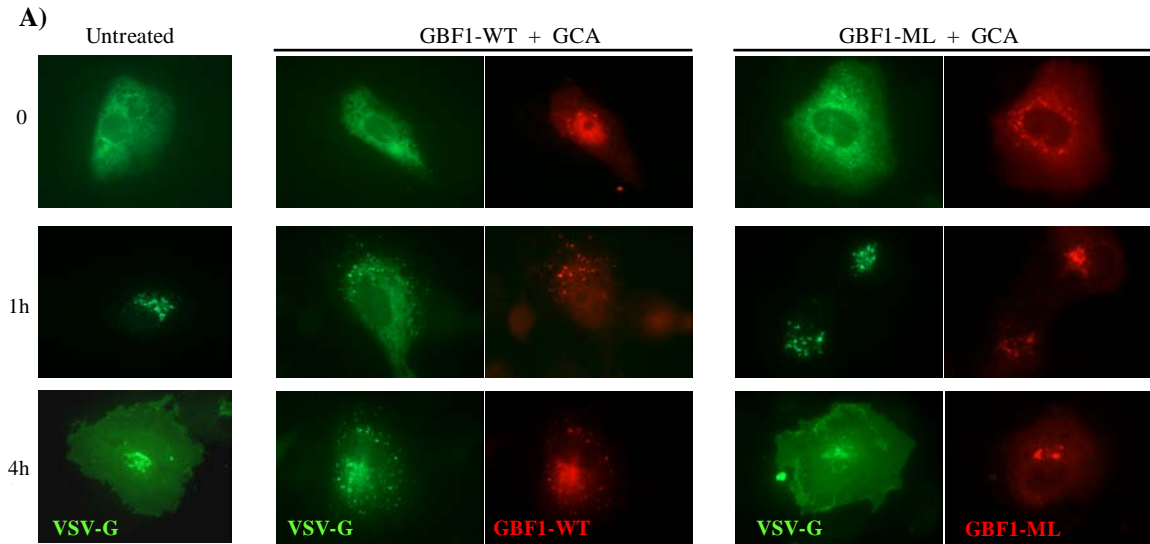
Figure 13. GBF1 mediates anterograde transport of membrane-bound proteins. (**A**) Transport of *ts*VSVG-GFP was monitored, at the various indicated times, in control cells (Untreated) and cells overexpressing wild-type (GBF1-WT) or GCA-resistant mutant GBF1 (GBF1-ML). Where indicated, cells were treated with GCA (10 µM) for 1 h prior to immunostaining. Overexpression of GBF1-ML restores VSVG trafficking to the cell surface. (**B**) VSVG-GFP is retained in the ERGIC following a 4-h treatment with GCA (10 µM). In Vero cells transfected with *ts*VSVG-GFP and treated with GCA, VSVG-GFP colocalizes with ERGIC-53-positive foci. Right panel indicates merged, magnified area of white box. Blue, nuclei.
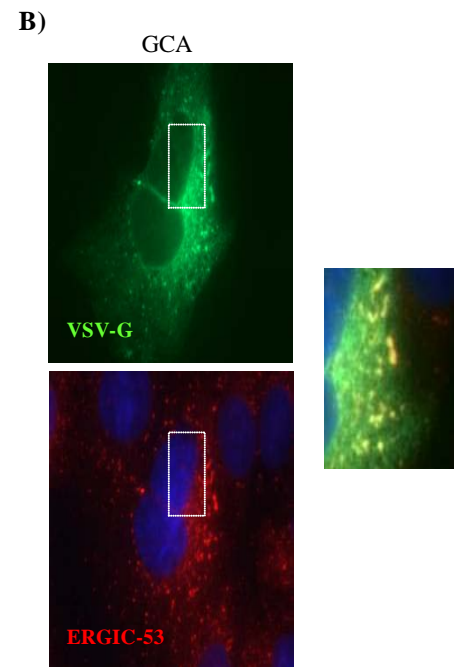
structures were identified as the ERGIC by their labeling with anti-ERGIC53, indicating that *ts*VSVG-GFP was capable of transport from the ER to the ERGIC in cells lacking GBF1 function. (Figure 13B).

To monitor the secretion of soluble cargo proteins, we expressed GFP bearing a neuropeptide Y secretion signal (NPY-GFP)[50]. This protein is secreted from Vero cells with a half life of approximately 60 min, as judged by pulse chase experiments[32]. Vero cells expressing NPY-GFP demonstrated markedly decreased GFP secretion in the presence of GCA (Figure 14). If inhibition of NPY-GFP secretion in GCA-treated cells was solely due to the inhibition of GBF1 function, then expression of the GCA-resistant GBF1-M832L mutant should restore protein secretion to levels seen with untreated cells. Whereas cells transduced with GBF1-WT failed to transport NPY-GFP to the plasma membrane in the presence of GCA, the expression of GBF1-M832L restored NPY-GFP transport through the Golgi to the plasma membrane (Figure 14). Together, these data
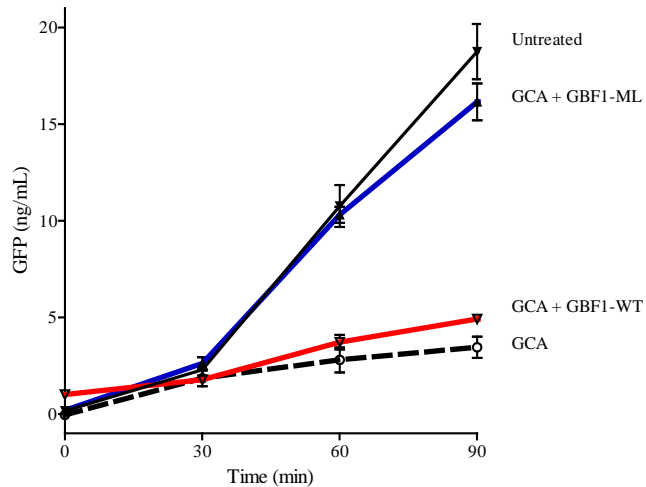
Figure 14. GCA inhibits secretion of soluble cargo. Cells were transduced either with adenovirus expressing NPY-GFP alone or co-transduced with NPY-GFP plus adenovirus expressing GBF1-WT or GBF1-ML. Cells were either left untreated or were exposed to GCA (10 mM) for 1 h. Secreted GFP concentration was assessed by ELISA (see Methods). GCA treatment decreases NPY-GFP secretion in untransduced cells (dotted), while overexpression of GBF1-ML (blue), but not GBF1-WT (red), restores NPY-GFP secretion to levels in untransduced, untreated cells (black).

97

indicate that GBF1 function is required for secretion of a soluble protein (NPY-GFP) as well as membrane-associated cargo (*ts*VSVG-GFP).

GBF1 is involved in retrograde toxin transport

The stepwise intracellular trafficking of bacterial toxins has been frequently used to probe host endocytic transport mechanisms[31]. STx transport to the TGN from endosomes can be quantified by assessing its sulfation by resident tyrosyl-protein sulfotransferases at the TGN[51,52]. We examined the effect of GCA on endosome-to-TGN transport using a STxB subunit that bears overlapping tyrosine sulfation sites (STxB-Sulf$_2$)[32]. Treatment with GCA markedly attenuated toxin sulfation (Figure 15A). Expression of GBF1-WT failed to rescue the transport of STxB-Sulf$_2$ to the TGN, while expression of GBF1-M832L completely restored toxin sulfation to control levels in GCA-treated cells. These results would suggest that GBF1 function is required for toxin transport from endosomes to the TGN, though we cannot rule out the possibility that inhibition of GBF1 prevents formation of a fully functional TGN to which STxB is targeted. We equally cannot rule out whether GCA alters the optimal pH required for sulfotransferase activity at the TGN.
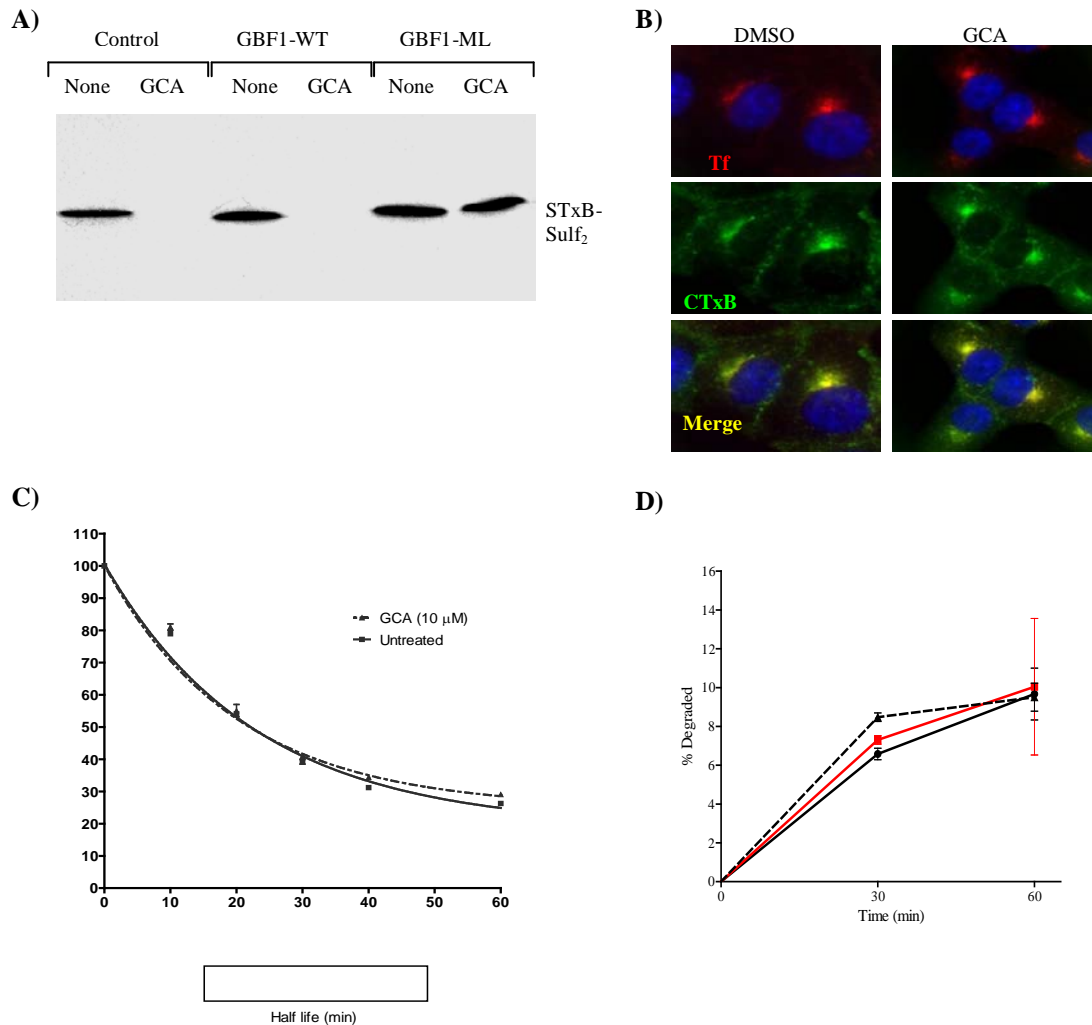
Figure 15. GCA impedes endosome-to-TGN transport of STx. **(A)** Transport of STx to the TGN was assessed by quantifying the degree of sulfation of a STxB construct bearing a tandem of sulfation sites (STxB-Sulf$_2$; see Methods). GCA treatment inhibited STxB-Sulf$_2$ sulfation, while overexpression of the GCA-resistant mutant GBF1-ML, but not wild-type GBF1 (GBF1-WT), restored it. **(B)** GCA does not affect toxin transport to early/recycling endosomes. Vero cells were treated with DMSO (0.5% v/v) or GCA (10 µM) for 1 h, and the transport of fluorescently-tagged cholera toxin B subunit (CTxB) and transferrin (Tf) was assessed at 22° C. GCA treatment has no effect on CTxB colocalization to Tf-positive endosomes. Blue, nuclei. **(C)** GCA treatment does not affect the kinetics of transferrin recycling. Vero cells were left untreated or were treated with GCA for 1 h. Cells were allowed to internalize AlexaFluor-488 labeled transferrin for 60 min. Fresh media containing quenching anti-AlexaFluor-488 antibodies were added, and at various times the cells were harvested and fixed (see Methods). Each time point represents triplicate data (mean ±S.D.). All data were fitted by nonlinear regression assuming one phase decay, and half-lives (in min; inset) were calculated using GraphPad Prism. **(D)** GCA treatment does not affect lysosomal degradation of bovine serum albumin (BSA). Vero cells were incubated with 1 µCi/ml [^{125}I]-BSA at 37°C in serum-free media containing no compound (untreated; solid line), BFA (10 µg/mL; red), or GCA (10 µM; dotted line). Supernatants were collected at 30 or 60 min, and TCA-soluble (degraded BSA) and –insoluble (undegraded BSA) counts were measured (see Methods). % Degraded refers to the percentage of degraded BSA (TCA-soluble counts) as a fraction of total BSA (TCA-soluble + TCA-insoluble counts). Radiolabeled Vero cells were also held at 4°C for 1 h prior to TCA precipitation of cell supernatants to account for BSA degradation in the absence of endocytosis. This value was subtracted from all samples prior to analysis. BFA, brefeldin A.

To rule out the possibility that GCA non-specifically inhibited endocytic transport

from the cell surface, we assessed the effects of endocytic transport of various ligands to recycling endosomes. Treatment with GCA did not affect accumulation of the cholera toxin B subunit (CTxB) in transferrin (Tf)-positive recycling endosomes at 22ºC (Figure 15B), a temperature shown to block endosome-to-TGN transport[53]. GCA treatment equally maintained the kinetics of transferrin recycling similar to untreated Vero cells (Figure 15C).

In addition, the degradation kinetics of radiolabeled bovine serum albumin was unaffected by GCA treatment, suggesting that generalized transport to lysosomes is unaffected in GCA-treated cells (Figure 15D). This observation was further supported by a lack of effect of GCA on LDL-BODPY transport to lysosomes by immunofluorescence (not shown). Together, these results suggest that GCA maintains endocytic transport to recycling endosomes and lysosomes.

GCA was initially identified in a high-throughput screen for its ability to inhibit the effects of STx on mammalian cells. Figures 15A-B indicate that retrograde toxin transport was arrested within the endocytic compartment. To determine whether the effects of GCA on toxin transport were due solely to GBF1 inhibition, we examined the ability of GBF1-M832L to restore toxin susceptibility to GCA-treated cells. Cells were transduced with the appropriate GBF1 constructs and treated with GCA. GCA strongly protected against STx in control cells and those transduced with GBF1-WT (Figure 16). In contrast, GCA was unable to protect against Shiga toxicity in cells overexpressing the GCA-resistant GBF1-M832L, indicating that the effects of GCA relied on GBF1 inhibition. Taken together, these results indicate that GBF1 function is not required for

transport of bacterial toxins to recycling endosomes, but this ARFGEF is required for retrograde transport of STx from endosomes to the TGN and Golgi.
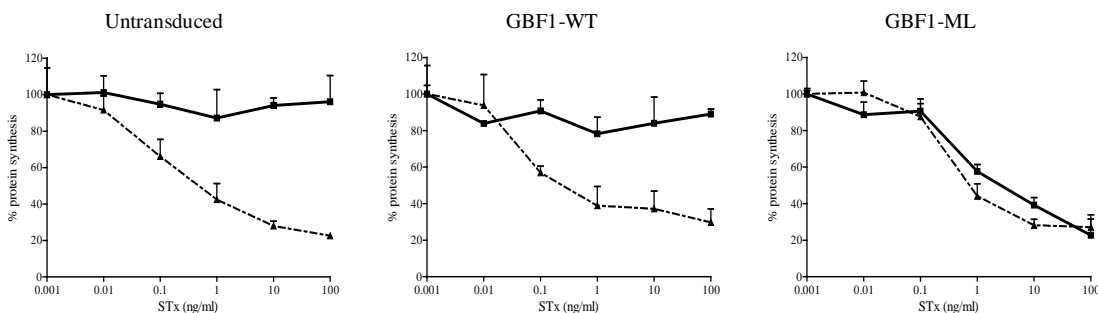
Figure 16. Overexpression of a GCA-resistant mutant restores STx susceptibility to Vero cells. Inhibition of Shiga toxicity by GCA is completely reversed in cells expressing GBF1-ML. Cells were either left untransduced or transduced with adenovirus expressing wild-type GBF1 (GBF1-WT) or a GCA-resistant GBF1 (GBF1-ML). Cells were then treated with either GCA (solid line) or no compound (dotted line) prior to exposure to increasing concentrations of STx. After a 4-h incubation, protein synthesis was assessed (see Methods). Data points represent triplicate data (mean ±S.D.) from one representative experiment.

DISCUSSION

We have described the identification and characterization of GCA, a potent, highly effective, and rapidly reversible inhibitor of intra-Golgi transport. Initial characterization of GCA revealed that it induced a BFA-like disruption of the Golgi. Unlike BFA, GCA specifically inhibited COPI coat recruitment to the *cis/medial*-Golgi while maintaining AP-1/GGA3 targeting to the TGN. The pleiotropic effects of GCA resulted from specific inhibition of the *cis/medial*-Golgi-localized ARFEGEF, GBF1. GCA thus represents a useful probe of the intracellular function of GBF1 in mediating vesicle transport and organelle integrity and will serve as a useful alternative to the more promiscuous transport inhibitor BFA.

The phenotypic effects of GCA were similar to those induced by expression of a catalytically inactive, dominant negative GBF1 (GBF1-E794K). Canine cells were found

101

to be resistant to the effects of GCA, and characterization of the canine GBF1 gene revealed a methionine for leucine substitution corresponding to residue 832 of the human GBF1. When introduced into the hamster GBF1, this substitution resulted in complete resistance to the phenotypic and functional effects of GCA. This residue is located within an alpha-helix of the Sec7 domain and forms part of a hydrophobic interfacial cleft that recognizes ARF1 in its GDP-bound state [7,54]. Interestingly, BFA binds within this cleft and substitution of methionine 832 to leucine results in BFA resistance[46]. Therefore, our finding that GBF1-M832L is also resistant to GCA suggests that these two compounds bind within the same interfacial cleft. However, unlike BFA, which inhibits BIG1 and BIG2 in addition to GBF1, GCA is highly specific for GBF1. Molecular modeling and mutagenesis studies revealed that a tripeptide loop present within the GBF1 Sec7 domain and absent from all other known ARFGEFS, accounts for the selectivity of GCA for its target. These structural findings may allow for the design of GCA analogues that specifically inhibit BIG1, BIG2, and related ARFGEFs.

We demonstrated that GCA inhibits ARF1 activation, and this effect is largely rescued by the expression of GBF1-M832L, indicating that GCA directly inhibits GBF1 function. We found that transport of *ts*VSVG-GFP was arrested in the ERGIC, indicating that GBF1 function was not required for exit of cargo from the ER but was required for transport past the ERGIC. These results are similar to those found with expression of a dominant negative GBF1 and by siRNA-mediated inhibition of GBF1 expression, which also found that GBF1 function was not required for exit of secreted molecules from the ER but was required for maturation of ER-Golgi transport intermediates and transport of *ts*VSVG-GFP past this compartment[55]. Inhibition of GBF1

102

function with GCA also blocked secretion of a soluble cargo protein. These results differ from a recent report that siRNA-mediated inhibition of GBF1 expression had no effect on the secretion of soluble cargo, though transport of transmembrane proteins was impaired[10]. Golgi morphology in these cells was relatively mildly affected, which was unexpected given the dramatic effects of BFA treatment, expression of dominant inhibitory GBF1, or inhibition of COPI expression or function. From these siRNA studies, GBF1 function and COPI recruitment were speculated to have relatively little role in secretion of soluble proteins and in the maintenance of medial-Golgi structure. We propose instead that the relatively milder effects of siRNA on Golgi morphology and secretion of soluble proteins resulted from less than complete inhibition of GBF1 expression.

The role of GBF1 in retrograde transport to the Golgi has not previously been investigated. We show that GCA treatment maintains endocytic transport from the cell surface to endosomes and lysosomes, suggesting that GBF1 function is not required for these pathways. However, GBF1 inhibition trapped bacterial toxins at the endosomal level, and these vesicles were unable to fuse with a dispersed TGN. These findings indicate that GBF1 function is required for endosome-to-TGN transport. It is currently not known whether GBF1 function is essential to maintenance of an intact TGN to which endosome-derived vesicles can be targeted. Inhibition of GBF1 at the *cis*/*medial*-Golgi could impede anterograde transport of soluble and membrane-bound proteins crucial for TGN membrane homeostasis. These possibilities would be amenable to investigation using GCA.

Small molecule inhibition offers several advantages over RNAi or transfection with dominant-negative mutants, most notably in its ability to rapidly inhibit protein function in essentially all treated cells independent of transfection efficiency. A reversible small molecule inhibitor offers the ability to dynamically monitor the role of protein function and affords the opportunity to examine mechanisms of recovery from perturbations in protein function. Moreover, RNAi cannot completely inhibit protein expression, and in some cases small amounts of residual protein are sufficient to maintain normal function and phenotype. However, an inherent caveat shared by RNAi, dominant negative expression, and small molecules is the possibility of non-specific or "off-target" effects. Demonstrating the specificity of small molecules can be relatively difficult, as these compounds often exhibit non-specific effects at higher concentrations. In the case of RNAi, specificity is often proven by expressing an siRNA-resistant version of the targeted gene and demonstrating reversal of the phenotypic effects. We have taken a similar approach to prove that GCA is highly specific for GBF1. Expression of the GBF1-M832L mutant renders cells completely resistant to the effects of this compound, indicating that the phenotypic and functional effects of GCA do not result from non-specific effects.

Phenotypic screens aimed at identifying inhibitors of endocytic and secretory transport have uncovered small molecules that are highly useful probes of intracellular transport. Exo1[56] and Exo2[57] were uncovered from an image-based screen for inhibitors of secretory transport and exhibited Golgi-disruptive effects. Studies with Exo2 revealed that treatment with this compound ablated the Golgi but maintained TGN integrity and suggested the existence of an alternative pathway for cholera toxin

transport. Exo1 exhibited BFA-like effects on ARF1 dissociation from Golgi membranes, but unlike BFA, it did not interfere with ARFGEF activity. The molecular targets of Exo1 and Exo2 have yet to be elucidated. A high-throughput screen for inhibitors of dynamin GTPase activity discovered dynasore, a particularly useful probe for studying the dynamics of dynamin-mediated clathrin coat formation[58,59]. Similarly, secramine was identified as a novel tool for dissecting the functions of Cdc42 and possibly other RhoGTPases[60]. Finally, SecinH3, an inhibitor of the cytoadhesins, was recently identified, and its use revealed a role for these BFA-insensitive ARFGEFs in insulin signaling[61]. Together, these studies underscore the utility of small molecules as alternative biological probes for dynamic intracellular processes.

The discovery of a small molecule inhibitor of GBF1 allowed us to demonstrate an essential role for GBF1 in anterograde and retrograde traffic through the Golgi and its requirement for maintenance of Golgi and TGN structure. Given its specificity, efficacy, and reversibility, GCA provides a unique and powerful means of elucidating the mechanisms underlying assembly and transport within the Golgi.

Diseases Research (MRCE) and an Investigators in Microbial Pathogenesis Award from the Burroughs Wellcome Foundation.

MATERIALS AND METHODS

Antibodies and reagents

Compound GCA was purchased from ChemDiv, reconstituted to 10 mM in DMSO, and stored at -20°C. Chemical characterization of GCA, along with validation of the structural isomers responsible for its activity, have been reported[62]. Shiga-like toxin 1 (List Biological Laboratories), trans [^{35}S] (MP Biomedicals), and [^{35}S]O$_4$ (American Radiolabeled Chemicals) were also used. Antibodies included rabbit anti-giantin polyclonal (Covance), rabbit anti-hemagglutinin polyclonal (Sigma-Aldrich), mouse anti-GM130 (BD Transduction), rabbit anti-human TGN38 (Santa Cruz), rabbit anti-βCOP (ABR), mouse anti-ERGIC-53 (Axxora), and fluorescently-labeled secondary antibodies (Molecular Probes). DMSO, BFA, cytochalasin B, and nocodazole were from Sigma.

Cell Lines and Cell Culture.

Vero (African green monkey kidney, CRL-1587), MDCK (Madin-Darby canine kidney, CCL-34), and 293A-HEK (Human embryonic kidney, CRL-1573) cells were obtained from the American Type Tissue Culture Collection (Manassas, VA). 293A cells were obtained from Invitrogen. Vero cells were maintained in DMEM supplemented with 10% fetal calf serum and 1% nonessential amino acids at 37°C under 5% CO$_2$. MDCK cells were maintained in EMEM supplemented with 10% fetal calf serum and 1%

nonessential amino acids at 37^oC under 5% CO_2. 293A cells were maintained in EMEM

with 10% heat-inactivated horse serum.

Transient transfections were performed using Lipofectamine 2000 (Invitrogen) in

OptiMem media, following the manufacturer's recommendations. Following overnight

incubation at 37^oC under 5% CO_2, cells were collected into chamber slides (Lab-Tek,

Campbell, CA) or appropriate dishes and incubated for 24 h before experimentation.

Radioactive protein synthesis assay

The luciferase-based high-throughput screen to identify inhibitors of STx

trafficking has previously been described[32,63]. Similarly, confirmation of positive hits

from the ChemDiv4 library screen was assessed by a previously described radioactive

[^{35}S] incorporation assay adapted to a multi-well format[32]. Briefly, Vero cells cultured

overnight at 37^oC and 5% CO_2 in 96-well plates (2.5×10^4 cells/well) were treated with

0.5% DMSO (v/v) or media containing GCA or BFA at the indicated concentrations.

Following a 0.5-h incubation at 37^oC, toxin was added to wells in triplicate, and cells

were shifted to $37^{\circ}C$ for an additional 4 h. Medium containing trans [^{35}S] label at 10

μCi/mL was added, and cells were incubated at 37^oC for 45 min, washed with PBS (pH

7.4), and lysed (1 mg/mL BSA, 0.2% deoxycholic acid, 0.1% SDS, 20mM Tris pH 7.4) at

4^oC for 12 h. Proteins from the lysed cells were TCA-precipitated (final concentration

15%), transferred to multi-screen HA plates (Millipore), and the filters were washed with

ice-cold 20% TCA. Filters were then removed from the plate, placed in 2 mL Bio-Safe

II scintillation fluid (RPI), and [^{35}S] incorporation quantitated using a beta counter

(Beckman). Independent experiments were performed at least three times for GCA and BFA, and data were analyzed using Prism v4.0 software (2003).

Immunofluorescence.

For all immunofluorescence experiments, cells were fixed in 4% paraformaldehyde in cold PBS, permeabilized with 0.1% Triton X-100 in PBS, blocked, then probed with primary and secondary (Alexa Fluor 488 or 594-labeled donkey anti-IgG) antibodies diluted in blocking buffer (DMEM containing 10% fetal calf serum plus 1 mg/mL BSA). Cells were rinsed thoroughly in PBS prior to mounting in SlowFade Gold reagent containing DAPI (Molecular Probes). Fluorescence imaging used epifluorescence (Zeiss) microscopy.

Toxin and transferrin internalization.

For CTxB and transferrin trafficking experiments, Vero cells grown in chamber slides (2.5×10^4 cells/chamber) were treated with serum-free medium containing DMSO, GCA, or BFA at the indicated concentrations and times at 37°C. Following the binding of toxin and transferrin at 4°C, cells were shifted to 19°C for 1 h to allow for toxin internalization. Cells were processed for immunofluorescence as described above.

Expression and trafficking of tsVSVG-GFP.

Vero cells were transiently transfected with VSVG-GFP *ts*045 using Lipofectamine 2000 (Invitrogen). In some experiments, cells were co-transfected with GBF1-HA WT or M832L plasmids. After overnight incubation at 37°C in 5% CO_2, cells

were collected and placed into chamber slides (Lab-Tek) for an additional 8-10 h at 37°C before their transfer to 42°C for 12-16 h. Cells were then treated with cycloheximide (100 µg/mL) to prevent *de novo* protein synthesis and either no compound, GCA (10 µM), or BFA (10 µg/mL), then transferred to 32°C. Cells were fixed following various incubation times at 32°C. Fixation, permeabilization, staining, and imaging were performed as described for immunofluorescence experiments.

Cloning and sequence analysis of canine GBF1 Sec7 domain

Total RNA was isolated from approximately 10^7 MDCK cells by silica membrane binding (RNeasy, Qiagen), and contaminating chromosomal DNA was removed by DNase treatment (Qiagen). The cDNA was prepared from isolated RNA with random primers and SuperScript II reverse transcriptase (Invitrogen) according to the manufacturer's instructions. The Sec7 domain of the canine GBF1 gene was amplified from MDCK cDNA using primers 5'-cgattttcctgtctcctgccagatccacggg-3' and 5'-ccacacatagttctcccgaaccaagcc-3' and the resulting product cloned into pcDNA3.1/V5/His. Four resulting clones were sequenced and compared to their human, hamster, and murine counterparts.

Site-directed mutagenesis

The hamster GBF1 cDNA (a gift from Paul Melançon, University of Alberta, Edmonton, AB) was used as template for constructing HA-tagged wild-type and mutant cDNA. GBF1-HA was generated by PCR using primers GBF1-HA (5'-gccgcgctagcctgaggcat agtcaggcacgtcataaggatagccgttgacttcagaggtgggaatagggtctgtag-3')

109

and the upstream GBF1 primer (5'-gacaggtttgccaagatggtggataagaatatt tacatc-3'). The resulting PCR product was cloned into pcDNA3.1D/V5-His-TOPO (Invitrogen) under control of the cytomegalovirus (CMV) promoter. The insert was sequenced to ensure its fidelity.

The GBF1 mutants were generated using the QuikChange II XL Site-Directed Mutagenesis Kit (Stratagene). Mutagenic primers were E794K sense (5'gccttccgtttgcccgggaaggcaccagttattcacaggttgc-3'), E794K antisense (5'gcaacctgtgaataactggtgccttcccgggcaaacggaaggc-3'), M832L sense (5'ggcctatgctgtcatcttgcttaatactgaccagc-3'), and M832L antisense (5'gctggtcagtattaagcaagatgacagcataggcc-3'). Mutant clones were sequenced to ensure their fidelity.

Preparation of adenovirus expressing GBF1-HA and GBF1-HA mutants

Adenovirus expressing GBF1-HA constructs, canine Arf1 switch mutants, and NPY-GFP were prepared by cloning the appropriate cDNA into plasmid pENTR-11, then transferring the cDNA insert to plasmid pAD/CMV/DEST using the Clonase II reaction (all from Invitrogen). Crude adenoviral stocks were isolated from transfected 293A cells, which were then used to generate high titer stocks. Each was aliquoted and frozen at -80°C until used for transduction. Control experiments were performed with each stock to determine conditions resulting in optimal transduction efficiency.

NPY-GFP secretion assay

The NPY-GFP assay was similar to that previously reported[32], with slight modifications. Briefly, 10^6 Vero cells were transduced overnight at 37ºC in 5% CO_2 with pAD-NPY-GFP. Cells were then washed, trypsinized, and seeded into a 96-well plate (~1 x 10^4 cells/well). The next day, the cells were washed once with PBS then incubated at 37ºC with media containing DMSO, BFA (10 µg/mL), or GCA (10 µM). Supernatants were collected at various times thereafter. GFP quantitation was performed by ELISA using anti-GFP coated plates (Pierce) and rabbit anti-GFP in solution. Mean absorbance for control wells containing DMEM alone were subtracted from sample wells. Calculation of GFP concentration was performed by interpolation from a recombinant GFP (rGFP; Boehring Manneheim) standard curve.

ARF1-GTP pulldown assay

Human ARF1 bearing a carboxy-terminal HA epitope tag was amplified from a human liver cDNA (Invitrogen) using flanking primers 5'-gtccttccacctgtccacaagcatgggg-3' and 5'-ccgcgctagcctgaggcatagtcaggcacgtcataaggatagccgttcttctggttccggagctgattg gacagcc-3'. The resulting product was ligated into plasmid pCDNA3.1/V5/His. Nucleotide sequencing was performed to verify fidelity of the HA-tagged wild-type cDNA. Following overexpression, the localization of ARF1 was tracked by indirect immunofluorescence using a mouse anti-V5 (Invitrogen) primary antibody, followed by staining with the corresponding secondary antibody.

The VHS and GAT domains from human GGA3 were amplified from a human cDNA library using primers 5- ggccgaattcatggcggaggcggaaggggaaagc-3' and 5'-

111

ccggctcgagtcagtcaggcagggttaaggtagccacctcg-3' The resulting product was initially cloned into plasmid pcDNA3.1/V5/His and sequenced to ensure its fidelity. The product was then released by digestion with EcoRI and XhoI and ligated into similarly digested plasmid pGEX-6p1. Expression of the recombinant GGA3-GST protein was induced by the addition of IPTG and the protein purified from crude bacterial lysates on a GSTrap column (Pharmacia). The protein was dialyzed into 50 mM Tris pH 7.5 plus 100 mM NaCl and used in ARF1 pulldown assays using the protocol of Santy and Casanova[48].

Vero cells were seeded in 10-cm^2 dishes and transduced with adenovirus expressing ARF1-V5 alone, or co-transduced with virus expressing ARF1-V5 and virus expressing GBF1-ML-HA. After overnight incubation, the cells were washed, trypsinized, and seeded into three 25- cm^2 flasks each. The following day, monolayers were treated at 37°C for 45 min with media alone, or media containing BFA (10 µg/mL) or GCA (10 µM). The cells were then washed with cold PBS and scraped into 1 mL lysis buffer (50 mM Tris pH 7.6, 100 mM NaCl, 2 mM MgCl$_2$, 1 % SDS, 1 % Triton X-100, 10% glycerol,). To each sample was added 48 µg of GGA-GST bound to 30 µL of glutathione agarose (Pierce Chemical Company). The samples were incubated with rocking at 4°C for 30 min, and the beads were pelleted and washed three times with cold GGA wash buffer (50 mM Tris pH 7.6, 100 mM NaCl, 2 mM MgCl$_2$, 1% NP-40, 10% glycerol). SDS-PAGE loading buffer was added, the samples were boiled, and equal aliquots separated by SDS-PAGE. ARF1 was detected by Western blot using anti-V5 antibody (Invitrogen), followed by enhanced chemiluminescence. Band intensity was determined using the program ImageJ. The results of duplicate experiments were averaged.

Molecular Modeling of GBF1-Arf1-GCA complex

The GBF1 homology model was built using Prime 2.0 software from

FirstDiscovery suite (Schrodinger, LLC, Portland, OR) and ARNO coordinates using the

ARNO-ARF1 complex (PDB id 1r8q) as a template[47]. Fully flexible ligand docking was

performed with Glide 5.0 (Schrodinger, LLC, Portland, OR). The protein was prepared

for grid generation and subsequent docking using the Protein Preparation Wizard tool

from FirstDiscovery suite. The default settings for grid calculations and docking were

used. Images were created with UCSF Chimera version 1.2540 for Windows[64].

Transferrin Recycling Assay

Transferrin (Tf) recycling was analyzed by modification of a previously published

assay for recycling of low density lipoprotein related protein[65]. 2×10^5 Vero cells were

seeded per well in seven 12-well dishes. The following day, media was removed and

replaced with 500 µL serum-free media containing Tf-488 (Invitrogen) at 5 µg/mL and

either no compound or GCA (10 µM). The samples were incubated at room temperature

for 60 min to allow Tf transport to recycling endosomes. Cells were washed twice with 1

mL PBS, then overlaid with 400 µL media containing 10% FCS, anti-AlexaFluor-488

antibody (Invitrogen) at 15 µg/mL, and either no compound, BFA (10 µg/mL), or GCA

(10 µM). t=0 min samples were maintained at room temperature to prevent recycling.

The remaining samples were incubated at 37ºC and at various times ranging from 10 to

60 min. Media was removed, and 500 µL prewarmed cell release buffer (Sigma) was

added. Cell suspensions were mixed with 250 µL 4% paraformaldehyde, and mean

fluorescence was determined by FACS on a Becton Dickenson FACSCaliber System.

Mean fluorescence of the t=0 samples was normalized to 100% fluorescence.

[^{125}I]-albumin degradation

Vero cells were seeded in 6-well plates (10^5 cells/well) and washed twice with cold serum-free media. Media was replaced with prewarmed serum-free medium containing 1 µCi/mL [^{125}I]-BSA and incubated at 37ºC for 30 or 60 min. Supernatants were collected, and unlabeled BSA was added to a final concentration of 2 mg/mL. Proteins were precipitated by TCA (final concentration 15%) for 30 min on ice, then centrifuged at 15,000 x g for 20 min at 4ºC. TCA-soluble and –insoluble fractions were analyzed by the Cobra II γ-counter and analyzed by Prism v4.0 software (2003).

STxB-SS-His Sulfation.

A STxB construct containing a tandem of carboxy-terminal sulfation sites and a histidine tag for purification (STxB-Sulf$_2$) has been described[32]. Vero cells seeded in a 6-well plate (1 x 10^6 cells/well) were washed three times in serum-free DMEM lacking sulfate (Washington University Tissue Culture Support Center), and then incubated in sulfate-free medium for 3.5 h at 37ºC. After treatment with DMSO (0.5% v/v), BFA (10 µg/mL) or GCA (10 µM) 30 min at 37ºC, media was replaced with sulfate-free media containing these compounds plus STxB-Sulf$_2$ (1 mg/mL) and 1 mCi/mL [^{35}S]O$_4$ for 3 h at 37ºC. Wells were washed with cold PBS (pH 7.4) and lysed with PBS containing 1% Triton X-100. Lysates were added to 40 µL Ni-NTA Superflow beads (Qiagen) and rotated at 4ºC overnight. Beads were washed once with PBS containing 1% Triton X-100

and twice with PBS, then resuspended in imidazole (1.5 M in PBS). Eluates were

resolved on a 10-20% Tris-HCl denaturing gel, treated with EnHance reagent (DuPont),

dried and exposed to film. Band intensity was determined using ImageJ software.

Statistical analyses

All statistical analyses were performed by GraphPad Prism 5. Toxin

concentrations were log transformed prior to curve fitting and statistical analyses. Toxin-

response curves were generated by nonlinear regression (least-squares fit) to correspond

to the observed data, and toxin IC_{50} and compound IC_{50} values were calculated using the

fitted curves. Toxin IC_{50} values were compared using the extra sum-of-squares F test

applied to the best-fit curves for the data. Differences between toxin IC_{50} values were

considered highly statistically significant for $p \leq 0.01$. For assessment of ARF1-GTP

levels, values were considered statistically significantly different for $p \leq 0.05$ (*), whereas

ns denotes a non-significant difference ($p > 0.05$).

REFERENCES

1. Donaldson, J.G., Honda, A. & Weigert, R. Multiple activities for Arf1 at the Golgi complex. *Biochim Biophys Acta* **1744**, 364-73 (2005).

2. Gillingham, A.K. & Munro, S. The small G proteins of the Arf family and their regulators. *Annu Rev Cell Dev Biol* **23**, 579-611 (2007).

3. Pasqualato, S., Menetrey, J., Franco, M. & Cherfils, J. The structural GDP/GTP cycle of human Arf6. *EMBO Rep* **2**, 234-8 (2001).

4. Cohen, L.A. et al. Active Arf6 recruits ARNO/cytohesin GEFs to the PM by binding their PH domains. *Mol Biol Cell* **18**, 2244-53 (2007).

5. Shmuel, M. et al. ARNO through its coiled-coil domain regulates endocytosis at the apical surface of polarized epithelial cells. *J Biol Chem* **281**, 13300-8 (2006).

6. Cherfils, J. & Melancon, P. On the action of Brefeldin A on Sec7-stimulated membrane-recruitment and GDP/GTP exchange of Arf proteins. *Biochem Soc Trans* **33**, 635-8 (2005).

7. Renault, L., Christova, P., Guibert, B., Pasqualato, S. & Cherfils, J. Mechanism of domain closure of Sec7 domains and role in BFA sensitivity. *Biochemistry* **41**, 3605-12 (2002).

8. Claude, A. et al. GBF1: A novel Golgi-associated BFA-resistant guanine nucleotide exchange factor that displays specificity for ADP-ribosylation factor 5. *J Cell Biol* **146**, 71-84 (1999).

9. Szul, T. et al. Dissection of membrane dynamics of the ARF-guanine nucleotide exchange factor GBF1. *Traffic* **6**, 374-85 (2005).

116

10. Szul, T. et al. Dissecting the role of the ARF guanine nucleotide exchange factor GBF1 in Golgi biogenesis and protein trafficking. *J Cell Sci* **120**, 3929-40 (2007).

11. Zhao, X. et al. GBF1, a cis-Golgi and VTCs-localized ARF-GEF, is implicated in ER-to-Golgi protein traffic. *J Cell Sci* **119**, 3743-53 (2006).

12. Zhao, X., Lasell, T.K. & Melancon, P. Localization of large ADP-ribosylation factor-guanine nucleotide exchange factors to different Golgi compartments: evidence for distinct functions in protein traffic. *Mol Biol Cell* **13**, 119-33 (2002).

13. Bonifacino, J.S. & Glick, B.S. The mechanisms of vesicle budding and fusion. *Cell* **116**, 153-66 (2004).

14. Boehm, M., Aguilar, R.C. & Bonifacino, J.S. Functional and physical interactions of the adaptor protein complex AP-4 with ADP-ribosylation factors (ARFs). *Embo J* **20**, 6265-76 (2001).

15. Robinson, M.S. Adaptable adaptors for coated vesicles. *Trends Cell Biol* **14**, 167-74 (2004).

16. Boman, A.L., Zhang, C., Zhu, X. & Kahn, R.A. A family of ADP-ribosylation factor effectors that can alter membrane transport through the trans-Golgi. *Mol Biol Cell* **11**, 1241-55 (2000).

17. Dell'Angelica, E.C. et al. GGAs: a family of ADP ribosylation factor-binding proteins related to adaptors and associated with the Golgi complex. *J Cell Biol* **149**, 81-94 (2000).

18. Doray, B., Ghosh, P., Griffith, J., Geuze, H.J. & Kornfeld, S. Cooperation of GGAs and AP-1 in packaging MPRs at the trans-Golgi network. *Science* **297**, 1700-3 (2002).

19. Ghosh, P. & Kornfeld, S. The GGA proteins: key players in protein sorting at the trans-Golgi network. *Eur J Cell Biol* **83**, 257-62 (2004).

20. Donaldson, J.G. & Jackson, C.L. Regulators and effectors of the ARF GTPases. *Curr Opin Cell Biol* **12**, 475-82 (2000).

21. Donaldson, J.G., Finazzi, D. & Klausner, R.D. Brefeldin A inhibits Golgi membrane-catalysed exchange of guanine nucleotide onto ARF protein. *Nature* **360**, 350-2 (1992).

22. Donaldson, J.G., Lippincott-Schwartz, J., Bloom, G.S., Kreis, T.E. & Klausner, R.D. Dissociation of a 110-kD peripheral membrane protein from the Golgi apparatus is an early event in brefeldin A action. *J Cell Biol* **111**, 2295-306 (1990).

23. Scheel, J., Pepperkok, R., Lowe, M., Griffiths, G. & Kreis, T.E. Dissociation of coatomer from membranes is required for brefeldin A-induced transfer of Golgi enzymes to the endoplasmic reticulum. *J Cell Biol* **137**, 319-33 (1997).

24. Weigert, R. et al. CtBP/BARS induces fission of Golgi membranes by acylating lysophosphatidic acid. *Nature* **402**, 429-33 (1999).

25. Manolea, F., Claude, A., Chun, J., Rosas, J. & Melancon, P. Distinct functions for Arf guanine nucleotide exchange factors at the Golgi complex: GBF1 and BIGs are required for assembly and maintenance of the Golgi stack and trans-Golgi network, respectively. *Mol Biol Cell* **19**, 523-35 (2008).

26. Citterio, C. et al. Unfolded protein response and cell death after depletion of brefeldin A-inhibited guanine nucleotide-exchange protein GBF1. *Proc Natl Acad Sci U S A* (2008).

27. Lefrancois, S. & McCormick, P.J. The Arf GEF GBF1 is required for GGA recruitment to Golgi membranes. *Traffic* **8**, 1440-51 (2007).

28. Holloway, Z.G. et al. Activation of ADP-ribosylation factor (Arf) regulates biogenesis of the ATP7A containing trans-Golgi network compartment and its Cu-induced trafficking. *Am J Physiol Cell Physiol* (2007).

29. Monetta, P., Slavin, I., Romero, N. & Alvarez, C. Rab1b interacts with GBF1 and modulates both ARF1 dynamics and COPI association. *Mol Biol Cell* **18**, 2400-10 (2007).

30. Zhao, L. & Haslam, D.B. A quantitative and highly sensitive luciferase-based assay for bacterial toxins that inhibit protein synthesis. *J Med Microbiol* **54**, 1023-30 (2005).

31. Saenz, J.B., Doggett, T.A. & Haslam, D.B. Identification and characterization of small molecules that inhibit intracellular toxin transport. *Infect Immun* **75**, 4552-61 (2007).

32. Saenz, J.B., Doggett, T.A. & Haslam, D.B. Identification and characterization of small molecules that inhibit intracellular toxin transport. *Infect Immun* **75**, 4552-61 (2007).

33. Lippincott-Schwartz, J. et al. Microtubule-dependent retrograde transport of proteins into the ER in the presence of brefeldin A suggests an ER recycling pathway. *Cell* **60**, 821-36 (1990).

34. Doms, R.W., Russ, G. & Yewdell, J.W. Brefeldin A redistributes resident and itinerant Golgi proteins to the endoplasmic reticulum. *J Cell Biol* **109**, 61-72 (1989).

35.   Puri, S. & Linstedt, A.D. Capacity of the golgi apparatus for biogenesis from the endoplasmic reticulum. *Mol Biol Cell* **14**, 5011-8 (2003).

36.   Donaldson, J.G. & Honda, A. Localization and function of Arf family GTPases. *Biochem Soc Trans* **33**, 639-42 (2005).

37.   Niu, T.K., Pfeifer, A.C., Lippincott-Schwartz, J. & Jackson, C.L. Dynamics of GBF1, a Brefeldin A-sensitive Arf1 exchange factor at the Golgi. *Mol Biol Cell* **16**, 1213-22 (2005).

38.   Mansour, S.J. et al. p200 ARF-GEP1: a Golgi-localized guanine nucleotide exchange protein whose Sec7 domain is targeted by the drug brefeldin A. *Proc Natl Acad Sci U S A* **96**, 7968-73 (1999).

39.   Shinotsuka, C., Yoshida, Y., Kawamoto, K., Takatsu, H. & Nakayama, K. Overexpression of an ADP-ribosylation factor-guanine nucleotide exchange factor, BIG2, uncouples brefeldin A-induced adaptor protein-1 coat dissociation and membrane tubulation. *J Biol Chem* **277**, 9468-73 (2002).

40.   Presley, J.F. et al. Dissection of COPI and Arf1 dynamics in vivo and role in Golgi membrane transport. *Nature* **417**, 187-93 (2002).

41.   Liu, W., Duden, R., Phair, R.D. & Lippincott-Schwartz, J. ArfGAP1 dynamics and its role in COPI coat assembly on Golgi membranes of living cells. *J Cell Biol* **168**, 1053-63 (2005).

42.   Helms, J.B. & Rothman, J.E. Inhibition by brefeldin A of a Golgi membrane enzyme that catalyses exchange of guanine nucleotide bound to ARF. *Nature* **360**, 352-4 (1992).

43. Sandvig, K., Prydz, K., Hansen, S.H. & van Deurs, B. Ricin transport in brefeldin A-treated cells: correlation between Golgi structure and toxic effect. *J Cell Biol* **115**, 971-81 (1991).

44. Prydz, K., Hansen, S.H., Sandvig, K. & van Deurs, B. Effects of brefeldin A on endocytosis, transcytosis and transport to the Golgi complex in polarized MDCK cells. *J Cell Biol* **119**, 259-72 (1992).

45. Hunziker, W., Whitney, J.A. & Mellman, I. Selective inhibition of transcytosis by brefeldin A in MDCK cells. *Cell* **67**, 617-27 (1991).

46. Peyroche, A. et al. Brefeldin A acts to stabilize an abortive ARF-GDP-Sec7 domain protein complex: involvement of specific residues of the Sec7 domain. *Mol Cell* **3**, 275-85 (1999).

47. Renault, L., Guibert, B. & Cherfils, J. Structural snapshots of the mechanism and inhibition of a guanine nucleotide exchange factor. *Nature* **426**, 525-30 (2003).

48. Santy, L.C. & Casanova, J.E. Activation of ARF6 by ARNO stimulates epithelial cell migration through downstream activation of both Rac1 and phospholipase D. *J Cell Biol* **154**, 599-610 (2001).

49. Hirschberg, K. et al. Kinetic analysis of secretory protein traffic and characterization of golgi to plasma membrane transport intermediates in living cells. *J Cell Biol* **143**, 1485-503 (1998).

50. El Meskini, R. et al. A signal sequence is sufficient for green fluorescent protein to be routed to regulated secretory granules. *Endocrinology* **142**, 864-73 (2001).

51.   Lin, W.H., Larsen, K., Hortin, G.L. & Roth, J.A. Recognition of substrates by tyrosylprotein sulfotransferase. Determination of affinity by acidic amino acids near the target sites. *J Biol Chem* **267**, 2876-9 (1992).

52.   Niehrs, C. & Huttner, W.B. Purification and characterization of tyrosylprotein sulfotransferase. *Embo J* **9**, 35-42 (1990).

53.   Mallard, F. et al. Early/recycling endosomes-to-TGN transport involves two SNARE complexes and a Rab6 isoform. *J Cell Biol* **156**, 653-64 (2002).

54.   Zeeh, J.C. et al. Dual specificity of the interfacial inhibitor brefeldin a for arf proteins and sec7 domains. *J Biol Chem* **281**, 11805-14 (2006).

55.   Garcia-Mata, R., Szul, T., Alvarez, C. & Sztul, E. ADP-ribosylation factor/COPI-dependent events at the endoplasmic reticulum-Golgi interface are regulated by the guanine nucleotide exchange factor GBF1. *Mol Biol Cell* **14**, 2250-61 (2003).

56.   Feng, Y. et al. Exo1: a new chemical inhibitor of the exocytic pathway. *Proceedings of the National Academy of Sciences of the United States of America* **100**, 6469-74 (2003).

57.   Feng, Y. et al. Retrograde transport of cholera toxin from the plasma membrane to the endoplasmic reticulum requires the trans-Golgi network but not the Golgi apparatus in Exo2-treated cells. *EMBO Reports* **5**, 596-601 (2004).

58.   Newton, A.J., Kirchhausen, T. & Murthy, V.N. Inhibition of dynamin completely blocks compensatory synaptic vesicle endocytosis. *Proc Natl Acad Sci U S A* **103**, 17955-60 (2006).

59.   Macia, E. et al. Dynasore, a cell-permeable inhibitor of dynamin. *Dev Cell* **10**, 839-50 (2006).

60.   Pelish, H.E. et al. Secramine inhibits Cdc42-dependent functions in cells and
       Cdc42 activation in vitro. *Nat Chem Biol* **2**, 39-46 (2006).

61.   Hafner, M. et al. Inhibition of cytohesins by SecinH3 leads to hepatic insulin
       resistance. *Nature* **444**, 941-4 (2006).

62.   Saenz, J.B. et al. Golgicide A reveals essential roles for GBF1 in Golgi assembly
       and function. *Nat Chem Biol* **5**, 157-65 (2009).

63.   Zhao, L. & Haslam, D.B. A quantitative and highly sensitive luciferase-based
       assay for bacterial toxins that inhibit protein synthesis. *Journal of Medical
       Microbiology* **54**, 1023-30 (2005).

64.   Pettersen, E.F. et al. UCSF Chimera--a visualization system for exploratory
       research and analysis. *J Comput Chem* **25**, 1605-12 (2004).

65.   van Kerkhof, P. et al. Sorting nexin 17 facilitates LRP recycling in the early
       endosome. *Embo J* **24**, 2851-61 (2005).

CHAPTER IV

The MAP kinase activated protein kinase-activated protein kinase 2 (MK2)

contributes to the STx-induced inflammatory response

OVERVIEW

Gastrointestinal infection with Shiga toxin (STx)-producing bacteria can lead to a toxemic condition known as hemolytic uremic syndrome (HUS). HUS is clinically characterized by hemolytic anemia, thrombocytopenia, and renal failure, and it is the leading cause of acute renal failure in children. HUS primarily results from the action of STx on endothelial cells lining intestinal and renal microvasculature, resulting in clot formation and occlusion of these small vessels (thrombotic microangiopathy). The mechanisms by which STx produces the pathologic features of HUS are debated, however. While some studies have pointed to a direct, cytotoxic role of STx on endothelial cells to explain some of the pathophysiology, recent studies have focused on the inflammatory component, suggesting that HUS could be an immunopathologic response to STx. In order to investigate the contribution of the immune response to STx, we have characterized the mitogen-activated protein (MAP) kinase-activated protein kinase 2 (MK2), a substrate of the p38 MAP kinase identified from a siRNA screen of the human kinome. We demonstrate that STx activates MK2 *in vitro* in both HeLa and human microvascular endothelial cells. Moreover, genetic and chemical inhibition of MK2 significantly decreases the inflammatory response to STx2 in HeLa cells and human macrophages. To correlate our findings to an *in vivo* model, we will adopt a murine model of HUS to compare HUS pathology in wild-type versus MK2-deficient mice.

SUMMARY

Infection with Shiga toxin (STx)-producing bacteria can progress to a toxemic, extraintestinal injury cascade known as hemolytic uremic syndrome (HUS), the leading cause of acute renal failure in children. Mounting evidence suggests that STx activates stress response pathways in susceptible cells and has implicated the p38 mitogen-activated protein kinase (MAPK) pathway. More importantly, some of the pathology associated with HUS is believed to be a result of a STx-induced inflammatory response. From a siRNA screen of the human kinome adapted to a high-throughput format, we found that knock-down of the MAPK-activated protein kinase 2 (MK2), a downstream target of the p38 MAPK, protected against Shiga toxicity. Further characterization of the *in vitro* role of MK2 revealed that STx activates the p38-MK2 stress response pathway in both p38- and MK2-dependent manners in two distinct cell lines. MK2 activation was specific to damage to the ribosome by an enzymatically active toxin and did not result from translational inhibition per se. Genetic and chemical inhibition of MK2 significantly decreased the inflammatory response to STx. These findings suggest that MK2 inhibition might play a valuable role in decreasing the immuopathological component of STx-mediated disease.

INTRODUCTION

Bacterial exotoxins are critical components of bacterial pathogenesis and constitute potential vehicles for bioterrorism. Among the most studied of the bacterial toxins are members of the AB family, including the bacterial toxins Shiga toxin (STx) and the plant toxin ricin. These toxins are characterized by their bipartite structure, consisting of a pentameric, receptor-binding B moiety that is non-covalently linked to a catalytic A subunit. Following a unique retrograde trafficking pathway that facilitates toxin access to the cytosol [1-4], these toxins shut off host protein synthesis by inactivating the ribosome through cleavage of a single adenine residue in the 28S rRNA [5-7].

STx was initially identified in *Shigella dysenteriae* type I, though it is now commonly associated with strains of STx-producing *Escherichia coli* (STEC), among which *E. coli* O157:H7 has become the most clinically relevant. In a subset of patients, gastrointestinal infection with STEC may progress to extraintestinal injury, leading to hemorrhagic colitis and hemolytic uremic syndrome (HUS). This toxemic syndrome is clinically defined by renal failure, thrombocytopenia, and hemolytic anemia, and it remains the leading cause of acute renal failure in children [8,9]. Extraintestinal complications of HUS correlate with circulating levels of STx, though the mechanism of STx-induced pathology in HUS remains unclear. One of the hallmarks of HUS is the development of thrombotic lesions within the intestinal and renal microvasculature that accounts for the associated hemorrhagic colitis, hemolytic anemia, and renal failure [10]. Though some evidence would suggest a direct role for STx in the thrombotic microangiopathy associated with HUS [11,12], various lines of evidence support the view that much of the systemic and focal pathology of HUS is immune-mediated [13-17].

127

In conjunction with the mounting evidence suggesting an inflammatory contribution to HUS pathology, various cellular stress pathways have been implicated. Perhaps the most studied are members of the mitogen activated protein kinase (MAPK) family. MAPKs are signal-transducing enzymes involved in a variety of regulatory roles in eukaryotes, including inflammation, differentiation, and apoptosis [18]. The p38 MAPK (p38) plays a critical role in the response to various stresses, such as UV radiation, cytokines, and toxic stress [19]. In the context of STx-mediated damage, numerous studies have clearly defined the role of p38 in inciting inflammatory cytokine release from toxin-treated cells [20,21]. One study, for example, showed that sequence-specific damage to 28S rRNA by STx stimulated a ribotoxic stress response that resulted in p38 activation [22].

Though the mechanisms behind STx activation of these signaling cascades remain unclear, a critical component is the function of kinases in propagating the stress signal and initiating a cellular response. As a result, kinases are tempting therapeutic targets for limiting STx-mediated cellular injury. For example, inhibition of p38 activation decreased cytokine release following exposure of macrophages to STx [23]. However, p38 inhibition may have limited therapeutic potential, given the ability of p38 to activate various downstream kinases involved in diverse cellular functions. Indeed, mice deficient in p38 are not viable post-natally [24-26], and in human clinical trials p38 inhibition has been met with unanticipated side effects [27]. Moreover, inhibition of p38 kinase activity by overexpression of dominant negative p38 isoforms [28] or by treatment with chemical inhibitors [29] has made probing of specific p38-dependent signaling pathways particularly difficult. Effectors downstream of p38 might therefore be more

specific and functionally relevant to the inflammatory signals induced in response to STx [30].

The mitogen-activated protein kinase-activated protein kinase 2 (MK2) has been recently shown to contribute to the inflammatory response [31]. MK2 is a member of the MAPK subfamily of calcium/calmodulin-dependent kinases that was originally identified as an *in vivo* substrate of p38 [32]. Activation of MK2 by p38 results primarily in the subsequent phosphorylation of its two main substrates, heat shock protein 27 (Hsp27) and tristetraprolin (TTP). Despite evidence demonstrating that STx elicits a p38-dependent stress response *in vitro* [22] and that MK2 has been implicated in an *in vivo* inflammatory response to lipopolysaccharide (LPS) [31], the role of MK2 in STx-mediated toxicity has yet to be explored. From a high-throughput siRNA screen of the human kinome, knock-down of MK2 was found to protect against Shiga toxicity. We present evidence demonstrating that STx activates MK2 *in vitro* in a p38-dependent manner and that inhibition of MK2 decreases the STx-induced inflammatory cytokine response. We extend our *in vitro* findings to an *in vivo* mouse model of HUS[33] and present preliminary evidence comparing the development of HUS pathology in wild-type and MK2-deficient mice.

RESULTS

Knock-down of MK2 protects against Shiga toxicity.

Various approaches have been employed to study the biological mechanisms underlying toxin-induced cell death. Of particular interest, high-throughput screens of small molecules have been developed to target varying aspects of bacterial toxin pathogenesis [34-36]. While small molecule compounds are amenable to high-throughput screening and allow for the reversible manipulation of cellular processes, the rate-limiting step in these studies is the identification of the compound's target[37].

As a result, we adapted an inherently target-based approach to specifically screen for kinases involved in Shiga toxicity. An siRNA library targeting 646 human kinase and kinase-associated genes (see Methods) was optimized to a high-throughput format and screened for kinases essential to Shiga toxicity in HeLa cells. A HeLa cell line (HeLa-Fluc) that constitutively expressed luciferase [38], where light expression served as a translational readout (Figure 1C), was transfected with a duplex of each of 646 siRNAs targeting the human kinome prior to treatment with STx (1 ng/mL) for 24 h. Each plate incorporated a series of controls to assess the screen for siRNA transfection efficiency and discriminatory ability (Figures 1A-B). We considered a hit any kinase knock-down that, in the presence of STx, maintained light levels at least 3 standard deviations above mock-transfected, STx-treated controls on replicate plates.
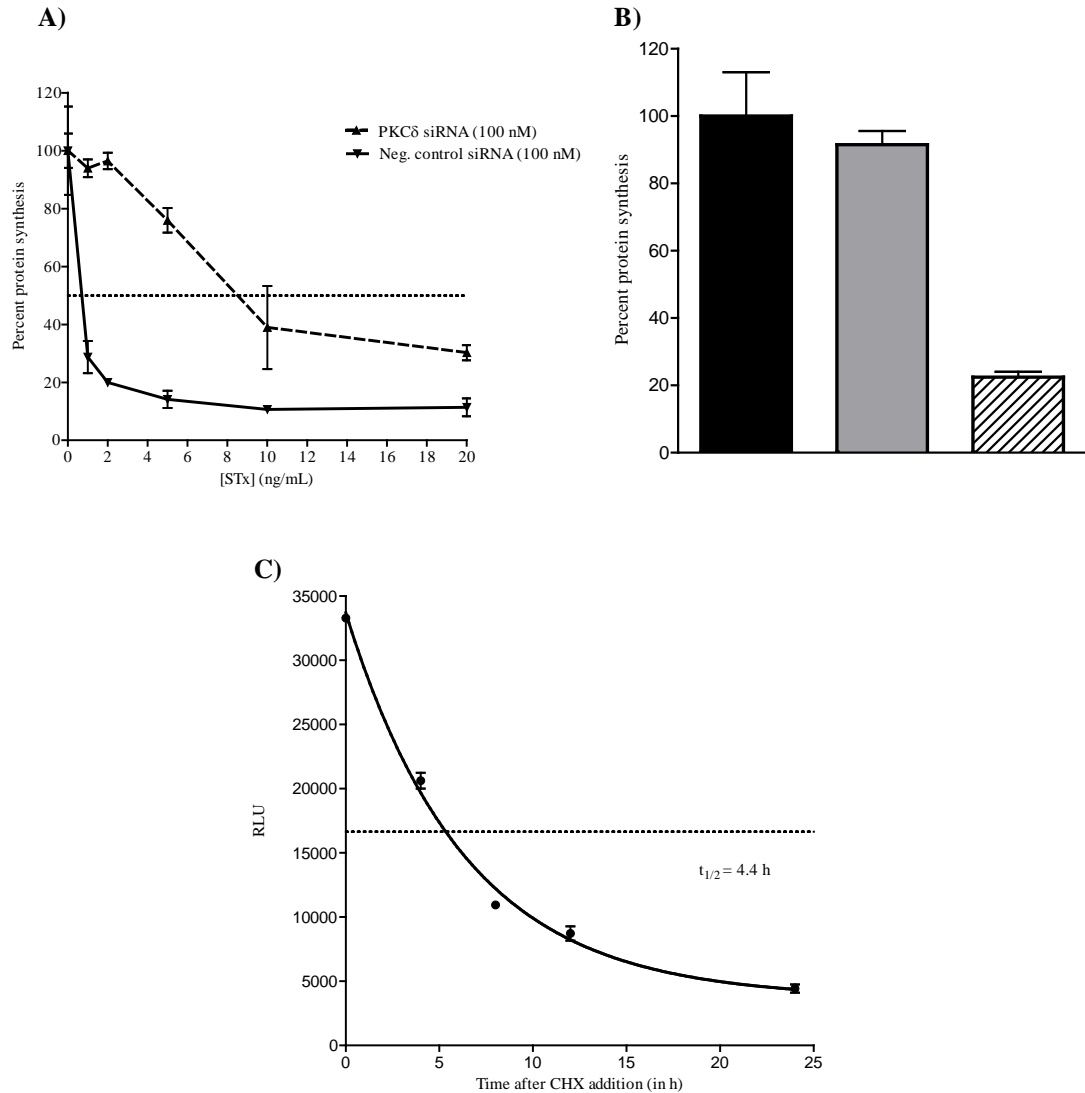
Figure 1. Optimization of the human kinome siRNA screen. **(A)** Identification of a positive control for the siRNA screen. Knock-down of the delta isoform of protein kinase C (PKCδ siRNA) protects against STx-induced inhibition of protein synthesis. HeLa-Fluc cells were transfected for 48 h with 100 nM negative control siRNA (solid line) or PKCδ siRNA (dotted line) prior to exposure to increasing concentrations of STx for 24 h. Percent protein synthesis denotes luminescence levels in transfected cells at a given STx concentration as a percentage of transfected cells lacking toxin treatment. Data points represent duplicate data (mean ±S.D.) for a given toxin concentration from one representative experiment. Data were analyzed using GraphPad Prism. Dotted horizontal line represents 50% protein synthesis. **(B)** GL3 siRNA was confirmed as a control for transfection efficiency. Transfection with GL3 siRNA effectively knocks down light levels in the HeLa-Fluc reporter cell line. HeLa-Fluc cells were transfected for 48 h with media alone (black bar), transfection reagent alone (gray bar), or GL3 siRNA (100 nM; hatched bar), and light levels were measured. Percent protein synthesis refers to light levels in transfected cells as a percentage of light levels in cells containing media alone. Data points represent duplicate data (mean ±S.D.) from one representative experiment. **(C)** The half-life of the Fluc reporter was determined using a CHX chase. HeLa-Fluc cells were treated with CHX (100 µg/mL) for the indicated times, and luminescence levels were measured. A non-linear fit to the duplicate data (mean ±S.D.) using a one-phase exponential decay model was performed using GraphPad Prism, and the half-life ($t_{1/2}$) was calculated. The horizontal dotted line denotes 50% of the baseline luminescence signal. CHX, cycloheximide.

131

Of six kinase hits identified, the mitogen-activated protein kinase-activated

protein kinase 2 (MK2) revealed the strongest protective effect (Figure 2), and its role in

STx-induced cytotoxicity was investigated.
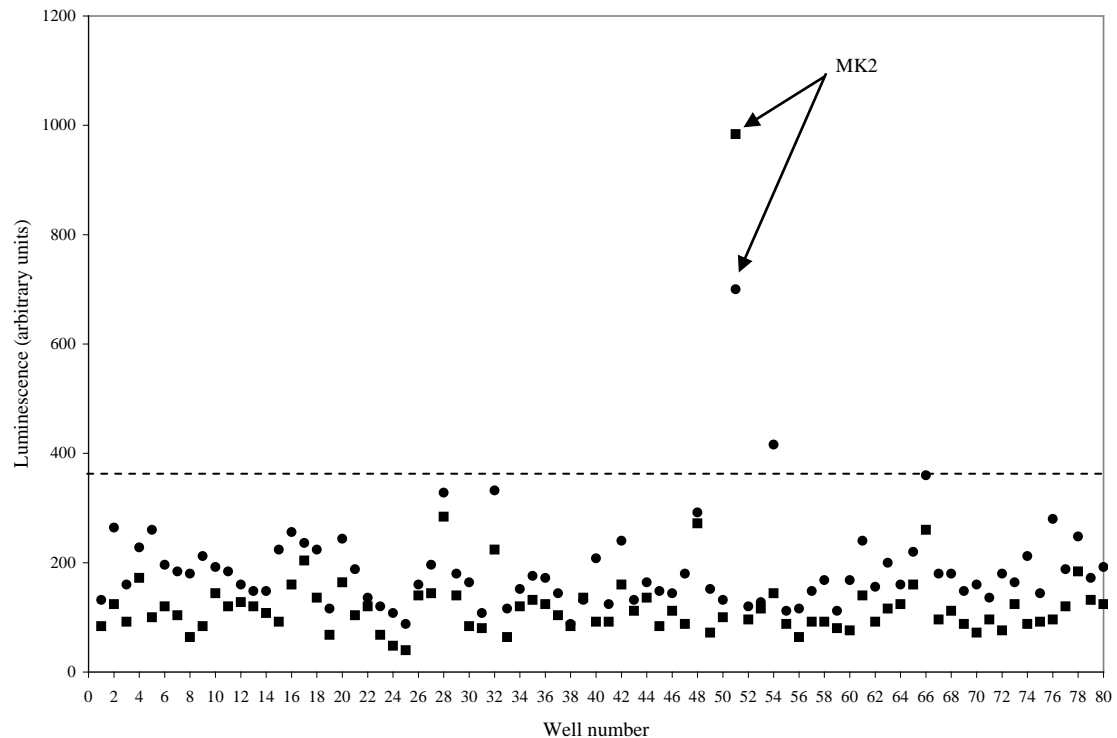
Figure 2. Knock-down of MK2 protects against Shiga toxicity. A siRNA screen of 646 human kinase and kinase-associated genes was adapted to a 96-well format (see Methods). Shown are two representative plates, run in duplicate (circles and squares), demonstrating light levels of 80 different kinase siRNAs after a 24-h treatment with STx1 (1 ng/mL). Well number represents each well of HeLa-Fluc cells transfected with 50 nM siRNA targeting a specific kinase, and corresponding light levels are shown on the y-axis. Control wells have been excluded (see Figures 1A-B). A hit was considered any knock-down that maintained luminescence at least 3 standard deviations above STx1-treated controls (dotted line). Knock-down of MK2 (siRNA sequence provided in Methods) conferred the highest protection against Shiga toxicity. Mean and standard deviations for each set of duplicate plates were determined by GraphPad Prism. MK2, mitogen-activated protein kinase-activated protein kinase 2.

STx activates MK2 *in vitro*.

MK2 is a member of the calcium/calmodulin-dependent superfamily of kinases

functioning downstream of the p38 MAP kinase [32]. Activation of MK2 by p38 results in

the subsequent phosphorylation by MK2 of its two main substrates, Hsp27 and

tristetraprolin (TTP). Hsp27 phosphorylation has been demonstrated to be completely

132

dependent on the kinase activity of MK2 [39], and we therefore used Hsp27

phosphorylation as an indicator of MK2 activation. Since the p38 MAPK pathway has

been shown to play a critical role in the response to various stresses, including UV

radiation, cytokines, and toxic stress, we assessed STx activation of MK2 in HeLa cells

A)

B)
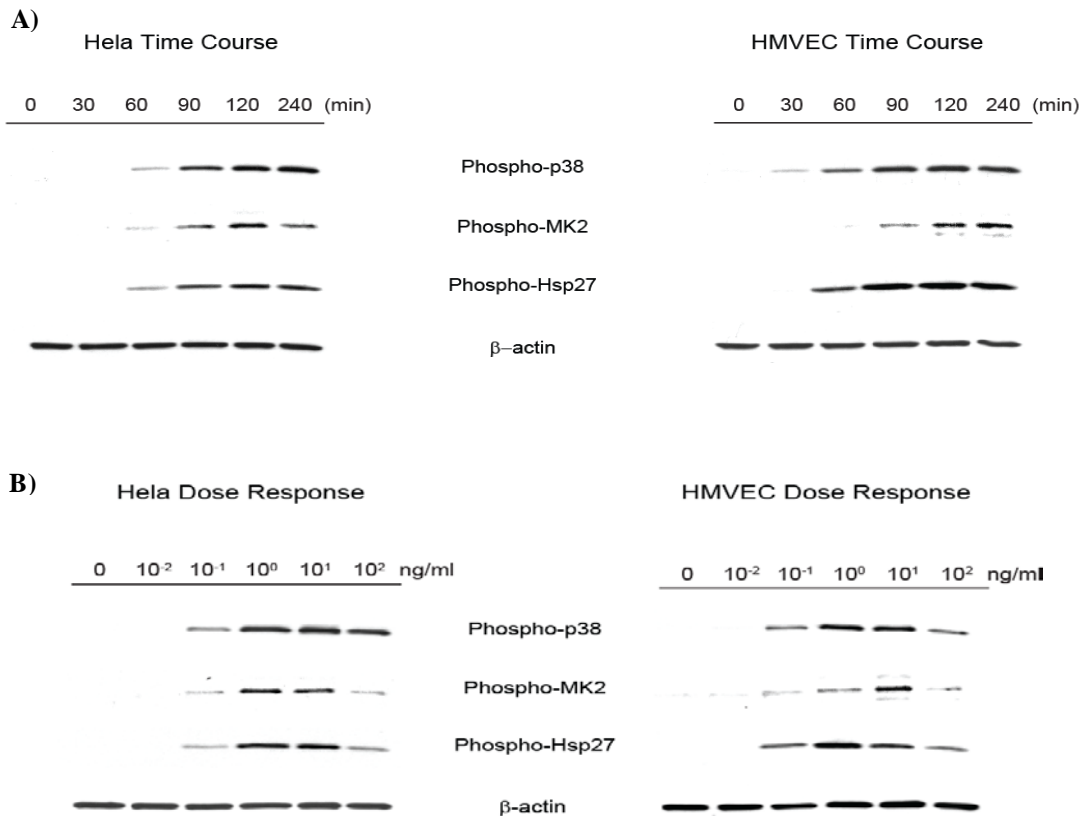
Figure 3. STx1 induces activation of the p38-MK2 pathway in both HeLa cells and HMVEC in time- and dose-dependent manners. (A) HeLa cells (left) or HMVEC (right) were treated with no toxin or STx1 (10 ng/mL) for the indicated times, and lysates were probed with the indicated antibodies. Activation of the p38-MK2 pathway is observed by 60 min following exposure to STx1, while stimulation of this pathway in HMVEC can be seen as early as 30 min. **(B)** HeLa cells (left) or HMVEC (right) were treated with either no toxin or increasing STx1 concentrations for 2 h. Lysates were probed as in (A). For both cell lines, as little as 0.1 ng/mL STx1 was able to activate the p38-MK2 pathway. For (A) and (B), actin staining served as a loading control. HMVEC, human microvascular endothelial cells.

by monitoring Hsp27 phosphorylation. Treatment with STx resulted in activation of

MK2 in both a time- and dose-dependent manner. As early as 60 min following exposure

to STx, phosphorylation of MK2 and its downstream target, Hsp27, were observed

(Figure 3A). Similarly, higher levels of phosphorylated MK2 and Hsp27 were observed

with increasing STx concentrations (Figure 3B). Time- and dose-dependent

phosphorylation of the p38 MAPK mirrored that of MK2, suggesting activation of the

p38-MK2 pathway (Figure 3).

Some studies have suggested that STxB binding to its receptor can stimulate

signal transduction cascades following activation of membrane-localized kinases, such as

Syk [40] and Yes [41], and that these effects were independent of the toxin's effect on

ribosome function. We found, however, that exposure of HeLa cells to the STxB subunit alone did not result in Hsp27 phosphorylation (Figure 4), implying that engagement of the STx receptor, Gb3, by the receptor-binding B

Treatment:	HI-STx1	STxB	STx1	STx1 + SB202190
Phospho-Hsp27				
MK2				

 Figure 4. Activation of MK2 is specific to catalytically active STx. HeLa cells were pretreated with DMSO (0.5% v/v) or the p38 inhibitor SB202190 (10 µM) for 1 h prior to a 30-min exposure to STx1 (100 ng/mL). Equal fractions of lysates were probed with the indicated antibodies, with MK2 serving as a loading control. Inhibition of p38 eliminates STx1-induced MK2 activation. In addition, treatment with 100 ng/mL heat-inactivated STx1 (HI-STx1) or the STxB subunit (100 ng/mL) did not activate MK2. Heat inactivation of STx1 involved incubating the toxin for 12 h at 95ºC.

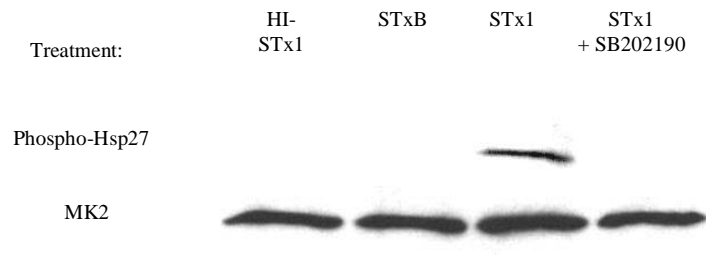subunit is insufficient for MK2 activation and that STx's catalytic activity is necessary

for induction of this pathway. Phosphorylation of MK2 in the presence of STx thus

appears to be specific to an enzymatically active toxin. In addition, we confirmed that

MK2 activation was not the result of a LPS contamination of the toxin preparation, as

heat-inactivated STx (HI-STx) failed to activate MK2 (Figure 4).

Activation of MK2 is p38-dependent.

To assess the role of p38 on STx-induced MK2 activation, we treated HeLa cells

with the p38-specific chemical inhibitor, SB202190, prior to STx exposure. As expected,

pretreatment with SB202190 blocked Hsp27 phosphorylation, indicating that STx

specifically activates MK2 through p38 and not through another stress activation pathway

(Figure 4). Moreover, pretreatment with other p38 inhibitors (SB 203580, p38 inhibitor

III) showed a similar effect, while pretreatment with the JNK inhibitor (SP 600125)

showed no decrease in MK2 activation in the presence of STx (Figure 5). Taken

together, these results indicate that STx-induced activation of MK2 is dependent on its

upstream MAP kinase, p38.
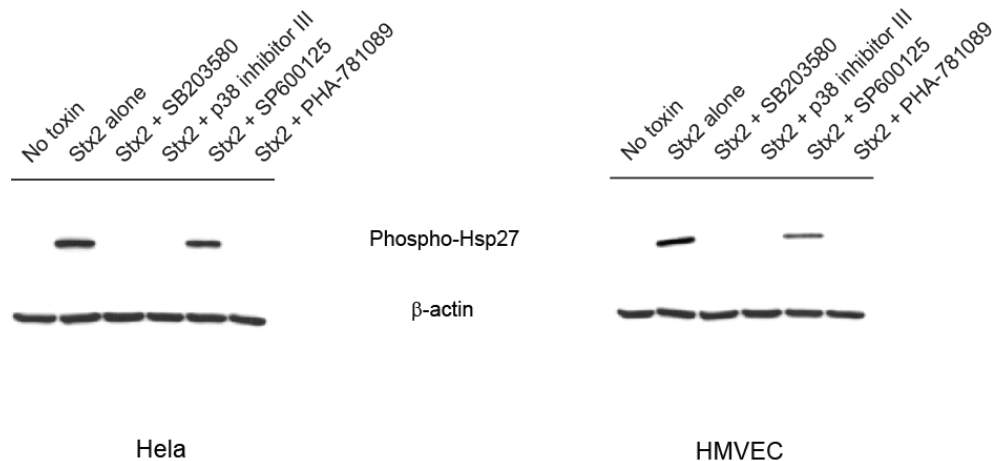
Figure 5. STx-induced MK2 activation is p38-specific. HeLa cells (left) or HMVEC (right) were pretreated with the indicated compounds 30 min prior to a 2-h exposure to STx2 (10 ng/mL). Lysates were probed with the indicated antibodies. Two distinct p38 inhibitors, SB203580 (2.65 µM) and the p38 inhibitor III (0.5 µM), prevented STx2-mediated Hsp27 phosphorylation, while the JNK inhibitor SP600125 (25 µM) showed no effect, similar to STx2-treated cells treated lacking compound treatment ("STx2 alone"). "No toxin" refers to cells lacking compound and toxin treatment. β-actin staining served as a loading control. HMVEC, human microvascular endothelial cells.

While we could confirm that STx stimulated the p38 MAPK pathway in HeLa

cells, we sought to validate these findings in a more physiologically relevant cell line.

Much of the *in vivo* systemic pathology resulting from infection with STx-producing

135

bacteria is related to the effects of circulating levels of STx on microvasculature [42]. STx-mediated endothelial cytotoxicity is believed to contribute to the thrombotic microangiopathy of HUS, and exposure of endothelial cells to STx has been shown to induce thrombotic changes to the endothelial cell surface, further contributing to the pro-coagulant state observed in HUS [43]. We investigated the *in vitro* effects of STx on human microvascular endothelial cells (HMVEC). As with HeLa cells, STx treatment of HMVEC stimulated MK2 activity in a time- and dose-dependent manner (Figures 3A-B), and MK2 activation was shown to be p38-dependent (Figure 5).

In these experiments, we measured cellular responses to STx1 (Figure 3) and STx2 (Figure 5), though we have found that HMVEC cells consistently showed similar sensitivity to both STx subgroups in terms of p38 activation (data not shown). While both subgroups differ in their toxicity in mice [44-46], they share indistinguishable toxicity in our cultured HMVEC and HeLa cells (not shown), consistent with similar observations in Vero cells [47]. However, epidemiological evidence suggests that *stx2*-producing enterohemorrhagic *E. coli* (EHEC) O157:H7 strains are more frequently associated with HUS than are *stx1*-producing strains [48,49]. We therefore found it relevant to study both STx subgroups in the context of p38-MK2 activation.

STx activation of the p38-MK2 pathway is MK2-dependent.

Activation of the p38-MK2 pathway by STx was equally found to be dependent on MK2 catalytic activity. Overexpression of a catalytically inactive adenoviral construct (MK2-DN) in HeLa cells eliminated STx1-induced Hsp27 phosphorylation compared to cells overexpressing wild-type MK2 (MK2-WT) or control vector (pAd-Luc; Figures 6A-

B). To validate this finding and further confirm the role of catalytically active MK2 in

the response to STx, pretreatment of endothelial cells with a recently identified inhibitor

of MK2, PHA-781089, blocked STx1-induced Hsp27 phosphorylation (Figure 6C). This

compound, at a dose of 20 µM, has been previously shown to inhibit Hsp27

phosphorylation of LPS-treated U937 macrophage cells [39]. We found a similar dose

response of PHA-781089 against Hsp27 phosphorylation in STx1-treated HeLa cells

(Figure 6D). Treatment of HMVEC with 20 µM PHA-781089 resulted in undetectable

levels of phosphorylated Hsp27, even after 4 h of STx treatment, while vehicle-treated

controls demonstrated MK2 activity beginning at 60 mins. This effect was not the result

of the MK2 inhibitor on STx transport, as treatment of HeLa cells with PHA-781089

showed no effects on STxB-488 transport to the Golgi (Figure 6D). These findings

suggest that STx stimulates the p38-MK2 pathway in two distinct human cell lines and

that activation of the p38-MK2 pathway may contribute to the endothelial cellular stress

response to STx *in vivo*.

A)

	MK2
	Phospho-Hsp27
	β-Actin

Virus	pAd-Luc	MK2-WT	MK2-DN
STx1 (10 ng/mL):	- +	- +	- +

B)

	MK2-WT	MK2-DN
Viral dilution:	Undil. 1:10 1:100 1:1000 No virus	Undil. 1:10 1:100 1:1000 No virus

MK2

β-Actin

C)

Treatment time (in min):	HI-STx2	0	30	60	120	240
β-Actin
Phospho-Hsp27
β-Actin
Phospho-Hsp27

D)

[PHA-781089] (µM)	0	0	1	2	10	20
STx1 (10 ng/mL)	-	+	+	+	+	+
Phospho-Hsp27
β-Actin

E)

| DMSO	PHA-781089	GCA

STxB

Giantin

Merge

138
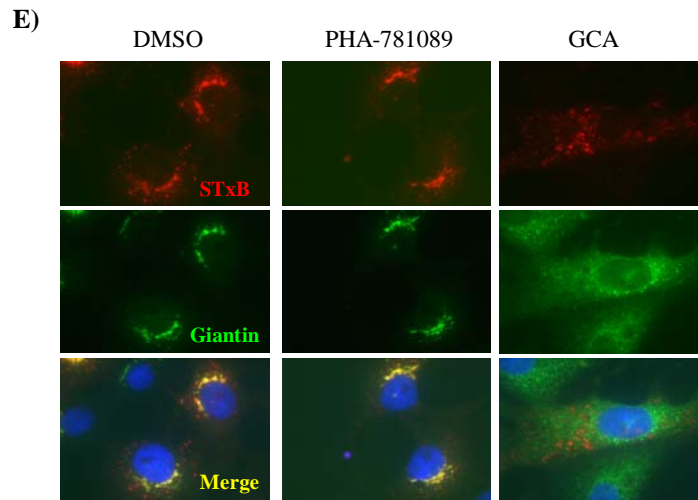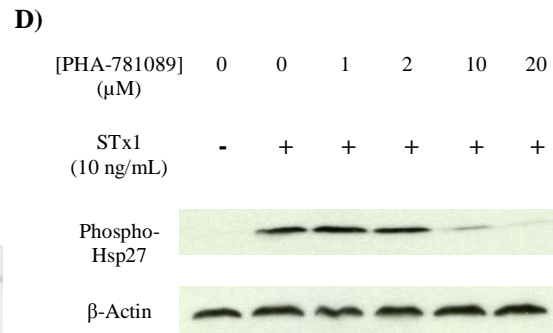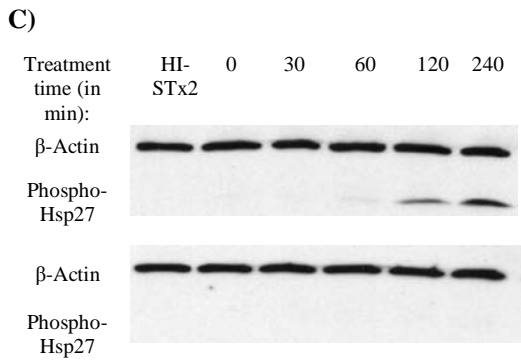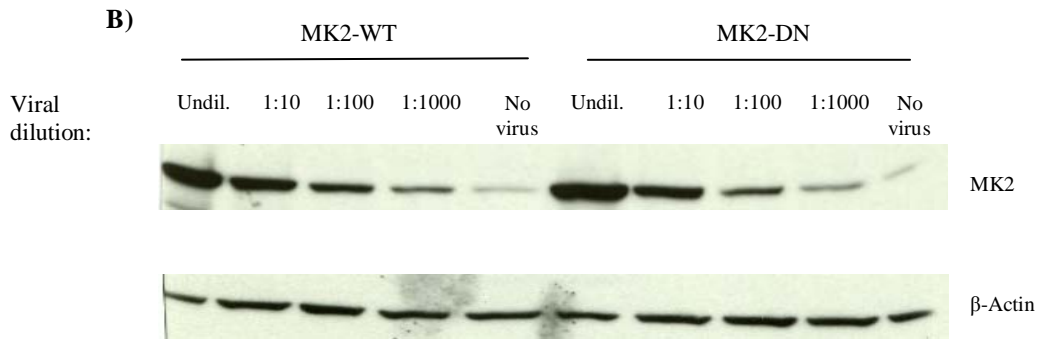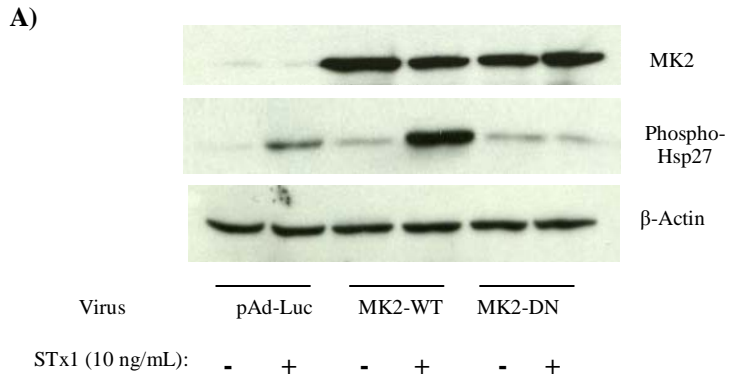
Figure 6. STx activation of the p38-MK2 pathway depends on MK2 activity. (A) Overexpression of catalytically inactive MK2 (MK2-DN) eliminates STx1-induced Hsp27 phosphorylation. HeLa cells were transduced with adenoviral constructs expressing luciferase (pAd-Luc), wild-type MK2 (MK2-WT), or catalytically inactive MK2 (MK2-DN; see Methods). Cells were then exposed to STx1 (10 ng/mL) for 6 h, and equal fractions of lysates were probed with the indicated antibodies. (B) Validation of the MK2 adenoviral vectors. HeLa cells were treated for 24 h with various dilutions of adenoviral constructs overexpressing either wild-type MK2 (MK2-WT) or a catalytically inactive, dominant negative MK2 (MK2-DN). Equal fractions of lysates were probed with the corresponding antibodies. Actin served as a loading control. Undiluted virus (corresponding to an MOI of approximately 100) resulted in the greatest level of MK2 expression and was used for all relevant experiments. (C) HMVEC were pretreated with DMSO (0.5% v/v; top) or the MK2 inhibitor PHA-781089 (20 µM; bottom) for 1 h prior to exposure to STx2 (1 ng/mL) for the indicated times. Lysates were probed with the indicated antibodies. Chemical inhibition of MK2 prevents STx-induced Hsp27 phosphorylation. HI-STx2, heat-inactivated STx2 (1 ng/mL). For (A) and (B), actin staining served as a loading control. (D) PHA-781089 exhibits maximal MK2-inhibitory activity at 20 µM. This concentration is consistent with a previous report [50]. HeLa cells were treated with increasing concentrations of PHA-781089 for 1 h prior to the addition of STx1 (10 ng/mL) for 4 h. Equal fractions of lysates were probed with the indicated antibodies. Actin served as a loading control. Figure is representative of two independent experiments. (E) MK2 inhibition has no effect on the intracellular transport of STxB to the Golgi. The fate of endocytosed fluorescently-tagged STxB (red) was monitored by immunofluorescence in HeLa cells pretreated with DMSO (0.5% v/v), PHA-781089 (20 µM), or GCA (10 µM) prior to staining with an anti-giantin antibody (green). Pretreatment with the MK2 inhibitor has no effect on STxB transport to the Golgi compared to DMSO-treated cells, while GCA prevents toxin colocalization with a giantin-positive structure. STxB, Shiga toxin B subunit; blue, nuclei.

MK2 activation by STx depends on toxin adherence and intracellular transport.

STx, like the plant toxin ricin, follows a retrograde trafficking pathway to reach its intracellular target. Following endocytosis into an early endosome, it is believed that these toxins hijack host trafficking mechanisms in order to bypass lysosomal degradation [51] and coordinate their rerouting to the ER via the Golgi [36]. The toxins are then retrotranslocated across the ER membrane in order to access the cytosol, where they can inhibit protein synthesis by directly damaging the ribosome [3,4,52]. To test whether MK2 activation relied on STx transport to the cytosol, HMVEC were initially incubated with P1 glycoprotein, a ligand of the Gb3 receptor. As STx is known to induce its uptake following binding to the glycosphingolipid Gb3 [53], we would expect that co-incubation of STx1 with the P1 glycoprotein would prevent toxin endocytosis. Indeed, the P1 glycoprotein reduced cell surface-associated STx1 and protected against STx1-mediated inhibition of protein synthesis (not shown). More importantly, the P1

glycoprotein was able to protect against STx-induced p38 and Hsp27 phosphorylation, suggesting that STx must be internalized to stimulate the p38-MK2 pathway (Figure 7A). Similarly, treatment of HMVEC with Golgicide A (GCA), a potent inhibitor of Shiga toxicity that arrests STx transport at the early endosome [54], was shown to also prevent STx-induced p38 and Hsp27 phosphorylation. In contrast, GCA had no effect on anisomycin, an established p38 agonist [55] that does not rely on intracellular transport and that rapidly equilibrates in the cytosol. If we equally consider that treatment with STxB alone did not activate MK2 (Figure 4), these results would collectively suggest that transport of catalytically active STx to the cytosol is required to activate the p38-MK2 pathway.
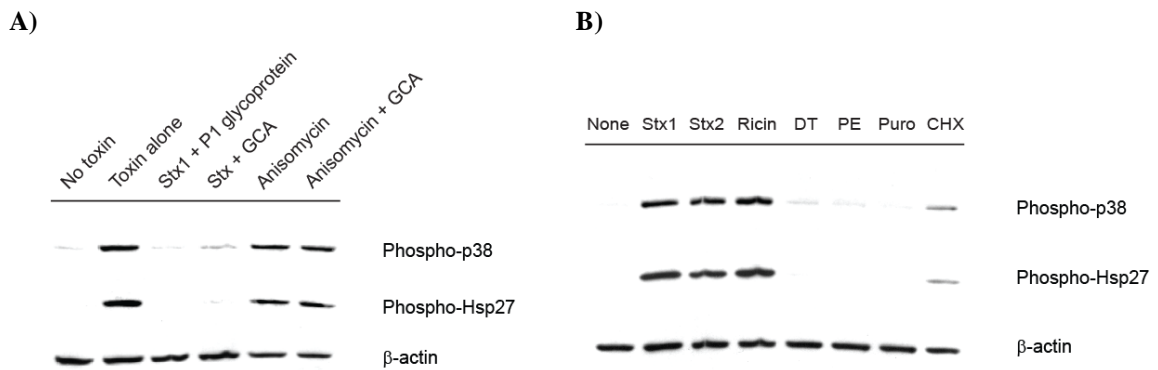
Figure 7. Activation of the p38-MK2 pathway by STx depends on toxin adherence and intracellular trafficking and appears to be part of a ribotoxic stress response. (A) HMVEC were pretreated with DMSO (0.5% v/v), GCA (10 µM), or P1 glycoprotein (1 µg/mL) for 30 min prior to exposure to STx1 (10 ng/mL) or media alone ("No Toxin"). Cells were allowed to internalize toxin for 2 h at 37°C prior to lysis and probing with the indicated antibodies. Pretreatment with the P1 glycoprotein inhibited STx1-mediated phosphorylation of p38 and Hsp27, and GCA treatment similarly blocked activation of the p38-MK2 pathway compared to DMSO-treated cells ("Toxin alone"). Pretreatment with GCA, however, had no effect on activation of this pathway following a 2-h exposure to anisomycin (10 ng/mL). **(B)** HMVEC were exposed to various translational inhibitors for 2 h, and the phosphorylation status of p38 and Hsp27 was assessed by Western blotting. Only inhibitors that are known to cause direct damage to the ribosome (STx1, STx2, and ricin) induced p38 and Hsp27 phosphorylation, while translational inhibitors acting through different mechanisms (DT, PE, Puro, CHX) showed little to no activation. "None" refers to cells lacking compound and toxin treatment. STx1, Shiga toxin 1 (10 ng/mL); STx2, Shiga toxin 2 (10 ng/mL); GCA, Golgicide A; DT, diphtheria toxin (1 µg/mL); PE, *Pseudomonas* exotoxin A (1 µg/mL); Puro, puromycin (10 µg/mL); CHX, cycloheximide (100 µg/mL). For both (A) and (B), actin staining served as a loading control.

MK2 activation relies on damage to the ribosome.

Following entry into the cytosol, STx and ricin inhibit protein synthesis through sequence-specific RNA damage to the α-sarcin loop in the 28S rRNA [56]. Both toxins consist of an enzymatic A subunit that has RNA *N*-glycohydrolase activity and depurinates a single adenine residue at position 4324 of the 28S rRNA. Given that MK2 activation relied on enzymatically active STx (Figure 4), we examined the possibility that MK2 activation was the result of ribosomal damage and not simply a stress response due to translational inhibition. To test this, HMVEC were treated with various inhibitors of protein synthesis acting through distinct mechanisms, and activation of the p38-MK2 pathway was assessed . As expected, STx and ricin treatments both stimulated p38 and Hsp27 phosphorylation (Figure 7B). In addition, both clinically relevant STx subgroups, STx1 and STx2, stimulated a similar response. These subgroups show approximately 60% similarity in the A subunits at the amino acid level [10] and share a common enzymatic mechanism. The bacterial exotoxins diphtheria toxin (DT) and *Pseudomonas* exotoxin A (PE), however, were unable to stimulate the p38-MK2 pathway at concentrations that have been previously shown to inhibit protein synthesis in HeLa cells [57]. Both toxins inhibit protein synthesis by catalyzing the ADP ribosylation of elongation factor 2 [58,59]. Similarly, the aminonucleoside antibiotic puromycin, which arrests translation by causing a premature release of the nascent peptide [60], also failed to activate the p38-MK2 pathway, while cycloheximide, which prevents ribosomal translocation during translational elongation [60], weakly activated it. These findings are consistent with activation of the p38-MK2 pathway following specific damage to the ribosome and not translational inhibition per se.

141

MK2 inhibition decreases the inflammatory response to STx.

MK2 has been implicated in a variety of stress responses, most notably inflammation [31], though no studies have directly assessed MK2's role in the context of the STx-induced inflammatory response. Multiple studies have lent an immmunological perspective to the pathology of HUS [13,14,17]. Given the activation of the p38-MK2 stress response pathway by STx and the contribution of this pathway to inflammation, we assessed the role of MK2 in generating an inflammatory response to STx. HeLa cells were transduced with adenoviral constructs expressing wild-type MK2 (MK2-WT) or a catalytically inactive MK2 (MK2-DN). Expression of these constructs was validated (Figure 6B) and exhibited the expected effects on STx1-induced MK2 activation (Figure 6A). MK2-DN overexpression significantly reduced mRNA levels of the inflammatory cytokines IL-6 and TNFα compared to cells overexpressing MK2-WT, as assessed by quantitative RT-PCR (qRT-PCR; Figures 8A-B). This suggests that catalytically active MK2 is required for the STx1-induced expression of the inflammatory markers IL-6 and TNFα.

A)

B)

C)

D)
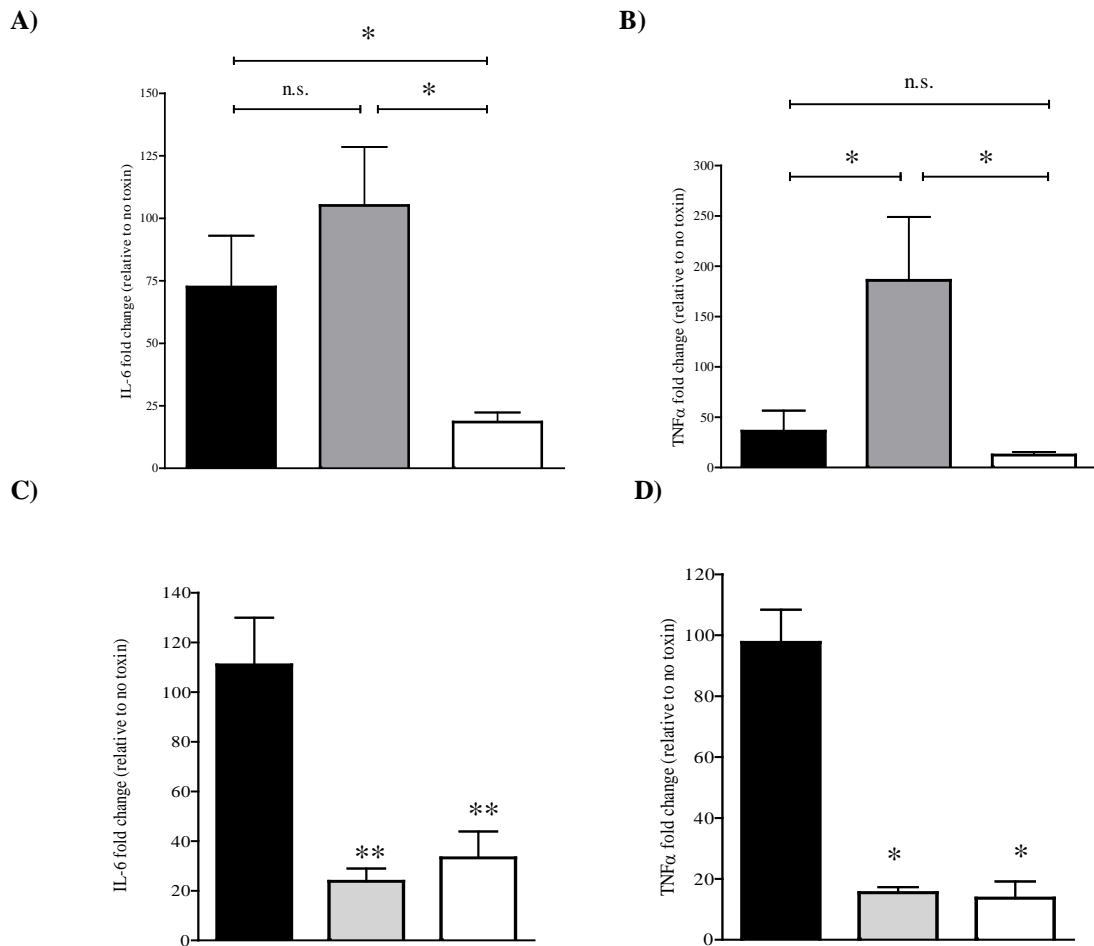
Figure 8. MK2 inhibition reduces the STx-induced inflammatory response in HeLa cells. **(A)** HeLa cells were transduced with a control adenoviral construct (pAd-Luc; black bars), a construct expressing wild-type MK2 (MK2-WT; gray bars), or a construct expressing a catalytically inactive MK2 (MK2-DN; white bars) for 24 h prior to treating with STx1 (10 ng/mL) for 6 h. The levels of IL-6 and TNFα mRNA were determined by qRT-PCR and are expressed as a fold change above mRNA levels in transduced cells lacking STx1 (see Methods). Data points represent duplicate data from three independent experiments (mean ±S.D.). Sample means were compared using a two-tailed Student's t-test for independent samples. **(B)** HeLa cells were pretreated with DMSO (0.5% v/v; black bars), the MK2 inhibitor PHA-781089 (20 µM; gray bars), or the p38 inhibitor SB202190 (10 µM; white bars) for 1 h prior to a 6-h exposure to STx1 (100 ng/mL). The levels of IL-6 and TNFα mRNA were determined by qRT-PCR and are expressed as a fold change above mRNA levels in compound-treated cells in the absence of STx1. Data points represent duplicate data from three independent experiments (mean ±S.D.). Sample means were compared as in (A). n.s. denotes no significant change, * significant change ($p<0.05$), ** highly significant change ($p<0.01$).

To further confirm that MK2 inhibition reduced the cytokine response to STx1, HeLa cells were pretreated with DMSO, an MK2 inhibitor, or a p38 inhibitor prior to a 6-h exposure to STx1. Chemical inhibition of MK2 significantly reduced IL-6 and TNFα mRNA levels (Figures 8C-D), consistent with overexpression of catalytically inactive MK2 (Figures 8A-B). Similarly, chemical inhibition of p38, the kinase upstream of

143

MK2, also significantly reduced the levels of these general inflammatory cytokines (Figures 8C-D). These trends could be duplicated in a human macrophage cell ine, THP-1. Chemical inhibition of MK2 in human macrophages (Figure 9A) reduced the levels of IL-6 and TNFα transcripts(Figure 9B). Together, our results collectively show that genetic and chemical inhibition of MK2 activity significantly reduces the inflammatory response to STx1. Chemical inhibition of MK2 thus presents a unique opportunity for targeting the immunopathological response to STx *in vivo*.

A)

Treatment:	Media	Media	PHA-781089 (20 µM)	PHA-781089 (20 µM)

STx2
(100 ng/mL)   -   +   -   +

Phospho-Hsp27

β-actin

B)
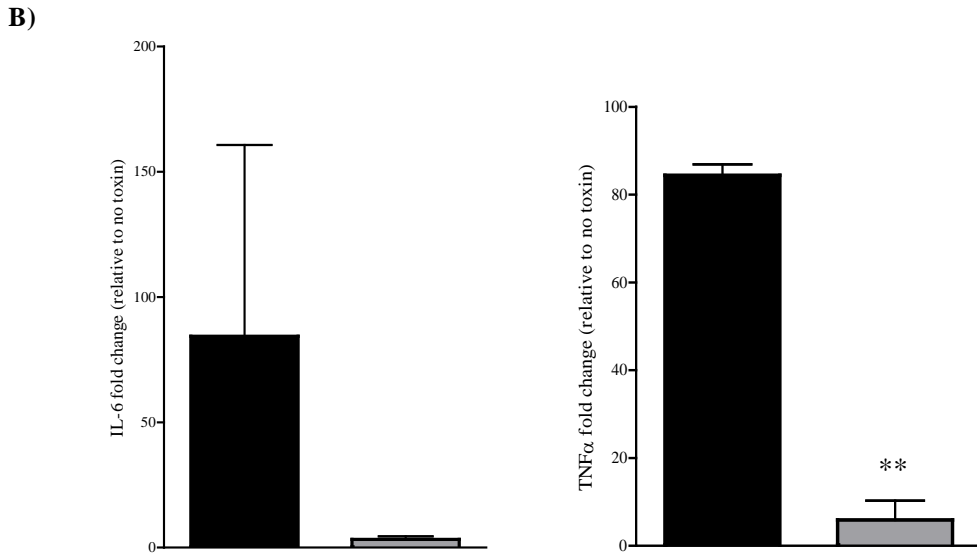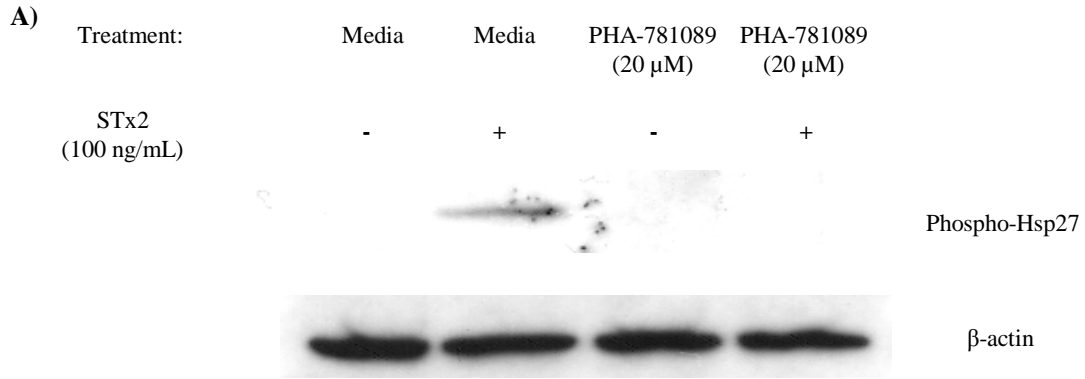
Figure 9. Chemical inhibition of MK2 reduces the inflammatory response to STx in THP-1 cells.
(A) THP-1 cells were pretreated with media alone or the MK2 inhibitor PHA-781089 for 1 h prior to a 6-h exposure to STx2 (100 ng/mL). Cell lysates were probed with the indicated antibodies. Staining with β-actin served as a loading control. **(B)** THP-1 cells were pretreated with media alone (black bars) or the MK2 inhibitor PHA-781089 (20 µM; gray bars) for 1 h prior to a 6-h exposure to STx1 (100 ng/mL). The levels of IL-6 and TNFα mRNA were determined by qRT-PCR and are expressed as a fold change above mRNA levels in compound-treated cells in the absence of STx1. Data points represent duplicate data from three independent experiments (mean ±S.D.). Sample means were compared as in (A). n.s. denotes no significant change, ** highly significant change (p<0.01).

DISCUSSION

In an effort to identify kinases involved in Shiga toxicity, we developed and adapted a siRNA screen targeting the human kinome to identify kinases essential to STx-induced cytotoxicity. Of the 646 kinases tested, six were identified as protective, with MK2 exhibiting the greatest protection. Compared to previous high-throughput screens aimed at identifying small molecule inhibitors of microbial toxicity [34-36,54], the siRNA approach represents an inherently target-based approach that is not hampered by potential intracellular "off-target" effects of small molecules.

While previous screens [36,54] focused on inhibitors of toxin trafficking and monitored Shiga toxicity over a shorter time period (~ 4-6 h), the siRNA screen relied on a 24-h exposure to STx due to the relatively long half-life of the Fluc translational reporter. As a result, we would expect that, following a longer exposure to STx, knock-down of kinases involved in STx transport as well as those involved in STx-induced cell death would show up as protective. Indeed, knock-down of MK2 exhibited strong protection against Shiga toxicity in our screen. A subsequent assessment of cell viability by Alamar Blue staining revealed that wells transfected with MK2 siRNA showed relatively higher cell viability (not shown; see reference), which may have accounted for the protective effects observed. The role of MK2 in STx-induced cell death remains unclear and is currently under investigation.

The central role of the p38 MAPK in propagating various cellular stress responses [18] has made specific inhibition of p38-dependent signaling pathways particularly difficult. MK2 thus appears as a tempting target, given that it functions downstream of p38 on a smaller set of substrates [32]. More importantly, MK2 has been

146

implicated in the inflammatory response in a lipopolysaccharide (LPS) mouse model [31]: MK2-deficient mice showed decreased TNFα and IL-6 levels and increased survival to LPS-induced shock. In an experimental asthma model, MK2 was found to be essential to Th2-type inflammation through sustained NF-κB activation [61]. Most recently, selective MK2 inhibitors have been developed for the treatment of animal models of rheumatoid arthritis and other inflammatory conditions mediated by TNFα [50]. The contribution of the inflammatory response in HUS remains debated, though several lines of evidence would suggest that some of the systemic pathology, namely the development of thrombotic lesions within the renal microvasculature, could be an immunopathological phenomenon [14,15,62]. Our studies suggest that catalytically active STx activates MK2 as a result of ribosomal damage, implicating MK2 in the STx ribotoxic stress response.

Biochemical evidence suggests that MK2 contributes to the stability of IL-6 and TNFα mRNA through the downstream phosphorylation of TTP in a process that involves AU-rich elements (ARE) in the 3' non-coding regions of these mRNAs [63-67]: phosphorylation of TTP by MK2 results in TTP sequestration and prevents TTP from directing degradation of these mRNAs. In our studies, MK2 inhibition by genetic and chemical means diminished the acute inflammatory response in STx-treated HeLa cells. Overexpression of catalytically inactive MK2 significantly decreased the mRNA levels of IL-6 and TNFα, and chemical inhibition of MK2 mirrored these effects.

Interestingly, HMVEC under the same tissue culture conditions did not exhibit the cytokine response that was observed in HeLa cells, despite demonstrating STx-dependent activation of the p38-MK2 pathway *in vitro*. Our studies utilized HMVEC of dermal origin, whose sensitivity to STx is similar to that of Vero cells [68]. Certain human

147

microvascular endothelial cell lines have been shown to mount a STx-dependent cytokine response *in vitro* [69,70], though these responses appear to be cell origin-dependent [71] and require pre-sensitization with inflammatory cytokines. Nonetheless, the observed cytokine response in both HeLa cells and human macrophages could be crucial to establishing a local inflammatory milieu *in vivo*. In particular, decreased *in vitro* levels of the general inflammatory markers TNFα and IL-6 in MK2-inhibited cells is consistent with decreased cytokine expression in MK2-deficient mice [31] and could translate to decreased immunopathology following exposure to STx. Inhibition of MK2 thus presents a viable therapeutic option in mitigating the toxemic effects of STx-mediated disease.

ACKNOWLEDGEMENTS

MATERIALS AND METTHODS

Reagents and antibodies

Shiga toxin 1 (STx1) and 2 (STx2) were kindly provided by Anne Kane (Tufts University) and diluted to 0.5 mg/mL in PBS (pH 7.4). Aliquots were frozen at -80°C until further use. Ricin, *Pseudomonas* exotoxin A, and diphtheria toxin were purchased from Sigma. The B subunit of STx1 (STxB) was purified and fluorescently tagged as previously described [36]. SB202190, SB203580, SP600125, anisomycin, puromycin, cycloheximide, and DMSO were purchased from Sigma, p38 inhibitor III from Calbiochem, Golgicide A from ChemDiv, and PHA-781089 from Pfizer. All chemical inhibitors were diluted to 10 mM in DMSO and stored at -20°C until further use. All antibodies used for Western blotting were purchased from Cell Signaling Technology, Inc. Dulbecco's modified Eagle's medium (DMEM), streptomycin, and penicillin were from Mediatech, and fetal bovine serum (FBS) was from Hyclone. Protease inhibitor cocktail was from Roche.

Cell culture

HeLa cells were obtained from the Tissue Culture Support Center (Washington University) and maintained at 37°C and 5% CO_2 in DMEM supplemented with 10% FBS and 0.1% penicillin/streptomycin. HeLa-Fluc cells were kindly provided by David Piwnica-Worms (Washington University) and maintained in DMEM supplemented with 10% FBS, 1% penicillin/streptomycin, and 1 mg/mL G418 (Washington University Tissue Culture Support Center). Human dermal microvascular endothelial cells (HMVEC) were purchased from Lonza and maintained in EGM-2MV medium (Lonza) at

37ºC and 5% CO_2. 293A cells were purchased from Invitrogen and maintained at 37ºC

and 5% CO_2 in DMEM supplemented with 10% FBS and 1% penicillin/streptomycin.

THP-1 cells were obtained from American Type Culture Collection and maintained in

DMEM supplemented with 10% FBS and 1% penicillin/streptomycin. For experiments,

THP-1 cells were seeded at 1 x 10^6 cells/well in 6-well dishes and subsequently

stimulated for 48 h with 50 ng/mL phorbol 12-myristate 13-acetate (PMA; Sigma).

Adherent cells were washed twice with DMEM and incubated in fresh medium lacking

PMA. Medium was changed every 24 h for 3 additional days, after which cells were

used for experiments.

siRNA kinome screen

The Human Kinase siRNA library set version 2.0 was provided by Qiagen. Fully

annealed duplex siRNAs were suspended in 1X annealing buffer (100 mM KOAc, 30

mM HEPES-KOH, 2 mM MgOAc, pH 7.4) and 0.25 nmol of pooled siRNAs were stored

at -80ºC until further use. HeLa-Fluc cells were seeded at 1 x 10^4 cells/well in thirty-six

96-well plates (Costar) and grown overnight at 37ºC and 5% CO_2. The next day, each

well was transfected with a duplex of siRNAs (50 nM) targeting a specific kinase, and

cells were subsequently incubated for 48 h at 37ºC. STx1 (1 ng/mL) was added for 24 h,

and light levels were determined using the PerkinElmer Envision XCite Multilabel

Reader (1 min delay, 1 s integration). Following luminescence readings, 10 µL of

Alamar Blue (440 µM resazurin sodium salt stock; Sigma) were added to each well, and

plates were incubated for 2 h at 37ºC. Alamar Blue levels were detected using the

FluoStar OPTIMA spectrophotometer (BMG Labtech).

150

Each plate contained a positive control and a series of negative controls, as well as a control for transfection efficiency. Positive controls included siRNA against the delta isoform of PKC (PKCδ siRNA, Dharmacon; Figure 1A), whose knock-down has been shown to protect against Shiga toxicity [72], or pretreatment for 1 h with GCA (10 µM), which has been equally shown to be protective against Shiga toxicity [54]. Negative controls included cells containing media alone, transfection reagent alone (DharmaFECT1, Dharmacon), negative control siRNA (Dharmacon), scrambled siRNA (Qiagen), and GFP siRNA (Qiagen). Transfection efficiency was controlled for by transfecting cells with siRNA targeting the luciferase reporter (GL3 siRNA; Dharmacon) and ensuring >75% drop in light levels (Figure 1B). All controls were validated prior to incorporating them in the screen. MK2 duplex siRNA sequences provided in the Qiagen library were as follows: 5'-CGCCATCATCGATGACTACAA-3' and 5'-CTACGAGCAGATCAAGATAAA-3'.

siRNA kinome library

The Human Kinase siRNA library set version 2.0 (Qiagen) consisted of 1292 HPP-grade siRNA duplexes targeting 646 human kinase and kinase-associated genes (two siRNA duplexes/gene). Targeted kinase genes included tyrosine kinases and tyrosine kinase-like kinases, calcium/calmodulin-dependent protein kinases, members of the protein kinase C family, cyclin-dependent protein kinases, mitogen-activated protein kinases, casein kinases, receptor guanyl cyclases, atypical kinases, and other less-characterized kinases. The siRNA kinase gene list can be found at

http://www1.qiagen.com/Products/GeneSilencing/LibrarySiRna/SiRnaSets/HumanKinase siRNASet.aspx?ShowInfo=1.

Western blotting

Following compound and toxin treatments, cells were lysed in lysis buffer (20 mM Tris-HCl pH 7.5, 150 mM NaCl, 1 mM Na_2EDTA, 1 mM EGTA, 1% Triton, 2.5 mM sodium pyrophosphate, 1 mM β-glycerophosphate, 1 mM Na_3VO_4, 1 µg/mL leupeptin, 1X protease inhibitor cocktail) and resolved on a 4-15% Tris-HCl gel (Biorad) prior to transfer onto PVDF membranes (Invitrogen). Membranes were probed with corresponding primary antibodies (1:1000) and anti-rabbit alkaline phosphatase-conjugated secondary antibodies (Invitrogen). Membranes were washed and developed using the Western Breeze kit protocol (Invitrogen). For experiments comparing multiple phospho-proteins, membranes were washed and reprobed with additional antibodies. Where indicated, equal fractions of lysates from the same experiment were run on separate gels and probed with the corresponding primary antibodies.

Overexpression of MK2-WT and MK2-DN

Recombinant wild-type MK2 (MK2-WT) and catalytically inactive MK2 (MK2-DN) adenoviruses were purchased from Cell Biolabs, Inc. and amplified in 293A cells using the manufacturer's protocol. The pAd-Luc adenoviral construct has been previously reported and validated [57]. Viral stocks were stored at -80ºC until further use. Confluent HeLa cells were transduced for 24 h prior to a 6-h expsoure to STx1 (10 ng/mL). Lysates were probed by Western blotting with antibodies to MK2, phospho-

Hsp27, and β-actin. For cytokine mRNA measurements, HeLa cells were transduced for

24 h, exposed to STx1 for 6h, and RNA was harvested using the RNeasy Mini Kit

(Qiagen), according to the manufacturer's protocol.

Immunohistochemistry

HeLa cells were seeded at 2.5 x 10^{4}cells/well and grown overnight on coverslips

(Labtek) at 37ºC. The next day, cells were treated with DMSO (0.5% v/v), PHA-781089

(20 µM), or GCA (10 µM) prior to treatment with STxB-488 (1 µg/mL; Molecular

Probes). Cells were kept at 4ºC, prior to internalization of STxB-488 for 1 h at 37ºC.

Cells were fixed in 4% paraformaldehyde for 15 min at room temperature, washed with

PBS, then permeabilized for 30 min at room temperature with permeabilization buffer

(PBS, 2% bovine serum albumin, 0.5% Triton X). Cells were washed and blocked in

blocking buffer (PBS, 2% bovine serum albumin, 0.1% Triton X) for 30 min at room

temperature prior to staining with rabbit anti-giantin antibody (1:500; Covance) for 1 h at

room temperature. Coverslips were washed and subsequently stained with AlexaFluor-

488 donkey anti-rabbit IgG (1:200; Molecular Probes) for 45 min at room temperature.

Cells were washed with PBS and mounted with SlowFade reagent (with DAPI;

Molecular Probes) for epifluorescence microscopy using a Zeiss microscope.

Quantitative RT-PCR (qRT-PCR)

For cells overexpressing MK2 adenoviral constructs, HeLa cells were transduced

for 24 h, exposed to STx1 for 6h, and RNA was harvested using the RNeasy Mini Kit.

For experiments involving chemical inhibition of MK2, HeLa cells were pretreated with

DMSO, PHA-781089, or SB202190 at the indicated concentrations for 1h at 37ºC. Cells were then left untreated or were exposed to STx1 (100 ng/mL) for 6 h. Cells were washed once with cold PBS, and RNA was extracted using the RNeasy Mini Kit. cDNA was synthesized in duplicate from 200 ng of each sample using commercially available primers for GAPDH, IL-6, and TNFα (Applied Biosystems). For each qRT-PCR run, the calculated threshold cycle (Ct) was normalized to the threshold cycle of the GAPDH gene amplified from the corresponding sample. The fold change was calculated using the $2^{-\Delta\Delta Ct}$ method [73] and represents the fold change above adenovirally-transduced or compound-treated cells lacking STx1 treatment.

Statistical analyses

Data were processed and analyzed using GraphPad Prism version 5.00 for Windows (GraphPad software). Cytokine mRNA levels were compared using the two-tailed Student's t-test (VassarStats, http://faculty.vassar.edu/lowry/tu.html) for three independent experiments. Differences were considered significant for $p < 0.05$ and highly significant for $p < 0.01$.

REFERENCES

1. Falguieres, T. et al. Targeting of Shiga toxin B-subunit to retrograde transport route in association with detergent-resistant membranes. *Molecular Biology of the Cell* **12**, 2453-68 (2001).

2. Falnes, P.O. & Sandvig, K. Penetration of protein toxins into cells. *Current Opinion in Cell Biology* **12**, 407-13 (2000).

3. Simpson, J.C. et al. Ricin A chain utilises the endoplasmic reticulum-associated protein degradation pathway to enter the cytosol of yeast. *FEBS Letters* **459**, 80-4 (1999).

4. Yu, M. & Haslam, D.B. Shiga toxin is transported from the endoplasmic reticulum following interaction with the luminal chaperone HEDJ/ERdj3. *Infection & Immunity* **73**, 2524-32 (2005).

5. Endo, Y. & Tsurugi, K. Mechanism of action of ricin and related toxic lectins on eukaryotic ribosomes. *Nucleic Acids Symp Ser*, 187-90 (1986).

6. Obrig, T.G., Moran, T.P. & Brown, J.E. The mode of action of Shiga toxin on peptide elongation of eukaryotic protein synthesis. *Biochem J* **244**, 287-94 (1987).

7. Reisbig, R., Olsnes, S. & Eiklid, K. The cytotoxic activity of Shigella toxin. Evidence for catalytic inactivation of the 60 S ribosomal subunit. *J Biol Chem* **256**, 8739-44 (1981).

8. Griffin, P.M. & Tauxe, R.V. The epidemiology of infections caused by Escherichia coli O157:H7, other enterohemorrhagic E. coli, and the associated hemolytic uremic syndrome. *Epidemiol Rev* **13**, 60-98 (1991).

9.   Karmali, M.A. Infection by verocytotoxin-producing Escherichia coli. *Clinical Microbiology Reviews* **2**, 15-38 (1989).

10.   Proulx, F., Seidman, E.G. & Karpman, D. Pathogenesis of Shiga toxin-associated hemolytic uremic syndrome. *Pediatr Res* **50**, 163-71 (2001).

11.   Obrig, T.G. et al. Direct cytotoxic action of Shiga toxin on human vascular endothelial cells. *Infect Immun* **56**, 2373-8 (1988).

12.   Louise, C.B. & Obrig, T.G. Shiga toxin-associated hemolytic uremic syndrome: combined cytotoxic effects of shiga toxin and lipopolysaccharide (endotoxin) on human vascular endothelial cells in vitro. *Infect Immun* **60**, 1536-43 (1992).

13.   Te Loo, D.M. et al. Shiga toxin-1 affects nitric oxide production by human glomerular endothelial and mesangial cells. *Pediatr Nephrol* **21**, 1815-23 (2006).

14.   Ramegowda, B. & Tesh, V.L. Differentiation-associated toxin receptor modulation, cytokine production, and sensitivity to Shiga-like toxins in human monocytes and monocytic cell lines. *Infect Immun* **64**, 1173-80 (1996).

15.   Kaye, S.A., Louise, C.B., Boyd, B., Lingwood, C.A. & Obrig, T.G. Shiga toxin-associated hemolytic uremic syndrome: interleukin-1 beta enhancement of Shiga toxin cytotoxicity toward human vascular endothelial cells in vitro. *Infect Immun* **61**, 3886-91 (1993).

16.   van de Kar, N.C., Monnens, L.A., Karmali, M.A. & van Hinsbergh, V.W. Tumor necrosis factor and interleukin-1 induce expression of the verocytotoxin receptor globotriaosylceramide on human endothelial cells: implications for the pathogenesis of the hemolytic uremic syndrome. *Blood* **80**, 2755-64 (1992).

17.   van Setten, P.A. et al. Effects of TNF alpha on verocytotoxin cytotoxicity in purified human glomerular microvascular endothelial cells. *Kidney Int* **51**, 1245-56 (1997).

18.   Ono, K. & Han, J. The p38 signal transduction pathway: activation and function. *Cell Signal* **12**, 1-13 (2000).

19.   Zarubin, T. & Han, J. Activation and signaling of the p38 MAP kinase pathway. *Cell Res* **15**, 11-8 (2005).

20.   Foster, G.H. & Tesh, V.L. Shiga toxin 1-induced activation of c-Jun NH(2)-terminal kinase and p38 in the human monocytic cell line THP-1: possible involvement in the production of TNF-alpha. *J Leukoc Biol* **71**, 107-14 (2002).

21.   Stone, M.K., Kolling, G.L., Lindner, M.H. & Obrig, T.G. p38 mitogen-activated protein kinase mediates lipopolysaccharide and tumor necrosis factor alpha induction of shiga toxin 2 sensitivity in human umbilical vein endothelial cells. *Infect Immun* **76**, 1115-21 (2008).

22.   Smith, W.E. et al. Shiga toxin 1 triggers a ribotoxic stress response leading to p38 and JNK activation and induction of apoptosis in intestinal epithelial cells. *Infect Immun* **71**, 1497-504 (2003).

23.   Cherla, R.P., Lee, S.Y., Mees, P.L. & Tesh, V.L. Shiga toxin 1-induced cytokine production is mediated by MAP kinase pathways and translation initiation factor eIF4E in the macrophage-like THP-1 cell line. *J Leukoc Biol* **79**, 397-407 (2006).

24.   Allen, M. et al. Deficiency of the stress kinase p38alpha results in embryonic lethality: characterization of the kinase dependence of stress responses of enzyme-deficient embryonic stem cells. *J Exp Med* **191**, 859-70 (2000).

25.   Mudgett, J.S. et al. Essential role for p38alpha mitogen-activated protein kinase in placental angiogenesis. *Proc Natl Acad Sci U S A* **97**, 10454-9 (2000).

26.   Tamura, K. et al. Requirement for p38alpha in erythropoietin expression: a role for stress kinases in erythropoiesis. *Cell* **102**, 221-31 (2000).

27.   Dominguez, C., Powers, D.A. & Tamayo, N. p38 MAP kinase inhibitors: many are made, but few are chosen. *Curr Opin Drug Discov Devel* **8**, 421-30 (2005).

28.   Somwar, R. et al. A dominant-negative p38 MAPK mutant and novel selective inhibitors of p38 MAPK reduce insulin-stimulated glucose uptake in 3T3-L1 adipocytes without affecting GLUT4 translocation. *J Biol Chem* **277**, 50386-95 (2002).

29.   Henry, J.R. et al. Potent inhibitors of the MAP kinase p38. *Bioorg Med Chem Lett* **8**, 3335-40 (1998).

30.   Gaestel, M., Kotlyarov, A. & Kracht, M. Targeting innate immunity protein kinase signalling in inflammation. *Nat Rev Drug Discov* **8**, 480-99 (2009).

31.   Kotlyarov, A. et al. MAPKAP kinase 2 is essential for LPS-induced TNF-alpha biosynthesis. *Nat Cell Biol* **1**, 94-7 (1999).

32.   Gaestel, M. MAPKAP kinases - MKs - two's company, three's a crowd. *Nat Rev Mol Cell Biol* **7**, 120-30 (2006).

33.   Sauter, K.A. et al. Mouse model of hemolytic-uremic syndrome caused by endotoxin-free Shiga toxin 2 (Stx2) and protection from lethal outcome by anti-Stx2 antibody. *Infect Immun* **76**, 4469-78 (2008).

34.   Carey, K.L., Westwood, N.J., Mitchison, T.J. & Ward, G.E. A small-molecule approach to studying invasive mechanisms of Toxoplasma gondii. *Proceedings of*

the National Academy of Sciences of the United States of America **101**, 7433-8 (2004).

35.   Hung, D.T., Shakhnovich, E.A., Pierson, E. & Mekalanos, J.J. Small-molecule inhibitor of Vibrio cholerae virulence and intestinal colonization. *Science* **310**, 670-4 (2005).

36.   Saenz, J.B., Doggett, T.A. & Haslam, D.B. Identification and characterization of small molecules that inhibit intracellular toxin transport. *Infect Immun* **75**, 4552-61 (2007).

37.   Saenz, J.B. et al. Golgicide A reveals essential roles for GBF1 in Golgi assembly and function. *Nat Chem Biol* **5**, 157-65 (2009).

38.   Gross, S. & Piwnica-Worms, D. Real-time imaging of ligand-induced IKK activation in intact cells and in living mice. *Nat Methods* **2**, 607-14 (2005).

39.   Anderson, D.R. et al. Aminocyanopyridine inhibitors of mitogen activated protein kinase-activated protein kinase 2 (MK-2). *Bioorg Med Chem Lett* **15**, 1587-90 (2005).

40.   Lauvrak, S.U. et al. Shiga toxin regulates its entry in a Syk-dependent manner. *Mol Biol Cell* **17**, 1096-109 (2006).

41.   Katagiri, Y.U. et al. Activation of Src family kinase yes induced by Shiga toxin binding to globotriaosyl ceramide (Gb3/CD77) in low density, detergent-insoluble microdomains. *J Biol Chem* **274**, 35278-82 (1999).

42.   Tarr, P.I., Gordon, C.A. & Chandler, W.L. Shiga-toxin-producing Escherichia coli and haemolytic uraemic syndrome. *Lancet* **365**, 1073-86 (2005).

43. Morigi, M. et al. Verotoxin-1-induced up-regulation of adhesive molecules renders microvascular endothelial cells thrombogenic at high shear stress. *Blood* **98**, 1828-35 (2001).

44. Lindgren, S.W., Samuel, J.E., Schmitt, C.K. & O'Brien, A.D. The specific activities of Shiga-like toxin type II (SLT-II) and SLT-II-related toxins of enterohemorrhagic Escherichia coli differ when measured by Vero cell cytotoxicity but not by mouse lethality. *Infect Immun* **62**, 623-31 (1994).

45. Paros, M., Tarr, P.I., Kim, H., Besser, T.E. & Hancock, D.D. A comparison of human and bovine Escherichia coli O157:H7 isolates by toxin genotype, plasmid profile, and bacteriophage lambda-restriction fragment length polymorphism profile. *J Infect Dis* **168**, 1300-3 (1993).

46. Samuel, J.E. et al. Comparison of the glycolipid receptor specificities of Shiga-like toxin type II and Shiga-like toxin type II variants. *Infect Immun* **58**, 611-8 (1990).

47. Tesh, V.L. et al. Comparison of the relative toxicities of Shiga-like toxins type I and type II for mice. *Infect Immun* **61**, 3392-402 (1993).

48. Ostroff, S.M. et al. Toxin genotypes and plasmid profiles as determinants of systemic sequelae in Escherichia coli O157:H7 infections. *J Infect Dis* **160**, 994-8 (1989).

49. Scotland, S.M., Willshaw, G.A., Smith, H.R. & Rowe, B. Properties of strains of Escherichia coli belonging to serogroup O157 with special reference to production of Vero cytotoxins VT1 and VT2. *Epidemiol Infect* **99**, 613-24 (1987).

50.   Anderson, D.R. et al. Pyrrolopyridine inhibitors of mitogen-activated protein kinase-activated protein kinase 2 (MK-2). *J Med Chem* **50**, 2647-54 (2007).

51.   Wilcke, M. et al. Rab11 regulates the compartmentalization of early endosomes required for efficient transport from early endosomes to the trans-golgi network. *Journal of Cell Biology* **151**, 1207-20 (2000).

52.   Yu, M., Haslam, R.H. & Haslam, D.B. HEDJ, an Hsp40 co-chaperone localized to the endoplasmic reticulum of human cells. *Journal of Biological Chemistry* **275**, 24984-92 (2000).

53.   Takenouchi, H. et al. Shiga toxin binding to globotriaosyl ceramide induces intracellular signals that mediate cytoskeleton remodeling in human renal carcinoma-derived cells. *J Cell Sci* **117**, 3911-22 (2004).

54.   Saenz, J.B. et al. Golgicide A reveals essential roles for GBF1 in Golgi assembly and function. *Nat Chem Biol* (2009).

55.   Wang, X. et al. Complete inhibition of anisomycin and UV radiation but not cytokine induced JNK and p38 activation by an aryl-substituted dihydropyrrolopyrazole quinoline and mixed lineage kinase 7 small interfering RNA. *J Biol Chem* **280**, 19298-305 (2005).

56.   Iordanov, M.S. et al. Ribotoxic stress response: activation of the stress-activated protein kinase JNK1 by inhibitors of the peptidyl transferase reaction and by sequence-specific RNA damage to the alpha-sarcin/ricin loop in the 28S rRNA. *Mol Cell Biol* **17**, 3373-81 (1997).

57. Zhao, L. & Haslam, D.B. A quantitative and highly sensitive luciferase-based assay for bacterial toxins that inhibit protein synthesis. *J Med Microbiol* **54**, 1023-30 (2005).

58. Yates, S.P. & Merrill, A.R. Elucidation of eukaryotic elongation factor-2 contact sites within the catalytic domain of Pseudomonas aeruginosa exotoxin A. *Biochem J* **379**, 563-72 (2004).

59. Deng, Q. & Barbieri, J.T. Molecular mechanisms of the cytotoxicity of ADP-ribosylating toxins. *Annu Rev Microbiol* **62**, 271-88 (2008).

60. Pestka, S. Inhibitors of ribosome functions. *Annu Rev Microbiol* **25**, 487-562 (1971).

61. Gorska, M.M. et al. MK2 controls the level of negative feedback in the NF-kappaB pathway and is essential for vascular permeability and airway inflammation. *J Exp Med* **204**, 1637-52 (2007).

62. Harel, Y. et al. A reporter transgene indicates renal-specific induction of tumor necrosis factor (TNF) by shiga-like toxin. Possible involvement of TNF in hemolytic uremic syndrome. *J Clin Invest* **92**, 2110-6 (1993).

63. Sun, L. et al. Tristetraprolin (TTP)-14-3-3 complex formation protects TTP from dephosphorylation by protein phosphatase 2a and stabilizes tumor necrosis factor-alpha mRNA. *J Biol Chem* **282**, 3766-77 (2007).

64. Carballo, E. et al. Decreased sensitivity of tristetraprolin-deficient cells to p38 inhibitors suggests the involvement of tristetraprolin in the p38 signaling pathway. *J Biol Chem* **276**, 42580-7 (2001).

65. Stoecklin, G. et al. MK2-induced tristetraprolin:14-3-3 complexes prevent stress granule association and ARE-mRNA decay. *Embo J* **23**, 1313-24 (2004).

66. Mahtani, K.R. et al. Mitogen-activated protein kinase p38 controls the expression and posttranslational modification of tristetraprolin, a regulator of tumor necrosis factor alpha mRNA stability. *Mol Cell Biol* **21**, 6461-9 (2001).

67. Neininger, A. et al. MK2 targets AU-rich elements and regulates biosynthesis of tumor necrosis factor and interleukin-6 independently at different post-transcriptional levels. *J Biol Chem* **277**, 3065-8 (2002).

68. Pijpers, A.H. et al. Verocytotoxin-induced apoptosis of human microvascular endothelial cells. *J Am Soc Nephrol* **12**, 767-78 (2001).

69. Guessous, F. et al. Shiga toxin 2 and lipopolysaccharide induce human microvascular endothelial cells to release chemokines and factors that stimulate platelet function. *Infect Immun* **73**, 8306-16 (2005).

70. Stricklett, P.K., Hughes, A.K. & Kohan, D.E. Inhibition of p38 mitogen-activated protein kinase ameliorates cytokine up-regulated shigatoxin-1 toxicity in human brain microvascular endothelial cells. *J Infect Dis* **191**, 461-71 (2005).

71. Obrig, T.G. et al. Endothelial heterogeneity in Shiga toxin receptors and responses. *J Biol Chem* **268**, 15484-8 (1993).

72. Torgersen, M.L., Walchli, S., Grimmer, S., Skanland, S.S. & Sandvig, K. Protein kinase Cdelta is activated by Shiga toxin and regulates its transport. *J Biol Chem* **282**, 16317-28 (2007).

73.	Livak, K.J. & Schmittgen, T.D. Analysis of relative gene expression data using real-time quantitative PCR and the 2(-Delta Delta C(T)) Method. *Methods* **25**, 402-8 (2001).

CHAPTER V

Conclusions and Future Directions

CONCLUSIONS

The study of Shiga toxin (STx) pathogenesis is inherently an investigation into host intracellular transport as well as into the activation of host stress response pathways. The unique trafficking mechanism of this bacterial exotoxin makes it an ideal probe for uncovering the host mechanisms underlying its transport. In addition, the development of hemolytic uremic syndrome (HUS) following Shiga toxicity highlights the need to understand the initiation and regulation of the host stress response in order to limit toxin-mediated systemic injury. Our studies have focused on inhibiting STx pathogenesis through a multi-faceted approach. A high-throughput screen aimed at identifying small molecules that block intracellular STx transport identified three potential inhibitors, one of which enhanced our understanding into the role of GBF1 in mediating anterograde and retrograde host transport. A subsequent siRNA screen adapted to a high-throughput format led us to pursue the role of the MAP kinase-activated protein kinase 2 (MK2) in mediating the inflammatory response to STx. The major conclusions of this work include: (i) small molecules are amenable to screens for inhibitors of STx transport, (ii) compounds 75 and 134 inhibit Shiga toxicity by blocking toxin transport at distinct stages along the STx retrograde trafficking pathway, (iii) Golgicide A (GCA) yielded insights into the role of GBF1 in mediating anterograde transport of soluble and membrane-bound proteins as well as endosome-to-TGN transport of STx, (iv) activation of MK2 is part of a ribotoxic stress response following exposure to STx, and (v) MK2 contributes to the acute inflammatory response to STx.

In terms of STx transport, characterization of small molecule inhibitors revealed that all three compounds studied protected against Shiga toxicity through perturbations in

166

Golgi structure. As compound 75 also protected against diphtheria toxicity and likely acted at the endosome-to-TGN stage of STx transport, it nonetheless disrupted Golgi architecture, possibly through an inhibition in bidirectional membrane recycling between endosomes and TGN. More importantly, the block in intra-Golgi transport consistently protected against Shiga toxicity, suggesting that STx must primarily transit through an intact Golgi in order to access the endoplasmic reticulum (ER). It therefore seems unlikely that a significant amount of STx can bypass the Golgi and reach the ER from an endosome, as has been previously suggested [1].

The discovery and functional characterization of GCA allowed for the study of intra-Golgi vesicular trafficking and clearly defined the role of GBF1 in mediating anterograde and retrograde transport. Previous experiments aimed at probing transport through the Golgi have relied on treatment with brefeldin A, and often the promiscuous effects of this small molecule on *cis*/*mediali-* and *trans*-Golgi have made specific dissection of transport through one of these Golgi compartments particularly difficult. We expect that GCA will serve as an effective tool for elucidating the mechanisms of COPI-dependent transport through the Golgi.

The siRNA screen of the human kinome led us to focus on the host stress response to STx. While the contribution of the immune system to HUS pathology remains unclear, MK2 appears to play a significant role in cytokine expression and stabilization as part of an acute inflammatory response to STx. MK2 represents a viable therapeutic candidate for the treatment of STx-mediated disease.

FUTURE DIRECTIONS

The use of small molecules to investigate STx transport has been shown to be an effective approach. Despite gaining insight into the host transport mechanisms that are exploited by STx, our studies have revealed additional complexity regarding intracellular retrograde transport. Similarly, the activation of MK2 following STx damage to the ribosome raises additional questions about the initiation and regulation of the inflammatory response to STx. The following section outlines some possible directions for strengthening the conclusions of these studies and enhancing our understanding of STx pathogenesis at the levels of toxin transport and host stress response.

Define a proteomic and lipidomic signature of toxin-containing vesicles

Perhaps the most understudied aspect of bacterial toxin trafficking is the recruitment of host molecules to the plasma membrane prior to the internalization of the toxin-receptor complex. A more detailed understanding of this process will help define the host molecules essential to this process. Moreover, as these membrane-bound toxins manage to bypass targeting to the lysosome for degradation, the composition of endocytic vesicles likely provides the localization signal to direct transport from endosomes to the TGN. The recruitment, and exclusion, of host factors determines the fate of endocytosed toxin. While studies have been undertaken to define host components of endosome-to-TGN transport[2], it remains unclear how bacterial toxins exploit host trafficking and dictate their transport.

We had previously shown that Vero cells treated with the fluorescently-tagged B subunits of Shiga toxin or cholera toxin (STxB-594 and CTxB-488, respectively)

168

internalize both toxins, and that these toxins, for the most part, colocalize to endocytic

compartments previously shown to be early/recycling endosomes[3]. However, a small

proportion of vesicles contained only one of the toxins (Figure 1A). These findings

suggested that STx and CTx are internalized into similar vesicles, but the mechanisms by

which these toxins reach this common compartment and the composition of these

endosomes remain to be determined. In addition, the endosomes containing only one

toxin could be of importance and suggest a different endosomal composition compared to

dually-labeled endosomes.

A)

B)
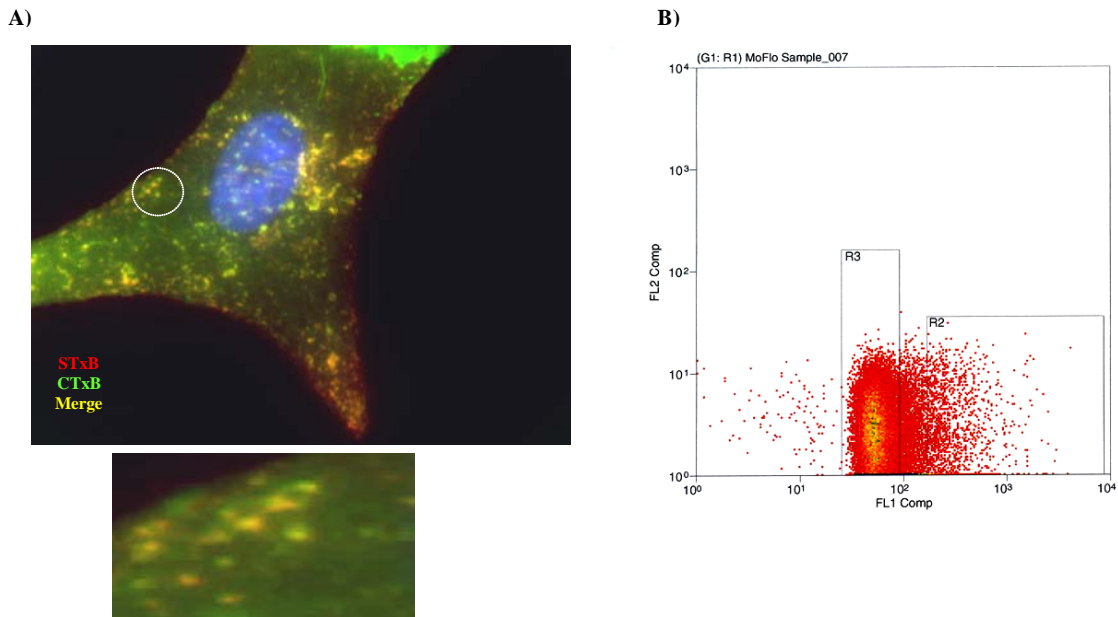
Figure 1. Isolation of toxin-containing vesicles. **(A)** STxB and CTxB converge on early endosomes. Vero cells were treated with fluorescently-tagged STxB or CTxB for 1 h at 4ºC, then allowed to internalize toxin at 22ºC for an additional hour. Cells were fixed and developed for immunofluorescence. **(B)** CTxB-488 vesicles can be isolated by FACS. CTxB was allowed to bind to Vero cells for 1 h at 4ºC, after which toxin was internalized for 1 h at 22ºC. Vesicles were isolated and sorted on a Dako MoFlo sorter, as outlined in the text. Approximately 6% of vesicles from toxin-treated cells were gated (R2) and collected, compared to 0.02% of vesicles falling into the R2 gate in untreated cells (not shown). STxB, Shiga toxin B subunit; CTxB, cholera toxin B subunit; FACS, fluorescent-activated cell sorting.

In an effort to define the composition of toxin-containing endosomes, our lab

attempted to isolate fluorescently-tagged vesicles by fluorescent-activated cell sorting

(FACS) and characterize their composition by proteomics and lipidomics. Isolation and purification of ligand-containing endosomes by FACS has proven difficult[4], as the small size of these vesicles are not amenable to detection using forward and side scatter. With the help of William Eades at the Cell Sorting Facility at Washington University, we were able to isolate CTxB-488-containing vesicles from Vero cells held at 22°C, a temperature known to block endosome-to-TGN transport[3]. The isolation could be achieved if the modular sorter was reconfigured with a smaller tip and rewired for detection on fluorescence instead of forward and side scatter. Compared to untreated cells, CTxB-488-containing cells showed an increased number of detectable vesicles in the gated region (see region R2 in Figure 1B; untreated cells not shown). Given the ability to isolate and purify these vesicles, the proteomic and lipidomic composition of toxin-containing vesicles can be determined.

This methodology could be extended to studying the composition of various ligand-containing endosomes to define their signature compositions. For example, STxB and CTxB are known to reach transferrin-positive endosomes; the transferrin-transferrin receptor complex reaches recycling endosomes, where the receptor dissociates from its ligand and is recycled to the cell surface. A comparison of STxB- or CTxB-containing endosomes to transferrin-positive endosomes would establish the host factors that constitute and distinguish these vesicles. In addition, the composition of ligands known to be targeted to lysosomes could also be compared to STxB- or CTxB-positive vesicles in order to identify host factors that may be excluded from toxin-containing vesicles to avoid lysosomal degradation. The composition of toxin-containing endosomes could also be studied for different cell lines and under various physiologic conditions (*e.g.*,

cholesterol depletion). As opposed to traditional immunofluorescence methods to define endosomal markers, this method provides a higher resolution of vesicle composition and could theoretically be applied to any fluorescently-tagged ligand.

Structural characterization of GCA inhibition of GBF1 ARFGEF activity

The mechanism by which the Sec7 domain of GBF1 catalyzes GDP/GTP exchange on ARF1 has been elucidated through studies with BFA. A crystal structure of the ARF1-Sec7-BFA complex revealed that BFA binds and stabilizes an abortive, ternary complex consisting of inactive ARF1-GDP, the Sec7 domain of GBF1, and BFA[5]. The mechanism by which GCA inhibits GBF1 catalytic activity is not known, though our studies implicated the essential role for a tripeptide loop unique to the Sec7 domain of GBF1[6] and responsible for GCA's selectivity for GBF1. The function of this loop in mediating the interaction of ARF1 with the Sec7 domain of GBF1 is not known but is amenable to investigation using GCA.

Preliminary studies would attempt to crystallize a complex of GCA with ARF1 and the GBF1 Sec7 domain. Previous structures that captured this complex relied on BFA binding to ARF1-GDP complexed to the Sec7 domain of the Gea1, the yeast homologue of GBF1. However, a sequence alignment of GBF1 with Gea1 reveals the absence of the GCA-susceptible tripeptide loop in Gea1[7]. As a result, crystallographic studies must rely on purification of recombinant GBF1 to accurately assess the significance of the tripeptide loop and the position of GCA in a putative complex.

It seems equally possible that GCA, like BFA, could stabilize an abortive complex of inactive ARF1-GDP with the Sec7 domain of GBF1. The current model for

171

the mechanism of GBF1-catalyzed GDP/GTP exchange on ARF1 argues that a conformational change in the hinge region of the GBF1 Sec7 domain releases the Sec7-ARF1 complex from the budding vesicle membrane following GTP exchange on ARF1[8]. BFA is believed to block this process and maintain the association between ARF1-GDP and GBF1. Since the hinge region on GBF1 contains the binding site of GCA, it is possible that GCA could function in a similar manner, given that it reduces intracellular levels of ARF1-GTP[6]. One could pull down GBF1 and probe by Western for the presence of ARF1 in cells overexpressing epitope-tagged constructs of GBF1 and ARF1. We would expect to see increased levels of ARF1 associated with GBF1 in GCA-treated cells compared to untreated cells, as has been seen in BFA-treated cells[8]. We would assume that ARF1 detected by this method would represent inactive ARF1-GDP. However, it is possible that GCA could stabilize a complex of GBF1 with active ARF1-GTP. In this instance, we would pull down ARF1-GTP using GST-GGA3, a specific probe for assessing levels of activated ARF1 *in vivo* [6], and look for GBF1 by Western blotting. This possibility seems less likely, as GCA has been shown to specifically target GBF1 and reduce ARF1-GTP levels by an amount proportional to the expected contribution of GBF1 to GDP/GTP exchange on ARF1[6].

Proteomic characterization of the STx-induced stress response

The activation of the host stress response by STx raises an interesting paradox. Given that STx inhibits host protein synthesis by inactivating the ribosome, how does the host manage to mount a stress response despite a drastically reduced translational rate? One hypothesis would be that the host cell diverts its remaining translational output to

172

preferentially translate host mRNAs related to the stress response. Our studies have consistently observed that, even at the highest toxin concentrations (0.1 – 1 µg/mL), *de novo* protein synthesis is not completely shut off [6,9]. This implies that a small pool of ribosomes maintains a low level of translation despite an overall reduction in protein synthesis. Host mRNAs relevant to the stress response would be preferentially targeted for translation or stabilized following the translational insult. Our evidence suggests that certain inflammatory cytokine mRNAs (IL-6, TNFα) are increased following STx exposure.

Some studies have looked at the transcriptional profile following STx exposure and not surprisingly found increases in transcripts primarily associated with apoptosis and the immune response[10,11]. However, these studies do not definitively address whether these transcripts are translated. Certain transcripts could be preferentially translated at sub-lethal STx doses, when a greater proportion of active ribosomes are available. Of particular importance in post-transcriptional mRNA regulation is the coordination of mRNA decay. MK2 has been shown to indirectly contribute to the stability of cytokine mRNAs containing AU-rich elements (ARE) in their 3'untranslated regions, including the acute inflammatory cytokines IL-6 and TNFα[12]. MK2 phosphorylates the cytokine-destabilizing protein tristetraprolin (TTP). Phosphorylated TTP is sequestered through its interaction with 14-3-3 proteins to stress granules, cytoplasmic foci where inactive components of the translational machinery accumulate under conditions of environmental stress.

To investigate the characteristics of proteins translated during ribotoxic stress, we would compare the proteomic profiles of cells treated with STx to those exposed to

catalytically inactive STxB. This would control for non-specific effects of STx transport

and would focus on the ribotoxic response. Proteomic profiles could be compared to

transcriptional data to identify the components of these mRNAs (*e.g.*, AU-rich elements)

responsible for their translation under conditions of toxic stress. The identity of these

proteins and transcriptional elements would not only provide a catalog of STx-induced

proteins but would also enhance our understanding of how these transcripts are targeted

for translation or stabilization.

REFERENCES

1. Llorente, A., Lauvrak, S.U., van Deurs, B. & Sandvig, K. Induction of direct endosome to endoplasmic reticulum transport in Chinese hamster ovary (CHO) cells (LdlF) with a temperature-sensitive defect in epsilon-coatomer protein (epsilon-COP). *J Biol Chem* **278**, 35850-5 (2003).

2. Bonifacino, J.S. & Lippincott-Schwartz, J. Coat proteins: shaping membrane transport. *Nat Rev Mol Cell Biol* **4**, 409-14 (2003).

3. Mallard, F. et al. Early/recycling endosomes-to-TGN transport involves two SNARE complexes and a Rab6 isoform. *J Cell Biol* **156**, 653-64 (2002).

4. Bananis, E. et al. Microtubule-dependent movement of late endocytic vesicles in vitro: requirements for Dynein and Kinesin. *Mol Biol Cell* **15**, 3688-97 (2004).

5. Mossessova, E., Corpina, R.A. & Goldberg, J. Crystal structure of ARF1*Sec7 complexed with Brefeldin A and its implications for the guanine nucleotide exchange mechanism. *Mol Cell* **12**, 1403-11 (2003).

6. Saenz, J.B. et al. Golgicide A reveals essential roles for GBF1 in Golgi assembly and function. *Nat Chem Biol* **5**, 157-65 (2009).

7. Jackson, C.L. & Casanova, J.E. Turning on ARF: the Sec7 family of guanine-nucleotide-exchange factors. *Trends Cell Biol* **10**, 60-7 (2000).

8. Szul, T. et al. Dissecting the role of the ARF guanine nucleotide exchange factor GBF1 in Golgi biogenesis and protein trafficking. *J Cell Sci* **120**, 3929-40 (2007).

9.   Saenz, J.B., Doggett, T.A. & Haslam, D.B. Identification and characterization of small molecules that inhibit intracellular toxin transport. *Infect Immun* **75**, 4552-61 (2007).

10.   Fujii, J. et al. Shiga toxin 2 causes apoptosis in human brain microvascular endothelial cells via C/EBP homologous protein. *Infect Immun* **76**, 3679-89 (2008).

11.   Keepers, T.R., Psotka, M.A., Gross, L.K. & Obrig, T.G. A murine model of HUS: Shiga toxin with lipopolysaccharide mimics the renal damage and physiologic response of human disease. *J Am Soc Nephrol* **17**, 3404-14 (2006).

12.   Anderson, P. Post-transcriptional control of cytokine production. *Nat Immunol* **9**, 353-9 (2008).

JOSE BERNARDO SAENZ
Curriculum Vita

PERSONAL INFORMATION

Date of birth: December 9, 1980
Place of birth: Miami, FL

CONTACT INFORMATION

Business:
Washington University School of Medicine
Department of Pediatrics
660 South Euclid Avenue, Campus Box 8208
Saint Louis, MO 63110
Phone: (314) 286-2872

Home:
329 Belt Avenue, #501
Saint Louis, MO 63112
Phone: (314) 583-6798
E-mail:
josesae@gmail.com

EDUCATION

GRADUATE SCHOOL
September 2005 – November 2009   Washington University   St. Louis, MO
- PhD in Microbiology and Microbial Pathogenesis
- *Dissertation:* Genetic and chemical genetic approaches to Shiga toxin inhibition
- Advisor: David Haslam, MD

Expected May 2011   Washington University   St. Louis, MO
- Medical Degree

COLLEGE
May 2003   Cornell University   Ithaca, NY
- B.A. in Chemistry
- B.A. in French Literature

HONORS/AFFILIATIONS

- Recipient of the Ruth L. Kirschstein National Research Service Award for Individual Predoctoral Fellows (F31; National Institute of Allergy and Infectious Diseases), 2009-2011
- Graduated *Cum laude* in Chemistry, 2003
- Merck Index Award in Chemistry at graduation (Cornell University), 2003

- Golden Key International Honor Society (Cornell University), 2002-2003

- National Society of Collegiate Scholars (Cornell University), 2000-2003
- American Cancer Society Fellowship (University of Miami), 2001
- Dean's List (Cornell University), 1999-2003
- Coordinator of SAFE (Sexual Awareness For Everyone) organization (Cornell University), 2002-2003
- Attended Student Global AIDS Conference (Williams University), 2003
- Cornell Biodiversity Program, 2001
- Salutatorian (Coral Gables High School), 1999
- Hispanic Outlook Scholarship (Coral Gables High School), 1999
- Inner City Youth Scholarship (Coral Gables High School), 1999

RESEARCH INTERESTS

- Study of bacterial and plant toxin trafficking through chemical genetic and siRNA approaches.
- Application of high-throughput chemical and siRNA screens for the identification of potential therapeutics in the treatment of toxin-mediated diseases (*i.e.*, Hemolytic Uremic Syndrome).

RELATED EXPERIENCE

Research

MEDICAL SCIENTIST TRAINEE, MD/PhD PROGRAM
August 2003 - present   Washington University   St. Louis, MO
- Screening of small molecule compounds that inhibit Shiga toxin-mediated cytotoxicity.
- Identification and characterization of two compounds that target distinct steps in the transport of Shiga and cholera toxins.
- Characterization of Golgicide A, a novel inhibitor of GBF1.
- Identification and characterization of kinases involved in Shiga toxin transport through a siRNA screen of the human kinome.

RESEARCH ASSISTANT
October 2001 - May 2003   Cornell University   Ithaca, NY
- Investigation of the binding domain of phosphodiesterase (PDE) and its role in the signal transduction pathway involved in vision, under the guidance of Dr. Richard Cerione.

- Biochemical assessment of the functional interactions of the inhibitory γ-subunit of PDE.
- Chemical cross-linking of trypsinized PDE.

<u>RESEARCH FELLOW, AMERICAN CANCER SOCIETY</u>

June 2001 - August 2001   *University of Miami*   *Miami, FL*

- Study on the affinity of Replication Protein A (RPA) for DNA polymerase delta and other essential DNA synthesis proteins, under the guidance of Dr. Antero So.
- Use of biochemical techniques for the purification of RPA.

<u>ABSTRACTS/PRESENTATIONS</u>

Saenz, J.B., Li, J., Haslam, D.B. (2009) The MAP kinase-activated protein kinase 2 (MK2) contributes to the Shiga toxin-induced inflammatory response. Speaker; *44th U.S.-Japan Conference on Cholera and Other Enteric Bacterial Infections*, San Diego, CA.

Saenz, J.B., Li, J., Haslam, D.B. (2009) The MAP kinase-activated protein kinase 2 (MK2) contributes to the Shiga toxin-induced inflammatory response. Poster; *American Physician Scientist Association*, Chicago, IL.

Saenz, J.B., Sun, W.J., Haslam, D.B. (2007) A small molecule inhibitor   of Shiga and cholera toxin transport. Speaker; *42nd U.S.-Japan Conference on Cholera and Other Enteric Bacterial Infections,* Austin, TX.

<u>PUBLICATIONS</u>

Saenz, J.B., Li, J., Haslam, D.B. The MAP kinase-activated protein kinase 2 (MK2) contributes to the Shiga toxin-induced inflammatory response. *Cellular Microbiology* (2009); submitted.

Saenz, J.B., Sun, W.J., Chang, J.W., Li, J., Bursulaya, B., Gray, N.S., Haslam D.B. Golgicide A reveals essential roles for GBF1 in Golgi assembly and function. *Nature Chemical Biology* 2009; 5(3):157-65.

Saenz, J.B., Doggett, T.A., Haslam, D.B. Identification and characterization of small molecules that inhibit intracellular toxin transport. *Infection and Immunity* 2007; 75(9):4552-61.

Medical

CLINICAL VOLUNTEER

March 2005   *Washington University*   *Nicaragua*
- Collaborated in setting up clinics in community centers and villages throughout Nicaragua.
- Provided general health care and dental care to local residents.
- Educated residents on appropriate hygiene procedures.

CLINICAL VOLUNTEER

September 2006   *Washington University*   *Belize*
- Collaborated in setting up clinics in rural areas of Belize.
- Provided general health care to local residents.
- Offered sexual education course to local school teachers.

Teaching

MCAT Instructor

January 2008 – March 2009   *MCAT Preparation Course*   *St. Louis, MO*
- Tutor for the General Chemistry and Verbal Reasoning portions of the Medical College Admission Test (MCAT).

TEACHING ASSISTANT

August 2005 - March 2006   *Washington University*   *St. Louis, MO*
- Laboratory instructor for the Histology course offered to first-year medical students.
- Held review sessions, graded exams, and proctored laboratory portion of exams.

TUTOR

September 1996 - June 1999   *Coral Gables High School*   *Miami, FL*
- Tutored middle and elementary school students in the subjects of Math and French grammar twice a week.

Languages
- Fluent in English, Spanish, and French.